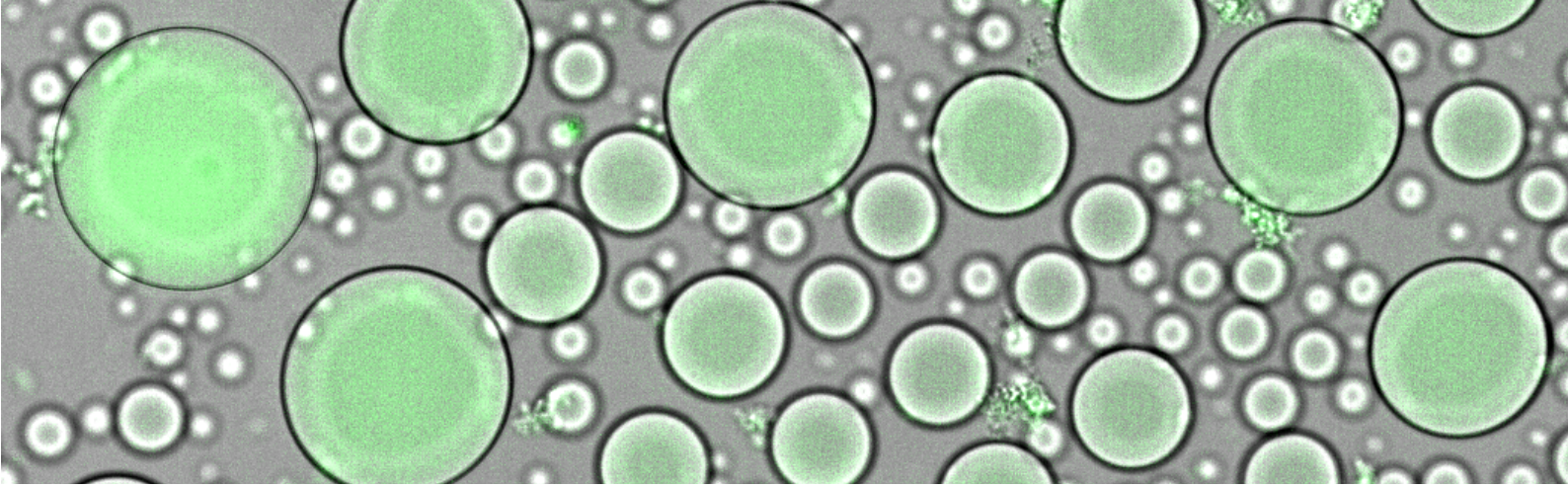

Biocompatible Reaction Compartments with Functionalizable Membranes

Thomas Frank

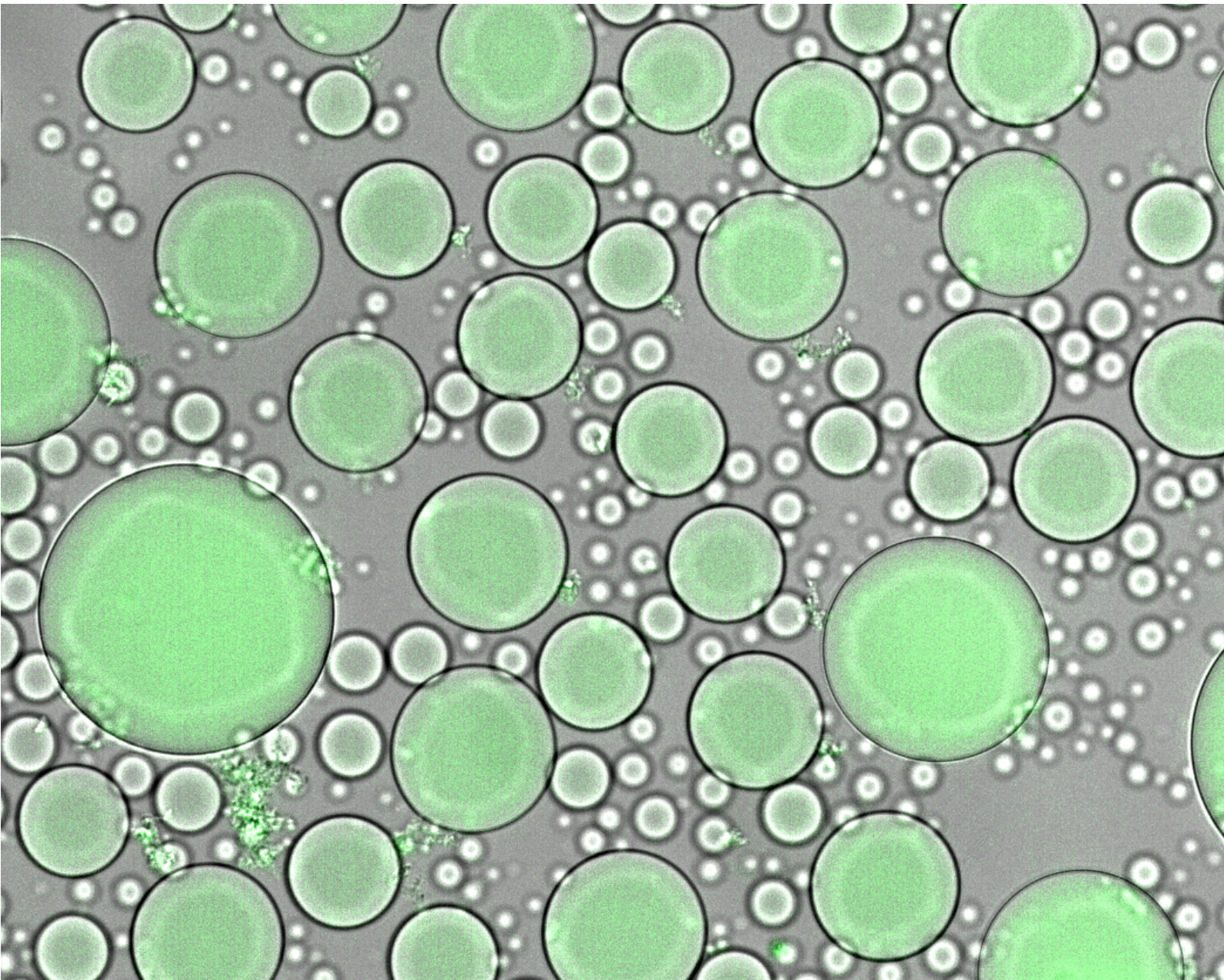

Technische Universität München
TUM School of Natural Sciences

Biocompatible Reaction Compartments with Functionalizable Membranes

Thomas Frank

Vollständiger Abdruck der von der TUM School of Natural Sciences zur Erlangung des akademischen Grades eines

Doktors der Naturwissenschaften (Dr. rer. nat.)

genehmigten Dissertation.

Vorsitz: Prof. Dr. Karen Alim

Prüfer*innen der Dissertation:

1. Prof. Dr. Friedrich C. Simmel
2. Prof. Dr. Petra Schwille

Die Dissertation wurde am 08.03.2023 bei der Technischen Universität München eingereicht und durch die TUM School of Natural Sciences am 07.04.2023 angenommen.

Contents

1 Introduction 11

2 Theoretical Background 15

2.1 Compartmentalization 15

2.1.1 Liposomes 18

2.1.2 Polymersomes 21

2.1.3 Hybrid Membranes 26

2.2 Membrane Effects 28

2.2.1 Phase Separation 28

2.2.2 Membrane Interactions 32

2.2.3 Proximity Labeling 35

2.3 *In Vitro* Transcription 37

2.4 Cell-Free Gene Expression 40

3 Materials and Methods 43

3.1 Protein Components 43

3.1.1 Cloning 43

3.1.2 Expression 43

3.1.3 Purification 43

3.2 Click Chemistry 45

3.3 Preparation of GUV 45

3.3.1 Solvent Evaporation 45

3.4 *In Vitro* transcription 46

3.4.1 Fluorescent aptamer 46

3.4.2 pRNA Aptamer 46

3.5 Cell-free Gene Expression 48

3.6 sAPEX2 Reconstitution 49

3.6.1 Production 49

3.6.2 Amplex Red Activity Assay 49

3.6.3 Biotinylation Assay 50

3.7 Western Blotting 50

3.8 Observation chambers 51

4 Results 53

4.1 Size Distribution of Giant Unilamelar Vesicles 53

4.2 Functionalized Hybrid Membranes 57

4.3 sAPEX2 Reconstitution 62

4.4 Encapsulation of Active Systems 66

4.4.1 In-vitro Transcription 66

4.4.2 Cell-free Gene Expression 71

5 Conclusion and Outlook 75
5.1 Conclusion 75
5.2 Outlook 76

List of Figures 81

List of Tables 81

Glossary 85
Bibliography 87
A Appendix 109

Abstract

The research on microscale compartments able to mimic cell-like behavior, serve a drug delivery tool, or being used as biosensors is ever-expanding over the last decades. Focused on different topics like the introduction of different functionalities in the compartments or the modification of their membrane, researchers push the boundary of applicability of vesicles in modern science. In this thesis the formation of giant unilamellar vesicles composed of biocompatible polypeptides and mixtures with phospholipids is investigated. Furthermore, functionalization of the membrane as well as encapsulation of active processes essential to mimic cell-like behavior are examined.

One aim of this thesis is membrane localized biotinylation activity triggered by addition of a multifunctional linker structure. For this, hybrid membranes of elastin-like polypeptides (ELP) and ELP-phospholipids were generated and examined. The combination of different membrane increases the average sizes of hybrid vesicles compared to liposomes. Hybrid vesicles interact with external molecules over biotin-streptavidin bonds which allows to visualize the membrane surface using biotinylated fluorophores. With the application of multivalent RNA-aptamers the colocalization of different fluorescent proteins on the surface as well as the reconstitution of the split enzyme sAPEX2 was achieved. Active sAPEX2 shows the ability to convert Amplex Red and to biotinylate ELPs used for encapsulation.

The second focus was set on the encapsulation of in vitro transcription (IVT) and cell-free gene expression (CFE) systems. These two systems are essential components of cellular life and their activity was observed within biocompatible ELP vesicles at micrometer scale. Observations of in vesiculo production of fluorescent RNA aptamers showed increasing fluorescent signals over time, while the monitored vesicles displayed growth at the same time. The growth or shrinkage of the vesicles correlates with the concentration of available ELPs in solution. As encapsulated CFE reactions showed a similar behavior while expressing YPET, changes in osmotic pressure are assumed to be the potential driving force behind this dynamic.

With these findings the addressability of membrane structures using streptavidin as linker molecule while enabling the encapsulation of essential cell processes within biocompatible membranes was shown.

Zusammenfassung

In den letzten Jahrzehnten hat sich die Forschung zu Mikrometer großen Kompartimenten, die zellähnliches Verhalten nachzuahmen, im Transport von pharmazeutisch aktiven Substanzen oder als Biosensoren eingesetzt werden können, stetig vergrößert. Durch das Implementieren verschiedener Funktionalitäten oder die Modifizierung ihrer Membran wird die Anwendbarkeit von Vesikeln in der modernen Wissenschaft durch Forscher erhöht. In dieser Abschlussarbeit wird die Herstellung von riesigen unilamellaren Vesikeln untersucht, die aus biokompatiblen Polypeptiden und deren Mischungen mit Phosoholipiden hergestellt wurden. Darüber hinaus werden die Funktionalisierung der Membran sowie die Enkapsulierung aktiver Prozesse untersucht, die für die Ausbildung eines Zell-ähnlichen Verhaltens notwendig sind.

Ein Ziel dieser Arbeit ist der Nachweis membranlokalisierter Biotinylierung die durch die Zugabe eines multifunktionalen Linkers gesteuert werden kann. Hierfür wurden elastinähnliche Polypeptid- (ELP) und hybride ELP-Phospholipidmembranen hergestellt und untersucht. Die durchschnittliche Größe der Hybridvesikel im Vergleich zu Liposomen kann auf die Kombination aus unterschiedlichen Membrankomponenten zurückgeführt werden. Hybridvesikel können mittels Biotin-Streptavidin-Bindungen mit externen Molekülen interagieren, was die Visualisierung der Membranoberfläche mit biotinylierten Fluorophoren ermöglicht. Die Anwendung multivalenter RNA-Aptamere ermöglichte die Kolokalisierung verschiedener fluoreszierender Proteine auf der Oberfläche sowie die Rekonstitution des gespaltenen Enzyms sAPEX2. Aktives sAPEX2 war in der Lage Amplex Red umzuwandeln und ELPs zu biotinylieren die für die Enkapsulierung verwendet wurden.

Der zweite Schwerpunkt lag auf der Enkapsulierung von In-vitro Transkriptionssystemen (IVT) und Systemen die zellfreie Genexpression (CFE) ermöglichen. Die Aktivität dieser beiden Mechanismen die essentielle Bestandteile des zellulären Lebens sind, konnte in biokompatiblen ELP-Vesikeln im Mikrometerbereich beobachtet werden. Bei der Messung der *in vesiculo* produzierten fluoreszenten RNA-Aptameren konnte ein steigendes Fluoreszenzsignal sowie ein Wachstum der Vesikel beobachtent werden. Es konnte eine Korrelation des Wachstumsverhaltens mit der verfügbaren ELP Konzentration in Lösung festgestellt werden. Da ein ähnliches Verhalten bei YPET prduzierenden CFE Reaktionen beobachtet wurde, wird angenommen, dass die Veränderung der osmotischen Druckverhältnisse die treibende Kraft des Wachstumsverhaltens ist.

Mit diesen Erkenntnissen konnte die Adressierbarkeit von Membranstrukturen unter Verwendung von Streptavidin als Linkermolekül gezeigt werden. Desweiteren konnte nachgewiesen werden, dass die verwendeten Vesikel in der Lage sind wesentliche Zellprozesse in biokompatiblen Membranen zu enkapsulieren.

1. Introduction

What is a cell? — According to the encyclopædia britannica a cell is defined as *'[...] the basic membrane-bound unit that contains the fundamental molecules of life and of which all living things are composed.'* [1] This definition spans over all domains of life and makes the cell the essential building block for life itself. Being separated in a solid-like membrane and a densely packed fluid-like cytoplasm, these two systems are responsible for different tasks within the cell but need to interact to properly regulate cell functions.

The cytoplasm consists of cell organelles and cytosol, which acts as the liquid matrix containing proteins, nucleic acids and metabolites. The cytoplasm's task is to harbour all essential components used for processes involved in cell functionality such as metabolism and gene expression. [2] Vital mechanisms of the cell like growth, [3] maintenance [4] [5] and differentiation [6] [7] are controlled by complex systems of interactions within the cytoplasm. In contrast to the sheer amount of interaction-based regulatory systems in the cytosol, the membrane has to provide fewer but also vital functions.

Although, the membrane itself does not possess such a complex repertoire of interacting components as the cytoplasm it introduces essential properties to the cell. [8] [9] As one of the major responsibilities, the interaction between the environment and the processing of external stimuli is mediated by the membrane as first barrier of contact. These can be handled by the coordinated transport to the inside [10] but also with signaling cascades generating defense mechanisms. [11] The protection of the cell itself also calls for a robust and impermeable barrier which is able to withstand external stress. This function is fulfilled by the interplay of cell membrane, cell wall and the cytoskeleton. [12] [13] The coordinated function of these systems is also responsible for cell division. This process regulating the proliferation of individual cells depends on the flexibility of cell membranes as well as its ability to interact with specific protein networks. [14] [15] Another aspect is the compartmentalization of smaller volumes, which allows the cell to organize specific functionalities into substructures. This can be seen as the introduction of membrane separated cell organelles in eukaryotic cells allowed an evolutionary leap towards the formation of more complex structures. [16] These dedicated substructures are responsible for specific tasks instead of a *de facto* one-pot reaction for all essential networks within the cell. [17] [18]

In possession of highly specialized functions depending on its composition, the membrane is an interesting scaffold structure which served as inspiration in syn-

thetic biology. The research on liposomes dates back to the 1960's and has brought forth a plethora of applications. Providing high biocompatibility, but showing poor stability and variability in their composition however restricts the potential implementations of liposomes. [19] This fact gave rise to the intense reasearch focusing on the formation of cell-like compartments composed from materials with a synthetic origin. [20] Polymersomes are vesicles made of (semi-) synthetic polymers able to form a stable membrane and even providing new characteristics in comparison to lipid double layers. As these two model systems developed in the recent decades, different fields of use formed for each of the systems.

One of these fields is the research of artificial minimal cells. Conducting experiments where vesicles encapsulate single molecular mechanisms without the complexity of the cytoplasm, provides the opportunity to explore the functions in a more detailed manner. Biological systems such as the bacterial cytoskeleton, [21] motion apparatus [22] and gene expression machinery [23] are only a few examples of cell-like processes observed in artificially formed vesicles. This way biomimetic functions can be tested within a designed environment with regulated parameters and a preformed membrane composition. The composition of the membrane influences its overall properties and has to be adapted to the systems involved in the measurements. Therefore, processes like cell division need the dynamic membrane behavior of liposomes while receptor activity is observed in a more robust membranes which can be provided by polymersomes. [24] [25]

In contrast to recreating mechanisms observed in nature, biosensors [26] [27] and synthetic drug delivery systems [28] [29] have extensive requirements for the desired vesicle properties. Instead of a biomimetic buildup, these fields focus on the functionality of their materials and how this could lead to a more precise application. Properties like responsiveness of the material itself are not mediated by membrane proteins or other regulatory mechanisms seen in nature. Instead, programming the materials themselves to react to specific stimuli is the key aspect used in this field of biotechnology. Triggers such as changes in pH, temperature and light as well as interaction of different ligands can change membrane properties. [30] [31]

Considering the progress made in all these fields, the aim of this thesis is the combination of active processes encapsulated within a reactive membrane. As the creation of stimuli-responsive vesicles shows high potential, [30] their combination with a regulatory system could produce autonomous cell-like compartments able to adapt to their environment. The combination of bio-compatible polymers with phospholipids can combine the dynamics observed in lipid bilayer membranes with the increased stability of polymers. Testing whether the implementation of a

reaction to outside stimuli can be achieved, a feedback mechanism consisting of localized biotinylation and protein co-localization was used. This mechanism used in proximity labeling can be used to locally increase membrane bound proteins and thereby increase membrane curvature. This way, tuning of the fluidity and composition of the membrane can induce deformation and fission events. [32] [24] [33]

The theoretical background on the systems and mechanisms used in this thesis are explained in chapter 2. Here we take a closer look on the physical laws behind the formation of compartments as well as on the properties of membranes. As the encapsulation of active systems like *in vitro* transcription (IVT) and cell free gene expression (CFE) were an essential goal of the thesis, these mechanisms are explained in more detail. The exact methods and materials for the production of vesicles composed of material able to interact in a pre-designed manner are explained in chapter 3. Measurements conducted during this thesis and evaluation of the achieved results are discussed in chapter 4. Lastly, the overall achievements of the work and potential improvements on the project are elucidated in chapter 5.

2. Theoretical Background

In this chapter the emphasis lies on the explanation of essential theoretical basics regarding compartmentalization, enzymatic processes and membrane interactions. Starting with the very essentials of compartment formation, we take a closer look on the characteristics of membrane forming molecules. These membranes can behave in different ways regarding their flexibility, mobility and stability. Properties like these and the potential means to manipulate them are explained in the following chapters. As encapsulation of active enzymatic processes was a major point for this thesis, we also take a closer look at *in vitro* transcription (IVT) and at cell-free gene expression (CFE).

2.1. Compartmentalization

Biological cells are able to contain complex reaction networks which are the building blocks of complex life on earth. One key component these cells need is the prescence of a barrier to physically separate themselves from their surroundings. [34] Only that way they are able to cope with potential threats [35], [36] create energy to proliferate [8] or to interact with one another. [9]

The creation of these barriers needs components with amphiphilic properties, where hydrophilic and hydrophobic domains are covalently bound. The works of Israelachvili thoroughly investigate the the laws of physics behind the process of compartmentalization. [37]

Aggregation of the molecules is driven by the hydrophobic effect, as well as by intermolecular Van der Waals forces. The hydrophilic domains establish hydrogen bonds with the surrounding water molecules. The energy of the system in each respective domain is lowered by minimization of unfavorable surface area between hydrophobic and hydrophilic moieties. This results in attractive forces between components demonstrating the same hydrophobic properties and repulsive forces between different properties. Furthermore, additional repulsive forces such as steric hindrance of the hydrophobic chains, electrostatic repulsion between charged headgroups as well as hydration energy influence this balance between attractive and repulsive forces. Looking at the overall energy within the system during the formation of an interface between hydrophobic core and hydrophilic surrounding, one has to consider the chemical potential μ of the molecules contributing to the phase separation

$$\mu_N^0 = \frac{2\gamma a_0 + \gamma}{a(a - a_0)^2} \tag{2.1}$$

As μ_N^0 also describes the energy difference between the individual molecule in solution and in aggregates of N particles, an optimal headgroup area a_O of amphiphilic molecules in an aggregate exists where the interaction surface of the hydrophobic domain and water is minimized. The positive interfacial free energy per unit area at the hydrophobic domain-water interface γ is specific for different hydrophobic domains. This energy difference is governed by the minimization of interfacial energy and repulsive forces between the individual molecules. Negative values of μ_N^0 promote the formation of small aggregates, so called micelles encapsulating the hydrohobic domains in the core and only presenting hydrophilic headgroups to the water molecules as seen in Fig.2.1.1 a. This however is only the possible when the number of molecules N in the system exceeds the critical micelle concentration (cmc), a concentration threshold under which amphiphilic molecules are not able to form micelles or even bigger aggregates by spontaneous self-assembly. [38]

$$c_{CMC} \approx e^{\frac{-N\epsilon_h}{k_B T}} \tag{2.2}$$

The monomer's effective interaction energy with the molecules in bulk ϵ_h is dependent on the material and their respective attractive forces. After establishing that amphiphilic molecules need an optimal surface area a_O for them to form aggregates which are energetically favorable, other parameters have to be defined for the formation of compartments. These 'packing parameters' include the volume occupied by the hydrophobic domain *v*, which remains incompressible but deformable and a critical chain length l_c as seen in Fig. 2.1.1 a. The critical chain length is described as the maximum length to which the hydrophobic chain can be elongated without energetic penalties.

The packing parameter influences the form of the resulting compartments extensively as different parameters promote different surface curvatures. As shown in Fig. 2.1.1 b , the packing paramter can be influenced by external stimuli like temperature and pH of the surrounding medium. High and low packing parameters favor the formation of micelles or inverted micelles, whereas a parameter of $\frac{V}{a_0 l_c} \approx 0.5-1$ is necessary for the formation of bilayer structures. This makes sense considering the low curvature needed to create two leaflets capable of forming membrane structures. The formation of spherical vesicles enables the membranes to

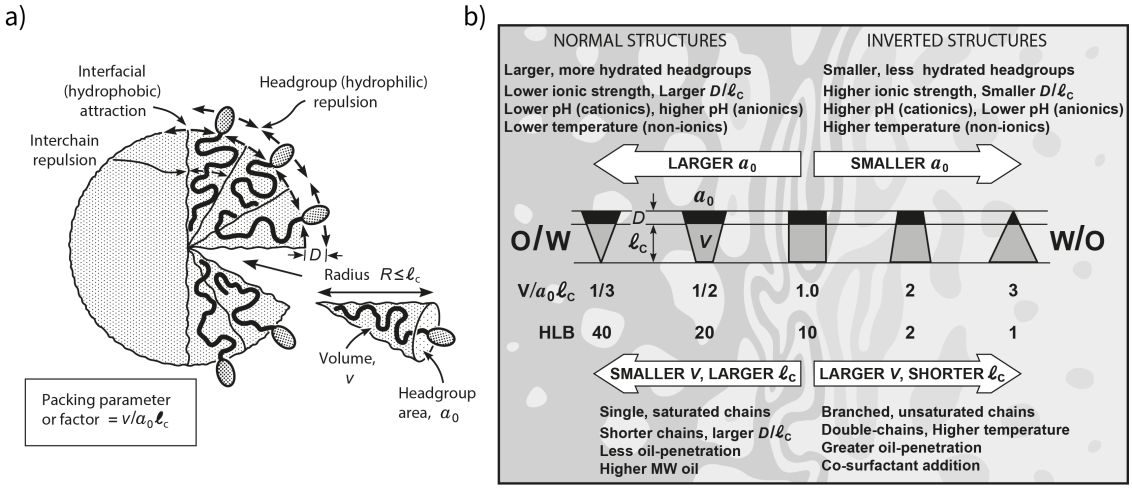

Figure 2.1.1: Packing Parameters: *Schematic overview of the influence of physical properties of amphiphilic molecules aggregating. a) Properties influencing the packing parameter due to repulsive or attractive forces exerted on molecules. b) Factors influencing the packing paramter and the resulting morphology of the individual molecules. The formation of water in oil emulsions (w/o) is promoted by outward directed conical molecules, composed of small a_0 and high v,whereas oil in water emulsions (o/w) need inverted proportions of these factors. The Hydrophilic-Lipophilic Balance describes the ratio between the two domains of the amphiphile and correlates with the packing parameter. Schematics taken from Israelachvili* [37]

take more stable conformation by reduction of energetically unfavorable edges in a system with a limited amount of amphiphiles. Resulting vesicles have certain constraints considering the stability of the formed membrane and their dimensions. Therefore, taking into account the specific packing parameter of an amphiphile, a critical radius R_c exists under which the membrane can not form without introducing packing stress on the individual components.

$$R_c \approx \frac{l_c}{(1 - v/a_0 l_c)} \tag{2.3}$$

The critical radius only applies for the outer leaflet, due to the fact that molecules incorporated in the inner leaflet deform and are not forced to extend over their specific l_c. Taking the critical radius of the vesicle shows the critical lower threshold of the size range a vesicle can attain. This can serve as an approximation of the size of vesicles formed by spontaneous self-assembly. Vesicle sizes are most commonly categorized in small unilamellar vesicles (SUV) with a size of up to 100 nm, large unilamellar vesicles (LUV) in a range of 100-1000 nm and giant unilamellar

vesicles (GUV) at sizes >1 µm (see Fig. 2.1.3), the latter being the main focus of this thesis. [19] The actual size is influenced by several other factors as well such as formation method and concentration of the amphiphiles. To estime the minimal amount of molecules necessary to at least theoretically form a vesicle with the radius R_c one has to determine the aggregation number N.

$$N \approx \frac{8\pi R_c^2}{a_0} \tag{2.4}$$

This sets the basic rules which are essential for the formation of compartments, but to form experiments depending on the formation of vesicles in the right size dimensions one has to keep specific material properties in mind. One specific aspect is the different architecture of vesicle forming amphiphiles. In the next chapters we take a more detailed look on the two most prevalently used materials for the formation of vesicles.

2.1.1. Liposomes

As already mentioned cell-like compartments can possess membranes consisting of different amphiphilic molecules. One group of these molecules prevalently used in research are lipids. Over the years a wide range of different preparation methods was introduced to enable the formation of compartments composed of a lipid bilayer encapsulating a aqueous phase inside. These liposomes are used as models to explore and mimic the mechanisms of specific cell functions or interactions. [39] [40] Instead of a highly complex cell environment, these models allow it to simplify the system and to observe specific functions. [21] [41]

The formation of lipid membranes is entropically driven by self-assembly of solved lipid molcules in an aqueous environment, which arrange in a bilayer structure. This bilayer is composed of an inner and outer leaflet which is held together by the hydrophobic core of the membrane. The membranes of liposomes can range between 3-5 nm in thickness and are slightly thinner than their biological counterparts (8-10 nm) as they are composed of a homogeneous mixture of lipids omitting associated proteins and carbohydrates. The artificial model membranes can be composed of a broad variety of different lipids. [39] The hydrophobic domains inside of the bilayer form intermolecular van der Waals bonds while simultaneously minimizing their interaction with the surrounding medium. Meanwhile the hydrophilic headgroups and surrounding water molecules interact via hydrogen bonds to keep the vesicle in solution. Even with different structures most lipids share the ability to form stable membranes due to their amphiphilic nature (see

Fig. 2.1.2). Following here is an overview over the most important lipids found in biological membranes. [42]

(a) **Glycerophospholipids:** These phospholipids are composed of a central glycerol linking a hydrophilic, mostly charged headgroup and hydrophobic acyl chains. Typical examples for headgroups connected via phosphate bonds are ethanolamine (PE), Choline (PC), Serine (PS), but can also contain saccharides or nucleic acids. One or two long hydrocarbon chains attached to the glycerol form the hydrophobic domain of the molecule. Commonly used chain lengths can range from C10 to C24. The structure is depicted in more detail in Fig.2.1.2 d. Depending on the degree of saturation of the carbohydrate chains, they posses different physical characteristics as seen in Fig.2.1.2 e.

(b) **Sphingolipids:** Similar to glycerophospholipids, all sphingolipids are composed of a central linker structure, the sphingoid base. The compostion ranges from carbohydrates, saccharides and small hydrophilic compounds as hydrophilic to fatty acid chains as hydrophobic domains. In contrast to phospholipids though, the exact composition can vary drastically ranging from structures with two acyl chains and a phosphate bound choline (Sphingomyelin) to sphingolipids composed of the central linker and three carbohydrate chains (Glycosphingolipids).

(c) **Sterol Lipids:** The structure of sterol lipids greatly differs from the blueprint of the lipids mentioned before. The common feature of all sterol lipids is the tetracyclic steran molecule composed of three C6 and one C5 rings. They can be categorized according to the number of carbon molecules in the core skeleton, steran. Attached functional groups defining the physico-chemical properties of the individual molecules can range from carbohydrates and saccharides to peptides and acids. In comparison to the former two groups the attached chain lengths of any attached molecule are rather short. Their structure also allows them to increase packing density of the membrane, which in turn has an impact on the stability and permeability of the membrane. [43] The overall structure of cholesterol can be seen in Fig.2.1.2 c,e.

Next to the lipid groups mentioned above, there are also other lipids involved in the maintenance of biological membranes as well as proteins and carbohydrates. For the context of this thesis however we focus on these three groups as they have proven to be essential components of model GUVs providing specific properties to the membrane.

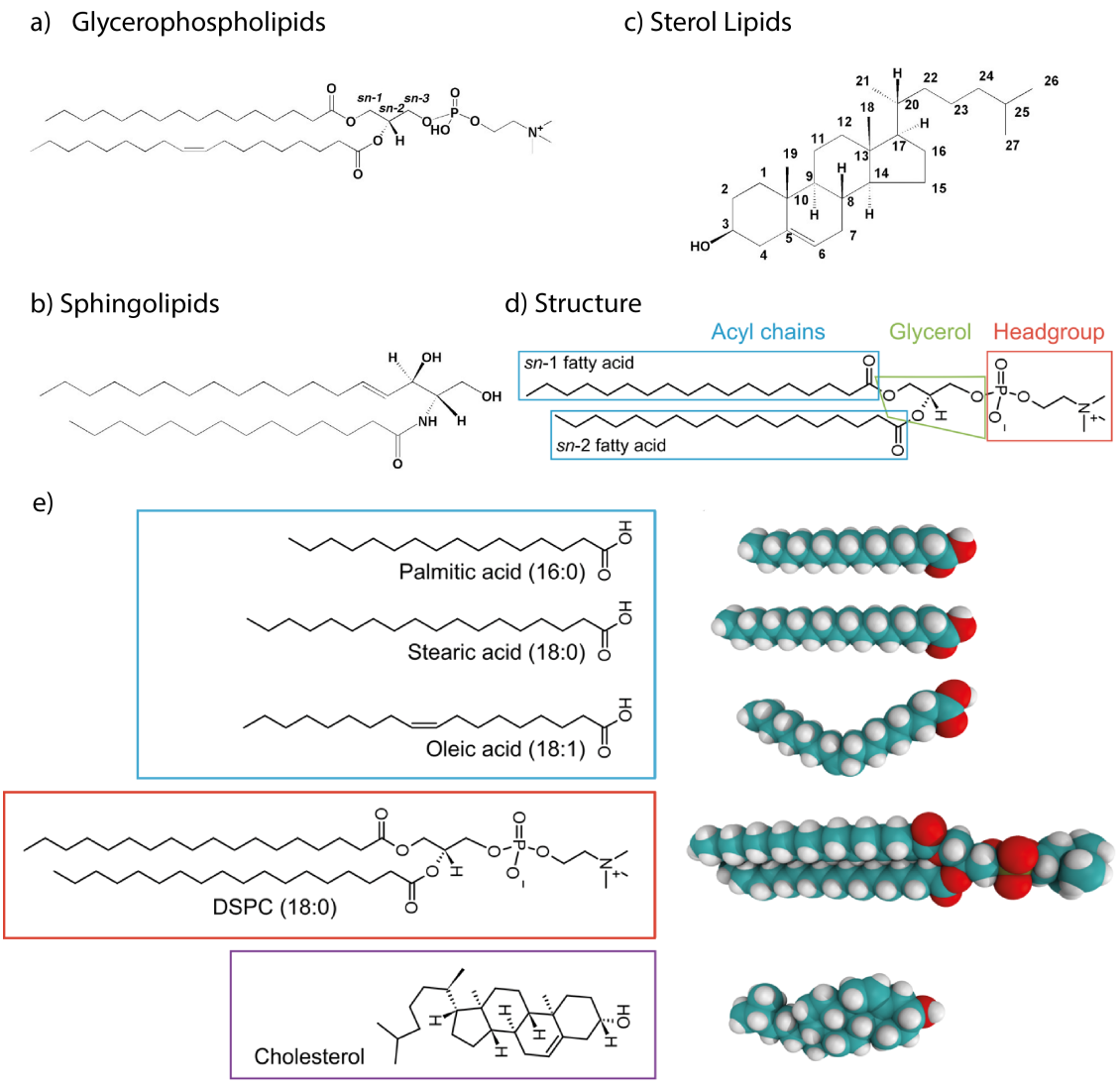

Figure 2.1.2: Overview Lipids: *Overview of structure of relevant lipid groups used in GUV model systems. a) Glycerophospholipids, 1-palmitoyl-2-oleoyl-glycero-3-phosphocholine (POPC), b) Spingolipids,N-myristoyl-sphingosine, c) Sterol lipids, Cholesterol (C27), d) The basic structure of glycerophospholipids where long acyl chains (blue) form the hydrophobic and the hydrophilic headgroup (red) are covalently linked via a glycerol backbone (green). e) The chemical structures (left) of commonly used fatty acids (blue), Glycerophospholipids (red) and sterols (purple) are projected with their stereochemical projection (right) as solid van der Waals spheres. Adapted from Fahy et al. [42] and Cebecauer et. al. [44] Copyright (2018) American Chemical Society.*

In nature, membranes act as a barrier partitioning different liquids and provide the ability to separate molecules from each other. As the membranes of liposomes tend to be leaky and are unselectively permeable for small molecules and ions like H_2O or H^+ (see Fig. 2.1.3). Therefore these models can only be seen as approximation for the characteristics of real cells, as the selective transport of ions using membrane proteins is an essential component of the cell's functionality. This

stems from the fluid-like characteristic of the membrane itself where individual molecules can freely diffuse within the barriers of the membrane at roughly 5-14 $\mu m^2/s$ and even can switch between the two leaflets at rates of 10^{-3}-10^{-8} s^{-1}. [45] [46] [47] Characterization of the fluid-like behavior of the membrane will be further explained in Chapter 2.2.

This dynamic behavior brings along advantages in the reconfiguration of the membrane composition itself but also makes it vulnerable to external forces. With a sensitivity towards external shifts in osmolarity, temperature, or pH and the proneness of its monomers to degradation, the overall stability of liposomes is rather low compared to cell membranes. [39] [48] The introduction of synthetical lipids alongside the implementation of a certain degree of tunability tries to counteract these restrictions. [49]

Overall, liposomes are mostly regarded as a platform to investigate molecular mechanisms of cells due to its similarity in composition and membrane dynamics rather than a sturdy carrier for chemical compounds.

2.1.2. Polymersomes

Comparing the structure of polymersome membranes shows that there is a broad variety of different polymer species used in research due to the convenient tunability of the modular components. The main characteristics to form membranes stays the same as mentioned in chapter 2.1, but polymersome yield a broader variety compared to liposome membranes. The structure of polymers and their resulting membranes allow more freedom in their design compared to liposomes. [50]

- **Diblock/Triblock Copolymers:** Polymers composed of two or three distinct modular blocks of repetitive identical subunits are called diblock or triblock copolymers repectively. In context of the formation of polymersomes only block copolymers with amphiphilic properties are discussed. The structure of the resulting membranes can differ between a bilayer and a monolayer depending on which copolymers are used, as triblock copolymers are able to either span the whole diameter of the membrane (**I**-form) or loop in the hydrophobic core and stay in one leaflet (**U** form). [51] Typical components with different chemico-physical properties used in the synthesis of polymersomes are polystyrene (PS), Polybutadiene (PB), polydimethylsiloxane (PDMS) as hydrophobic and polyethylene oxide (PEO), polyacrylic acid (PAA), polyethylene glycol (PEG) as hydrophilic blocks. [52]
- **Graft Copolymers:** Graft copolymers are also composed of distinct polymer units like block copolymers, but instead of being linked linearly, a central polymer functions as the backbone for the molecules and side chains are attached

to the central backbone giving it a brush-like appearance. Resulting from this difference in structure of the polymers themselves, membranes also differ from the mono- or bilayer structure we looked at so far. Instead of an hydrophobic core and hydrophilic outside of the membrane, here we have a far thicker membrane with a mesh-like structure containing hydrophobic and hydrophilic domains within.

- **Alternating Copolymers:** Like block copolymers, alternating copolymers are formed of linear linked polymer species presenting different properties. However, these polymers are made up of a high number of small block repeats instead of two or three major blocks as seen in block copolymers. Due to their different structure and their assembly, alternating copolymers can form smaller vesicles compared to block copolymers. [53] [54]

Besides the structure of the individual polymer, the choice of monomers is essential for the properties of the membrane. Looking at the different structures as well as different composition of polymers it shows that there is a vast amount of different components available for the design of polymersome membranes. While liposome membrane diameters range 3-5 nm, polymersome membranes can span 5-50 nm as depicted in Fig.2.1.3. [19] [55] This parameter is mostly defined by the molecular weight (MW) of the hydrophobic block. [56] [57] [58] The correlation between membrane thickness and MW of the polymer scales according to following power law. [59]

$$d_{mem} = \phi \cdot (MW_{phob})^{\zeta} \tag{2.5}$$

Here we can predict the increasing membrane thickness with ϕ being a constant and ζ being a polymer-specific variable. In case of ideal random coil forming polymers with MW $\geq$ 3kDa, ζ $\approx$ 1/2. [59] This variable changes depending on the conformation of the polymer and its size, as fully streched polymer chains predict ζ= 1 and smaller polymers as well as phospholipids are subject to the strong segregation limit with ζ = 2/3. In the theory of strong segregation, the tension between hydrophobic and hydrophilic blocks is minimized by the minimization of their interface area resulting in distinct distribution of the polymer chains. [60]

Also size and morphology of the polymersome heavily depend on the type and size of polymers used in the formation of the membrane. [61] [62] Looking at the influence the choice of polymer can have on the properties of the membrane one has to also look at the dynamics within the membrane. The observations made

by Itel et. al. show the influence of the size and the conformation of membrane components on their motility within the membrane. [56]

As longer polymer chains can form coil structures in contrast to the linear structure of acyl chains connected to phospholipids, the possibility of entanglement between molecules rises. This leads to the formations of specific domains within the membrane, where the prescence of coiled structures is influenced by material specific temperatures, so called transition glass temperatures (T_g). This temperature is described as transition point between a solid-like pseudocrystalline state and a highly viscous state of thermoplastic polymers. [63]

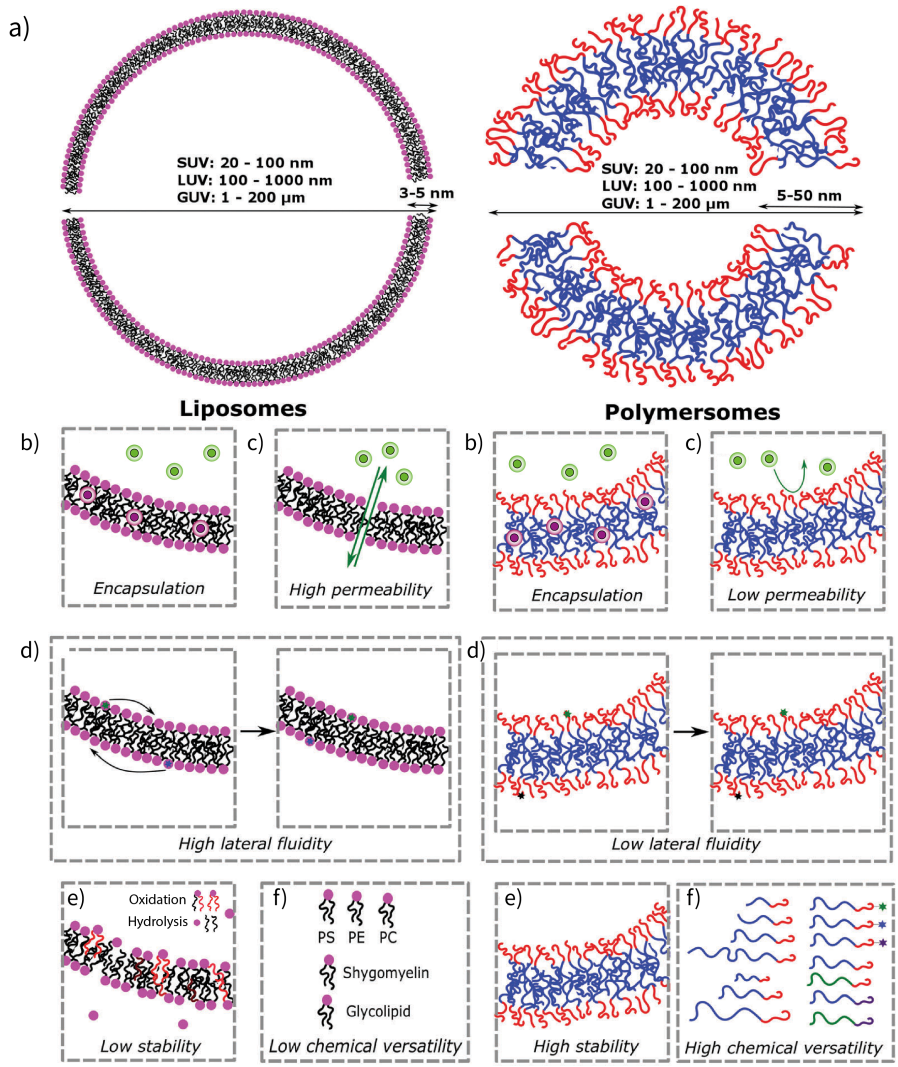

Figure 2.1.3: Overview Liposome Polymersome: *Comparison between the physical and morphological properties of polymersomes and liposomes. a) Comparison between dimensions of liposomes (left) and polymersomes (right). Comparison of specific attributes between liposomes and polymersomes in respect to b) encapsulation of hydrophilic (green) and hydrophobic (purple) cargo, c) permeability, d) lateral diffusion, e) monomer stability and f) monomer variety. Adapted from Rideau et. al. [19] with permission from the Royal Society of Chemistry.*

Another aspect of the increased intermolecular forces introduced by bigger polymers are the increased stability and rigidity of polymersome membranes compared to liposomes. [64] [65] As not only the volume occupied by the molecules alone is larger compared to liposomes also the interdigitization of individual molecules contribute to the denser build-up of the membrane and increasing the bending rigidity. [66] [59]

The condensed hydrophobic core of the membrane reduces permeability of hydrophilic compounds encapsulated. [67] Combining this characteristic with the capability to store hydrophobic molecules in the membrane, researchers were able to build dual-cargo carrier compartments. [68] [69] Using these specifically designed transporter vesicles can increase the efficiency of drug delievery by far. As most polymers used for the formation of GUVs show higher stability against degradation, they are promising candidates for chemical modification. These modifications create "smart materials" able to react to specific conditions in their immediate surroundings. [70] [71] [72] [30]

Another interesting field of research is the application of polymersomes as nano reactors facilitating enzymatic processes within or on their surface. [73] [60] Enabling to encapsulate complex systems in more robust GUVs compared to liposmes contibutes to the approaches in bottom-up synthetic cell-like systems. Not only can the enzymatic components be positioned on the surface of the membrane or the lumen, but can also be integrated into the membrane and enhance the functionality of membrane and polymersome itself. [67] [74]

In contrast to liposomes, polymersomes show a broader variety of individual monomers due to their high tunability and modular structure. Showing increased rigidity, stability and tightness comes at the price of lowered membrane dynamics and limited biocompatibility as depicted in Fig.2.1.3. These properties make polymersomes far more interesting in applications revolving around cargo transport and triggered release as well as platform for nanoreactors in need of resisting high stresses and sturdy inert membranes.

Elastin-like Polypeptides

Whereas polymers span a broad variety of different materials most of them are of synthetic origin. Peptides however can be described as polymer structures as their serial and modular structure composed of amino acids can also possess amphiphilic properties. Elastin-like polypeptides (ELP) are a specific group of peptides and were predominantly used in this thesis for the formation of GUV structure.

The basic repeating unit of ELPs is the pentameric amino acid sequence (Val-Pro-Gly-X-Gly), where the guest residue X can be any other proteinogenic amino

acid besides proline. This biogenic polymer derived from the structural protein elastin found in the extracellular matrix of higly flexible tissues like lung tissue or the vascular system. ELPs possess a peculiar lower critical solution temperature (LCST) behavior, being able to perform reversible aggregation surpassing a specific temperature. [75] This inverse transition temperature T_t can be modified by several intrinsic factors like concentration, polypeptide length [76] and composition of the pentapeptide. [77] [78] Also external parameters like salt, [79] pH [80] [81] and additional proteins [82] in the surrounding medium influence the transition temperature. The influence of salts on the transition temperature have to be distinguished between kosmotropic and chaotropic activity. [83] Kosmotropic anions show a rather linear correlation between salt concentration and increase in transition temperature as shown in equation 2.6.

$$T_t = T_0 + c[M] \tag{2.6}$$

Where the change of the transition temperature T_t is determined using the salt concentration with a molarity of M and the initial transition temperature T_0. In contrast to that, chaotropic salts show increased solubility at low concentrations before lowering the LCST values at higher concentrations. The change in T_t can be described as follows:

$$T_t = T_0 + c[M] + \frac{B_{max} K_A[M]}{1 + K_A[M]} \tag{2.7}$$

The additional term represents the Langmuir binding isotherm, with K_A as equilibrium association constant for anions and B_{max} to introduce temperature units as the isotherm is unitless.

The overall molecular process orchestrating this transition between solved monomeric polypeptides and accumulated aggregates is only partly understood and was first described by Urry et. al. [75] His hypothesis postulates a multi-step process for the formation of an ordered helical secondary structure from a random coil as soon as T_t is exceeded. According to this hypothesis the reconfiguration of the peptide chain promotes the expulsion of hydrating water molcules and a β-spiral structure can be formed. This structure composed of several β-turns exhibits higher intermolecular forces and promotes the interaction between individual ELP chains. [84] [85]

Due to newer data achieved by NMR measurements, this hypothesis has to be revised. [86] [87] Current findings do not emphasize the necessity of specific sec-

ondary structures or a hydrophobic core to promote the formation of hydrophobic intermolecular interactions. [88] This would be supported by the high contents of water still residing in the core of ELP aggregates. [89] [78] Furthermore, synergistic effects from entropically driven early stage oligomer formation can amplify the formation process, showing an increased concentration dependency of the aggregation process. [90]

Their tunability, modular nature and stimulus responsiveness make ELPs an attractive material for a wide range of different applications like drug delivery [91], [31] tissue engineering [92] or protein engineering. [93] [94] In context of this thesis, the ELP's ability to form compartments was of interest as its basic structure resembles polymers and should in theory reflect its ability to form complex membrane structures. [95] Due to its aforementioned tunability as well as its capability to interact with lipid bilayers the potential functionalities embedded within the membranes can be designed. [96] [97] Compartments solely made of ELPs were produced in different forms ranging from artificial *in vivo* compartments, [98] *in vitro* SUVs [99] [100] to GUVs encapsulating complex enzymatic reactions. [101] [102]

2.1.3. Hybrid Membranes

As both liposomes and polymersomes have their individual advantages, researchers are looking for a way to harness the full capabilities of the materials used. A topic gaining popularity is the production of giant hybrid unilamellar vesicles (GHUV) which enable the creation of 'smart' drug delivery compartments, nanoreactors and synthetic cell-like models. [20] [55] [103] The combination of materials showing completely different chemical structures can influence functionalities of the resulting vesicles like permeability [104], [105] integration of membrane proteins [106] and stability. [107] [108]

Different parameters are influencing the properties of the membrane and are a vital point in the experimental design involving GHUVs. One of these factors is the choice of different polymers and lipids in the first place. Due to the different structure of polymers and lipids the degree of interaction has to be estimated by comparison of different compatibility parameters. [109] Furthermore, different molecular mechanisms such as lyotropic phase behavior and microphase segregation are influencing the order within the membrane. Additionally also the difference in MW plays an important role as lipids (≤ 1 kDa) and polymers (≥ 1 kDa) can differ significantly in size. [19] The hydrophobic mismatch caused by the discrepancy in size of the hydrophobic domains can substantially influence the morphology of the membrane. Revealing hydrophobic moieties of the copolymer increases the line tension

between the lipid and polymer monomers within the membrane. Minimizing the hydrophobic surface area, the polymers can either (i) deform their hydrophobic block in exchange for a higher internal entropy or, more prevalently observed, (ii) they form bigger clusters of polymers to minimize the phase boundary between lipids and polymers. [20]

Taking this into consideration for the planning of experiments involving GHUV, one can achieve interesting membrane characteristics. This includes complex behavior in case of interaction with surrounding ligands or the spontaneous deformation of the membrane which are explained in more detail in the following chapters.

2.2. Membrane Effects

2.2.1. Phase Separation

As biomembranes possess complex properties to cope with a multitude of external stimuli and interactions, homogeneous mixtures of membrane components would be insufficient. Consisting of different types of lipids and membrane proteins embedded within biological membranes, they are able to form a flexible and dynamic cell surface. [110] This dynamic behavior is crucial for the proper functionality of processes like endocytosis, [111] cell division [112] and formation of protein complexes within the membrane [113] to name only a few. By using multi-component mixtures of membrane monomers, researchers try to imitate these intricate processes in experiments.

A central aspect of the membrane mobility is the presence of different phases, meaning different microdomains within the membrane. Influencing the lateral diffusion of individual molecules, [114] permeability [115] and insertion of membrane proteins, [106] phase separation is an important regulator for the dynamics within membranes. Depicted in Fig.2.2.1 b, the separation of distinct phases can be seen using fluorescently labeled lipids. The labeled lipids remain predominantly in their specific phases and can therefore signalize their position on the vesicle membrane. Considering the ambient temperature and the composition of the lipid mixture, these solutions can exist in a liquid-crystalline (L_α) or solid-like gel phase (L_β). Following, we take a look at the relevant phases in respect to the fluid-like dynamics of the membrane we want to observe. [116] [117]

- **Liquid-disordered phases (L_d):** The liquid-disordered phase is predominantly composed of unsaturated lipids with acyl chains showing one or multiple kinks in their molecular structure (Fig.2.1.2). The enlarged surface of the hydrophobic tail undergoing constant conformational changes prevents tighter packing of the molecules, which reduces the attractive forces between molecules. This behavior is schematically depicted in Fig.2.2.1 a. Due to the reduced interaction the L_d phase is more dynamic compared to the L_o phase.
- **Liquid-ordered phases (L_o):** This phase is composed of mostly saturated lipids, which means the hydrophobic domain is constituted of linear acyl chains. This promotes a tighter packing of the individual molecules due to the increased strength of the intermolecular Van der Waals forces between the acyl chains (Fig.2.2.1 a). The strength of these intermolecular forces dictate the specific melting temperature T_m of the lipids, at which the transition between liquid (L_α) and solid-like gel phase (L_β) takes place. The addition of sterol molecules into

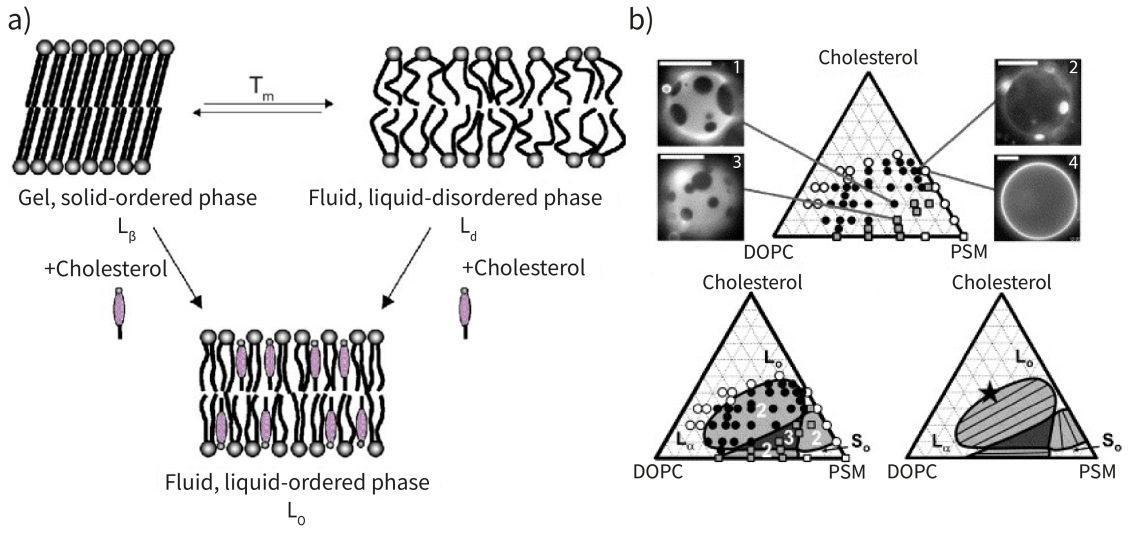

Figure 2.2.1: Phase Separation: *Overview of different lipid phase behavior inside of the membrane depending on their structure. a) Schematic phase behavior of lipids in the presence of cholesterol and without it. Gel, liquid-disordered and liquid-ordered phase and the dependence of of cholesterol ond specific $T_m$shown to visualize phase transition behavior. b) Showing the phase behavior of ternary lipid mixtures composed of DOPC, palmitoylsphingomyelin (PSM) and cholesterol corresponding to the respective ratios. Fluorescence micrographs are used as indicator for phase separation (upper). Individual spots on the phase diagram signify the presence of one phase (white circles), two phases (black circles) and three phases (grey squares) (lower left). The speculative tie lines partitioning the phase diagram into regions of different regions of phase coexistence (lower right). The depicted star illustrates the miscibility critical point. Adapted from Eeman et. al. [118] and Veatch et. al. [116]*

these mixtures is essential to keep the fluid-like status of the lipids by addition of 'spacer'-like molecules reducing the T_m by blocking the formation of intermolecular forces. [119] [120] The influence of cholesterol on the conformation within the membrane can be seen depicted in Fig.2.2.1 a.

- **Gel-phase (L_β):** Portions of the membrane containing high T_m lipids forming solid-like aggregations are called gel phase. This increase in T_ms is caused by (i) linear saturated acyl chains enabling the formation of stronger interactions between the individual lipids or (ii) weaker repulsive forces between headgroups. [114] Resulting from the changing ratio between attractive and repuslive forces a tighter packing of the molecules within the membrane is enabled and different phase behaviors can be observed (Fig.2.2.1 a). In contrast to the L_o phase, the gel-phase does not possess fluid-like behavior and can undergo diffusion only in form of membrane patches where individual high T_m lipids stay bound as aggregates. This can be seen in Fig.2.2.1 b showing clear separation between flu-

orescently labeled and non-labeled lipids.

These individual phases can be modulated by their respective compositions and the changing properties certain molecules implement in the membrane as mentioned in chapter 2.1.1.

The composition of complex biological membranes is not only limited to phospholipids, steroids and fatty acids. As already explained in chapter 2.1.1, also membrane proteins are essential components for the functionality of membranes. Anchoring of the proteins within the membrane of model liposomes is achieved by composition of raft-like assemblies within the membrane. [113]

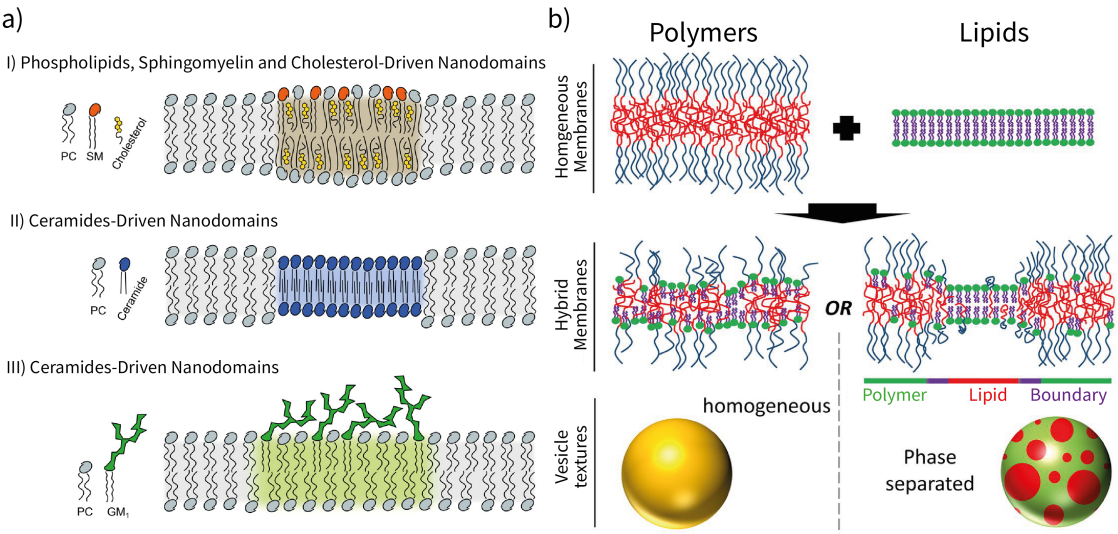

Figure 2.2.2: Phase Separation in hybrid membranes: *A schematic overview over phase separation formed within mixtures of different lipds (a) or mixtures of polymers and lipids (b). a) Drawings of lipid mixture phase separating in distinct manner due to structural characteristics of lipids. Domain formation is promoted by different forces exhibited by prescence of cholesterol and high $T_m$lipids (I), interdigitation of acyl chains (II) and modified hydrophilic headgroups (III). b) Schematic comparison between polymer and lipid hybrid membranes demonstrating different phase behavior. The molecular structure within homogeneous polymer and lipid membranes is depicted (upper). The phase behavior depends on the bending rigidity of the polymer to either favor the formation a mixed phase of polymers interspersed with single lipid molecules (left) or the formation of distinct microdomains (right). Adapted from Beales et. al. [74] and Cebecauer et. al. [44] Copyright (2018) American Chemical Society.*

So far only the interaction between different kinds of lipid molecules were discussed but as it was already mentioned in chapter 2.1.3 hybrid membranes composed of polypeptide block polymers and phospholipids were used for this thesis. Looking at the different properties between lipids and polypeptides like length and structure, the ratio and the size of their hydrophobic mismatch are influencing the

morphology of the membrane and the molecule distribution within. [121] [55] Using high T_m lipids can promote the formation of distinct domains due to lateral interactions where the lipids aggregate under their specific T_m and phase separation is promoted which can be seen in Fig.2.2.2 a. [122] [123] An increased bending rigidity of the individual copolymers can impair the potential to form domains within the membrane due to the lack of the deformation of the hydrophobic block at the phase boundaries between lipids and copolymers which can be seen in Fig.2.2.2 b. [20] [124]

As long as these parameters are not within a specific range, no domain formation is visible and only a homogeneous phase with interstitial lipids can form as seen in the case of the hybrid mixture seen in Fig.2.2.2 b on the left side. Otherwise distinct microdomains can be formed due to the deformation of polymers neigboring lipid-rich sections of the membrane as seen in Fig.2.2.2 b on the right side. With growing domains and the interplay between (i) hydrophobic mismatch, (ii) line tension, (iii) bending rigidity and (iv) polymer/lipid ratio the membrane surface deforms to the point of budding and even fission. [123] [125] [103] The molecular dynamics of the individual monomers within the membrane with increasing stress exerted can be characterized from a thermodynamic point of view. Therefore, one has to look at the domain energy E_1 built-up within the aggregated phase of lipids seen in Eq. 2.8:

$$E_1 = 2\pi L_d \lambda + 2A_d \kappa_d m_d \tag{2.8}$$

The domain of an amphiphilic molecule within a hybrid membrane with a radius L_d and a surface area A_d has a specific spontaneous curvature m_d, a bending rigidity κ_d and a line tension λ. This line tensions depends on the hydrophobic mismatch between polymer and lipid monomers in the membrane. The energy E_2 of a bud formed of the same membrane in Eq 2.9

$$E_2 = 8\pi\kappa_d(1 - \frac{1}{2}L_d|m_d|) \tag{2.9}$$

shows that the formation of a bud as soon as the radius L_d exceeds as certain threshold and $E_2 > E_1$. [126]

As mixed membranes composed of polymers and lipids have a broader range of attributes compared to the homogeneous membranes, they possess the potential for a whole set of new applications. By combining the stability provided by polymersomes and the biocompatibility of lipid membranes, new versions of drug delivery

can be created. [28] [29] Additionally, the targeted design of membrane domains with specific physico-chemical properties allows the construction of specialized reaction compartments [104]

2.2.2. Membrane Interactions

The multifaceted tasks the cell membrane is responsible for, can not be maintained by complex mixtures of lipids and steroids alone. Essential components for the reactivity and the capabilities are coordinated by proteins. Be it proteins embedded within or peripheral proteins interacting with the membrane. The interaction between proteins can influence different properties like membrane tension or its dynamics. This interaction can take place in different manners considering the intercating components and the duration of their interaction. Upcoming is a list of potential targets for protein-membrane interactions. [127]

1. **Hydrophilic Headgroups:** These kinds of interactions can either take place due to the charged state of the headgroups or their specific chemical structure. Additionally, the presence of divalent cations (Ca^{2+}, Mg^{2+}) can alter the strength of interaction. [128] [129]

2. **Hydrophobic Tails:** In contrast to the headgroups a lipid's hydrophobic domain is embedded within the membrane and is much harder to access from the surrounding medium. To circumvent this problem, proteins use small hydrophobic moieties like α-helices, [130] hydrophobic loops [131] or conjugated lipids to integrate an anchor within the membrane.

3. **Lipidation:** The process of covalently binding amino acid side chains of proteins to lipids is called lipidation. [132] In nature this process is catalyzed enzymatically to enable the cells to communicate. [133] [134]

4. **Protein-Protein Interaction:** So far only interaction between proteins and lipids were mentioned, but as membrane proteins embedded within the membrane play an important role for the functionality of biological membranes, they pose an important target for interactions. Ranging from receptors essential for signal transduction [135] to Protein secretion and translocation, [136] there are different mechanisms in which the protein complexes can interact with each other.

5. **Protein-Ligand Interaction:** Next to membrane proteins other non-lipid molecules can bind to peripheral proteins in a specific way. These interactions can be facilitated by introduction of specific complexes like Ni-NTA to the membrane components. [137] As this is a rather synthetic approach, more biological

relevant targets for these proteins are modifications of the membrane structure. For this thesis, Biotinylation of membrane components was of special interest. As the interaction between Streptavidin and Biotin shows one of the strongest non-covalent bonds in nature, the potential of stable protein-membrane interaction was the highest using this approch. [138]

Considering the number of components within the cell, these diverse interactions show sheer amount of mechanisms necessary to structure membrane organization and functions. Proteins can change properties like tension, viscosity, elasticity and the bending rigidity of biological membranes to control cell functions. By influencing all of those individual characteristics the overall shape of the cell can be controlled. In Fig.2.2.3 two different ways of how protein-membrane interaction can alter the form of the cell.

Polymerization-driven Deformation: The localized polymerization on the membrane surface creates forces able to overcome the bending rigidity of the membrane by continous elongation of filaments. This creates protrusions of the membrane as long as the forming filaments are bound to components achored in the membrane as seen in Fig.2.2.3 a. An example for this mechanism is the formation of filopodia, which are formed by coordinated creation of parallelized filaments from a complex branched actin network. [139] The mechanism itself is founded on the interplay of different proteins and their localized concentration, which shows the dynamic nature of mechanisms controlling the shape of cells. [22] [140] [141]

Crowding-driven Deformation: Like with the aforementioned mechanism, the driving force for the crowding-driven deformation is the localized high concentration of proteins. But instead of polar polymerization of proteins to create forces to overcome the bending rigidity of the membrane, here the interaction of each individual protein with the membrane is important. As depicted in Fig.2.2.3 b deformation can be promoted by scaffolding and intrinsically bent proteins [142], [143] insertion of amphiphilic helices into the membrane [144] [145] and the crowding of unspecific proteins on the surface. [144] [32] Due to the size of the proteins they are not able to freely diffuse in the membrane without colliding. Due to these collisions and the constraints in their movement forces are created that enable the membrane to bend out of the previous curvature.

Taking the results of literature into consideration shows that there are numerous ways the interaction of proteins can influence biological membranes. As even

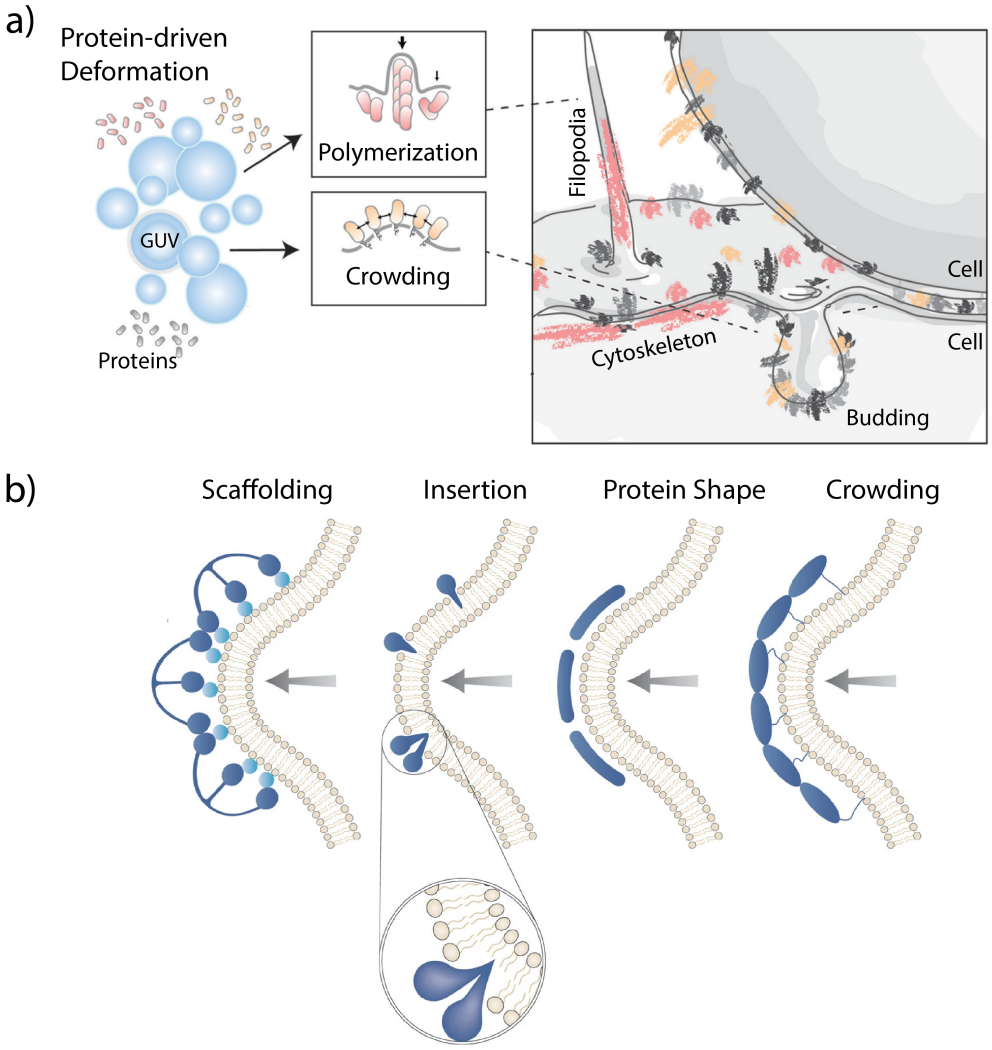

Figure 2.2.3: Schematic Overview of Protein-driven Deformation: *A schematic overview of different mechanisms of protein induced membrane deformation. a) Schematic overview of the different modes of action of polymerization- and crowding driven membrane deformation in a simplified cell environment. Cell functionalities like budding events and formation of filopodia are regulated by protein-driven deformation in different ways. b) Different modes of crowding-driven deformation of membranes due specific protein structures. Scaffolding: Interaction of protein scaffolds interacting with the membrane or adaptor proteins exterting forces onto the membrane. Insertion: Deformation driven by assymetric insertion of hydrophobic moieties into the outer leaflet introduce curvature. Protein Shape: Membrane curvature introduced by the presence of intrinsically curved proteins interacting with the membrane. Crowding: High local concentration of unspecifically binding proteins can induce membrane deformation due to restrictions in the motility of the associated membrane components. Adapted from Dimova et. al.* [126] *and Kirchhausen et. al.* [146]

unspecific protein aggregation can alter the curvature of membranes, [32] the implememtation of a positive feedback mechanisms. These mechanisms promoting localized protein aggregation can be used to trigger membrane deformation. Po-

tential tools to facilitate this mechanisms are explained in the following chapter.

2.2.3. Proximity Labeling

Looking for potential techniques that provide the ability to localize proteins onto membranes, proximity labeling was chosen. This tool is used in proteomics to identify interaction partners. The targets are labeled *in vivo* and can range from proteins to nucleic acids. [147] For this application fusion proteins of a target protein and a specific labeling enzyme are expressed *in vivo*. In the prescence of specific substrates like biotin [148] or biotin tyramide [149] molecules interacting with the target protein can be labeled and identified. The enzymes produce reactive substrate molecules which label the side chains of Lys, His, Cys, Trp, Tyr as well as with other amine containing molecules like the N-terminus of peptides. These molecules can freely diffuse and provide reliable labeling in a radius of 1-10 nm, but lose efficiency with increasing distance due to degradation of the reactive species of the substrate. [150] Furthermore, the activated substrates are membrane impermeable which allows specific labeling of individual leaflets. [151] In modern research two groups of labeling enzymes are predominantly used.

Biotin Ligase: In this approach a mutated, more promiscuous version of BirA, a biotin ligase involved in the biosynthesis of fatty acids, catalyzes bound biotin to biotinoyl-adenylate (bio-AMP) under consumption of ATP. The mutated version has a lower affinity towards the product and releases it before it can be bound to its target. [152] This way reactive species of bio-AMP can diffuse freely and react with the primary amines of lysine side chains. Research and optimization of efficiency and reactivity of the mutated version of BirA resulted in a wide variety of different enzymes used for proximity-dependent biotin identification (BioID) like BioID 1/2 [152], [148] TurboID and miniTurbo [153] [154]

Peroxidase: Peroxidases unlike aforementioned biotin ligases do not specifically bind biotin, but are able to catalyze a broader variety of substrates under usage of H_2O_2 as oxidant. Instead substrates, like biotinyl-tyramide where reactive groups are linked to biotin can be utilized to label interacting proteins. In this case the peroxidase catalyzes the reaction of phenol to produce a radical able to interact with the residues of specific amino acids as well as the N-terminal amine group of the protein. The two scientifically relevant enzymes are horseradish peroxidase (HRP) and ascorbate peroxidase (APEX), which have undergone optimization to improve their efficiency *in vivo* and functionality. [155] The potential for detection of even more interaction partners of these two enzymes could be achieved after producing split enzymes with restored activity after reconsitution. [156] [157]

Comparing the different possible mechanisms utilized for proximity labeling, we chose the split version of APEX2 (sAPEX2) for further experimentation, as it showed a high efficiency of its split construct as well as far higher reaction speed. [156]

The aim for this system was to precisely control the activity of sAPEX2 on the membrane surface and therefore also to control the localized accumulation of proteins on the surface to promote membrane bending. An essential component for this control was the localization and reconstitution of the split enzyme. Fortunately, Han et. al. already screened for the potential of specific secondary structures introduced into non-coding RNA to interact with specific peptide domains. [156] As this problem was solved, there still remained the issue of localization on the surface of the membrane. For this a modular RNA aptamer construct composed of three orthogonal binding domains was used. [158] This enabled us to control the activity of sAPEX2 as well as its localization with the addition of only one molecule.

2.3. *In Vitro* Transcription

With the development of *in vitro* transcription (IVT) processes researchers were able to get a deeper understanding of the physical properties of RNA molecules and thereby to design specific interaction networks. [159] While the cellular transcription apparatus is a highly complicated system between several interacting agents, the implementation of this process in a simpler environment was accomplished by using transcription machinery of bacteriophages. IVT systems often use the much simpler RNA polymerase systems of bacteriophages, such as T3, T7 and SP6 phages. [160]

Especially the T7 transcription system is well established and shows high compatibility with a broad range of applications. [161],[160] Possessing a single subunit RNA polymerase and high specificity for its DNA binding region, makes the T7 phage transcription system an interesting target for further optimization. [162] For example, this binding specificity can even be used for the creation of T7 RNA polymerases using orthogonal binding regions. [163]

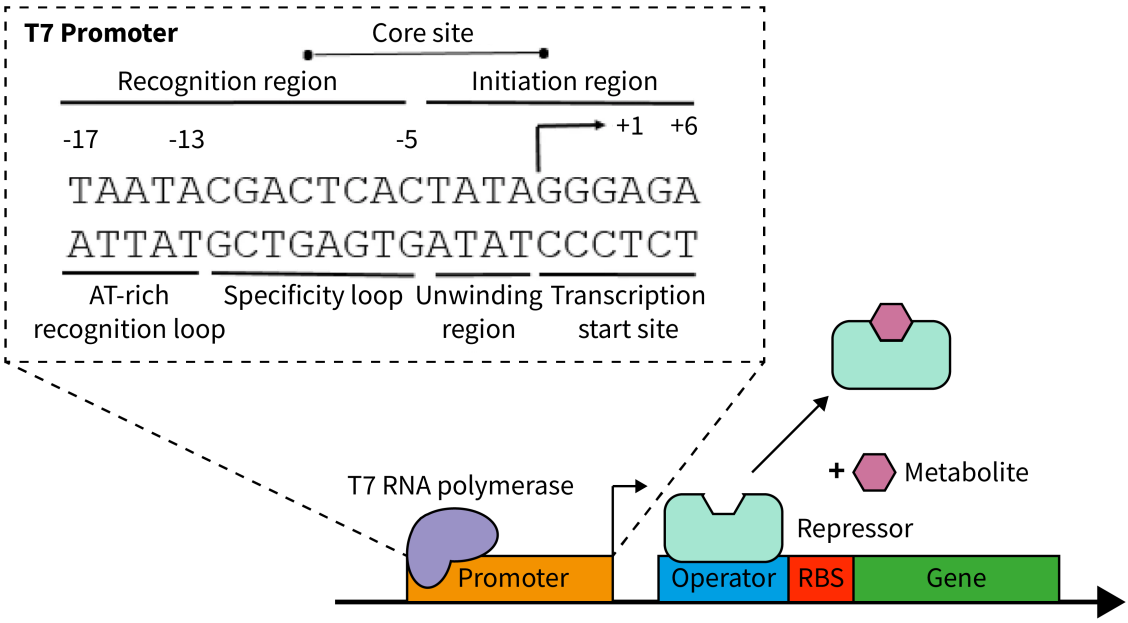

Figure 2.3.1: Gene Regulation: *Schematic overview of gene regulation components necessary under the control of the T7 RNAP promoter (upper left). Specific binding and regulatory sites of the T7 promoter in respect to their position from the transcription start. A simplified regulation scheme containing repressors regulated by metabolites within the system depicted on the lower right. Partly adapted from Padmanabhan et. al.* [164]

The transcription activity is regulated by the T7 promoter on the 5'-end of the DNA template as well as by regulatory sequences flanking the binding site. Specific operator sequences introduced into the DNA templates can serve as tools to control

the overall binding and activity rate of the RNA polymerase as indicated in Fig.2.3.1. Transcription factor dependent regulation mechanisms such as the lac operon use specific recognition sequences up- and downstream of the RNA polymerase binding sequence as recognition sites for protein activators or repressors. [165],[166],[167] As gene regulatory mechanisms like the lac operon are optimized for the RNA polymerase of their respective original organism, they are not completely compatible with the T7 transcription machinery. It is possible to regulate the *in vivo* the expression of proteins under the control of T7 mediated transcription with specific metabolites. [168] The repression of the transcription however, is not completely given as the T7 RNA polymerase is able to displace the DNA binding repressor. [169] This way a low non-repressable transcription rate, also called leakage, is observed which could influence the experimental results. [170]

The composition of the T7 promoter itself is able to modify the transcription rate more precisely. The different regions within depicted in Fig.2.3.1 show a separation in a recognition region, responsible for the T7 RNAP binding and a initiation region which controls the start of the transcription reaction. [164] These regions contain domains which regulate their functionality in different ways such as both loop domains bind different sites within the T7 RNAP. The AT-rich unwinding region presumably plays an important role in the melting of the template DNA and therefore make the first template nucleotide (+1) of the transcription start site accessible. This first nucleotide is conserved in all bacteriophage promters and always presents a guanine.

The termination of the transcription process in contrast is rather simple and involves mainly two different mechanisms in an *in vitro* context. While linear gene constructs like PCR products or hybridized DNA oligonucleotides stop the transcription by "Run-off", where the enzyme basically migrates over the end of the DNA template, circular templates depend on sequence specific termination. This can either be controlled by the insertion of an hairpin structure followed by a poly-U sequence or the presence of a specific termination sequence. [171]

The production of RNA is involved in a range of different applications like interaction studies of RNA binding proteins [172] [173] , genetic circuits [174] , or discovering the transcriptome of the cell. [175] Most of these fields rely on the ability to hybridize with nucleic acids or to bind to proteins based on the RNA's secondary structure. So-called riboswitches combine the secondary structure of the RNA with a regulatory function. [176] These sequences regulate the binding properties of messenger RNA (mRNA) *in vivo* with their secondary structure and fine tune translation of produced RNA. The fast responsiveness of these structures is due to their ability to

bind small molecules like metabolites and undergo conformational change upon interaction. Their structure can be separated into two parts, the aptamer domain that facilitates the interaction and the expression platform that reacts to conformational change and enables ribosome binding. [177]

This specific ligand binding activity of the aptamer domain represents an interesting field for futher research as data suggested that interaction was not only facilitated with small molecules but also proteins and specific cell types. [178] Furthermore, interaction between aptamer domains and specific phage proteins could be observed. [179] [180] Using systematic evolution of ligands by exponential enrichment (SELEX) combines the phenotypical structure of the interacting nucleotides with their genotype of the aptamer domains. [181]

For the process to discover new interaction based RNA structures, SELEX uses randomized DNA libraries to screen for new secondary structures. In this process random DNA sequences are transcribed and evaluated for their binding affinity in several cycles in high-throughput approach. The increasing number of aptamers developed this way is predominantly used as biosensors in different fields due to their high specificity, small size and designability. [178] These sensors can create a fluorescent signal upon interaction with a specific ligand [182] or even create a response from the cells they are expressed in. [183] Even the combination between different domains to create multifunctional RNA species facilitating protein interactions and creating a fluorescent signal is possible due to their modular nature. [158]

Overall the process of IVT enables scientists to design RNA-based interaction networks, produce highly specific aptamers and take a closer look at the overall transcription regulation of cells within a simplified environment. Furthermore, the implementation of these reactions within the context of artficial cells can prompt hints on how to approach this topic in a bottom-up approach. This, however, can only explain a fraction of the problems connected to the creation of artificial cell structures and has to be observed in a more complex system involving the proteome of bacterial cells.

2.4. Cell-Free Gene Expression

On the way to create synthetic autonomous compartments the encapsulation of an active transcription system is the first step to implement the functionalities of an artificial cell in a designable manner. Nevertheless, RNA molecules alone are not able to control complex mechanisms observed in biological cells. As one of the goals of this thesis was the implementation of responsive mechanisms of artificial compartments mimicking cell-like behavior, we also needed to test a more complex system.

To enable this, a system is required that is able to harness the whole repertoire of a biological cell. The first steps were made in the 1970's where it was possible to extract the essential components from *E. coli* and to produce proteins without intact bacterial cells. [184] Starting from crude cell lysates supplemented with buffers, the production of *in vitro* gene expression solutions has become much more detailed and dedicated to optimize the performence of the protein expression. Over the years these cell free gene expression (CFE) systems have achieved high standards concerning the reproducability and protein yield. [185] Besides clearing the cell lysate from genomic DNA and membrane fragments, buffers solutions supplement essential components needed for the protein synthesis such as rNTPs, amino acids, t-RNA and an ATP regeneration system to elongate the functionality of the system. [186]

The decoupling between protein expression and biological cells opens the door for completely new possibilities regarding the testing of protein functionalities, design of complex genetic circuits and creation of protocells. [188] Designability of the reactions by omitting or adding molecules of interest or potential interaction partners in the gene expression reactions enables experimentation without the constraints of bacterial cells. Production of complex protein structures, [189] insertion of high amounts of foreign DNA [190] or the construction of molecular machines [191] can be performed *in vitro*.

This approach is not only restricted to *E. coli* cells but can already be reproduced with a variety of prokaryotic and eukaryotic cells. [187] This collection of different organisms brings different characteristics to specific fields of application as schemtically depicted in Fig. 2.4.1a. A special interest throughout this thesis lay on the potential to encapsulate CFE solutions within artificial GUVs to form artificial cells or organelles. [192] [193] The ability to design a specific environment with adjustable parameters like membrane composition, DNA templates and non-native ligands present within a compartment provides a wide variety of new experimental designs. Limitations like bacterial metabolism and physical constraints of

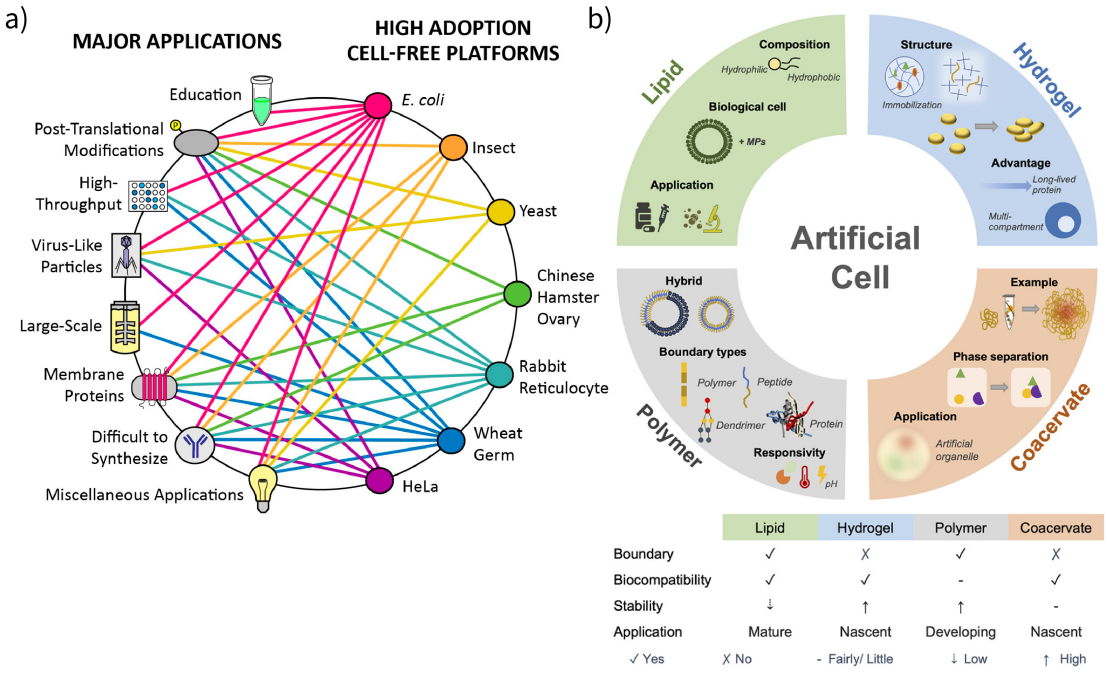

Figure 2.4.1: Overview CFE: *An overview over the variety of CFE derived technologies and applications. a) A web of applications shows the fields of research currently conducted using cell-free gene expression. Additionally, the variety of available CFE systems originating from different organisms are shown and their specific field of application is depicted by connection over a colored line. Proteins declarated as difficult to synthesize include antibodies, large proetins, ice structuring proteins and metalloproteins. Miscellaneous applications sum up fields of research like genetic circuits an metabolic engineering. b)A small overview over the different components building a reaction compartement and their potential application is given. The basic characteristics of each of the mentioned groups is given in respect to presence of a boundary structre, biocompatibility, stability and their current state of application. Adapted from Gregorio et. al. [187] and Cho et. al. [23] Copyright (2020) American Chemical Society.*

the cell wall can be overcome by the construction of artificial cells in a bottom-up approach using CFE. [23] [188] Complex mechanisms like cell division [194],[195], [195] adaptive production of membrane components [196] [99] as well as sustaining energy consumption [197] are only a few of the new fields of research.

Due to the different applications of these synthetic reaction compartments there is also a need for different membranes supporting the functionality of the encapsulated gene expressions system (Fig. 2.4.1 b). Initially, liposomes were the compartment of choice due to its similar characteristics to biological cells, this decision was only sensical. However the rapid evolution in the field of polymer membranes as well as the creation of membrane-less compartments as hydrogels and coacervates brought along new ways of functionality for *in vitro* gene expression. [23] Introducing the ability of localized compartmentalization of enzymes and other

components within an membrane-less matrix makes hydrogel systems using CFE an interesting field for organelle-like systems. The same can be said for coacervates which are able to entrap enzymes in specified confined volumes. Being able to form sub cellular organization units can provide an advantage in comparison to liquid-filled vesicular structures. Due to the insufficiency in matters of permeability of the hydrogel or coacervate compartments, it is however advisable to optimize their individual performance in combination with membrane based reaction compartments. [198] [199]

3. Materials and Methods

In the following chapter the methods and materials used in this thesis are described more precisely. All buffer compositions used are noted in chapter A.2.

3.1. Protein Components

3.1.1. Cloning

Cloning of the used proteins was performed either by Golden Gate Cloning or Gibson Assembly. The sequences of the used constructs can be seen in chapter A.3. All synthetically produced gene fragments were designed using Benchling and the Codon Usage Database provided by the Kazusa DNA Research Institute, JP. All plasmids were either transformed in NEB stable cells for DNA storage or in *Rosetta (DE3) pLys*/*Rosetta-gami B (DE3) pLys* for protein expression. Correct plasmid sequences were confirmed by Sanger sequencing provided by Microsynth AG.

3.1.2. Expression

All protein constructs were expressed in *Rosetta-2 (DE3)* unless stated otherwise. For the expression 2x750 mL 2xYT medium was placed in 1.5 L shaking flasks with 50 µg/mL chloramphenicol and 10 µL Antifoam 204. Depending on the used plasmid backbone for the expression either 50 µg/mL Kanamycin (for pET21, pET24 and pET28 plasmids) or 50 µg/mL Carbenicillin (for pET20) were added as well. An 5 mL overnight culture of the bacteria containing the desired protein were added to the medium. The bacteria were incubated at 37°C at 350 rpm until they reached an optical density (OD) of 0.6. At this point the protein expression was induced at 1 mM Isopropyl-β-d-thiogalactopyranoside (IPTG) and then further incubated at 16°C, 350 rpm for 16 h.

3.1.3. Purification

All steps of the lysis of the cells are performed on ice to conserve the protein stability. After protein expression over night, the bacteria are peletted at 4000 rcf, 4°C, 20 min. The pellet is solved in 1xPBS and again pelleted at 7100 rcf, 4°C, 20 min to remove remaining components of the growth medium. The cell pellet then is dissolved in lysis buffer containing 1 mg/mL lysozyme, 1 µM benzamidin, 1µM phenylmethylsulfonylfluoride (PMSF) and 0.001 U/µL Turbo DNase and incubated on ice for 1 h. After incubation the cell walls are disrupted by usage of a sonotrode with a power output of 8 W for 20 minutes using pulses of 15 seconds. The resulting

lysate is yet again centrifuged for 20 min, 4°C at 7000 rcf. For further purification of the supernatant two different purification methods were used.

Inverse Transition Cycling

Most of the used non-conjugated ELP constructs were purified using inverse transition cycling. Depending on the ELP construct the cleared supernatant of the lysate is heated in a water bath at 60°C in case of $(R_5Q_5)_2F_{20}$. Step by step NaCl was added to a maximum of 3 M to the suspension until cloudiness within the liquid could be observed. The aggregated proteins were pelleted for 20 min, RT at 7200 rcf. The resulting pellet was dissolved in pure and pre-cooled H_2O_{bidest} and incubated on ice for 10 min. The clear solution is again centrifuged for 20 min, 4°C at 7200 rcf. This supernatant is yet again heated and the process is repeated at least 3 times while decreasing the volume of the resuspension of the pellet. For EF constructs the protein purification was induced by changes in pH, where HCl was added until aggregation could be observed. The following steps were conducted analogous to the aforementioned protocol. All protein solutions were dialysed against H_2O_{bidest} in a 10 kDa-cutoff dialysis cassette under constant stirring at 4°C for 18h. The final concentration of the protein solution is measured by A_{280}. The purity of the peptides was evaluated by Sodium Dodecyl Sulfate Polyacrylamide Gel Electrophoresis (SDS-PAGE).

Affinity Chromatography

All proteins and ELP-conjugates not stable enough to be purified by the ITC method, were purified using immobilized metal affinity chromatography (IMAC). The cell lysate was applied to an HisTrap FF crude 1 mL column using an ÄKTA pure protein purification system. The column was cleaned using 10 column volumes (CV) of washing buffer before proteins were eluted using a gradient of 10% CV of elution buffer. The collected fractions were analysed using SDS-PAGE, pooled and concentrated using 10 kDa-cutoff Amicon centrifugation filters and finally dialysed against H_2O_{bidest} in a 10 kDa-cutoff dialysis cassette under constant stirring at 4°C for 18h. The final concentration of the protein solution is measured by A_{280}.

Size Exclusion Chromatography

Further purification was used for sAPEX split proteins using Size Exclusion chromatography (SEC). Therefore, the samples were concentrated to a total volume of 500 µL using Amicon centrifugational columns with an appropriate cut-off. The samples were loaded into an 0.5 mL sample loop and afterwards flushed through a SEC column of appropriate size and resolution. The samples were eluted over an isocratic gradient of 1.5 CV using gel filtration buffer. The resulting fractions were yet again screened using a SDS-PAGE and quantified by A_{280}.

3.2. Click Chemistry

Some of the purified ELP components were fluorescently labeled using Cu(I)-catalyzed azide alkyne Huisgen cycloaddition (CuAAC). The lyophilized ELPs were resuspended at a concentration of 500 µM in 1xPBS. The ELPS were mixed with a 15 fold excess of NHS-PEG_5-alkyne and incubated shaking overnight (roughly 12 h) at 4°C at 300 rpm. Residual bifunctonal linker were removed by dialysis with a 10 kDa dialysis cassette in 1xPBS at 4°C over night. Atto488-azide or Cy5-azide were mixed to the alkynated ELPs in a equimolar ratio. The reaction was started by the addition of 1 mM $CuSO_4$, 0.1 mM Tris(3-hydroxypropyltriazolylmethyl)amine (THPTA) and 1 mM Tris-(2-carboxyethyl)-phosphine (TCEP) and incubated at RT for 3-6 h. The residual dye was removed by dialysis in 1xPBS using a 10 kDa dialysis cassette at 4°C over night. The degree of labeling and the dye concentration was determined using wavelength specific absorption of the dialyzed sample.

3.3. Preparation of GUV

3.3.1. Solvent Evaporation

Peptides and phospholipids are freeze-dried in a 10 mL round flask, by freezing the solutions in liquid nitrogen and sublimation within a dessicator for 20 min. The solids are then re-solved in 10 mL pure tetrahydrofuran (THF) and agitated within a sonication water bath for 30 minutes at RT. Encapsulation of the inner solution (IS) containing 1.5 M sucrose is achieved by addition of the IS to the peptide-THF mixture and followed by agitation for roughly 3 seconds on a vortexer. This mixture is incubated at RT for 60 minutes and then transferred to a rotary evaporator. During the evaporation process that takes place for 15-20 minutes, depending on the temperature of the environment, a double layer forms around the aqueous IS.

For observation the formed vesicles are transferred in an isotonic glucose solution and afterwards placed within the designated observation slides. All experiments conducted in chapter 4.4 were performed with $(R_5\ Q_5)_2F_{20}$and all experiments in chapter 4.1 and chapter 4.2 were performed with EF_{20} unless stated otherwise. Depicted in Fig.3.3.1 is a schematic overview over the structure of the polypeptides and the formation process.

All following experiments including GUVs were prepared in this manner unless stated otherwise. The composition of the membranes is stated in the appendix A.4. Microscopy images were analyzed using ImageJ and Matlab. The image correction specifically was performed using the BioVoxxel Toolbox. [200] Automated

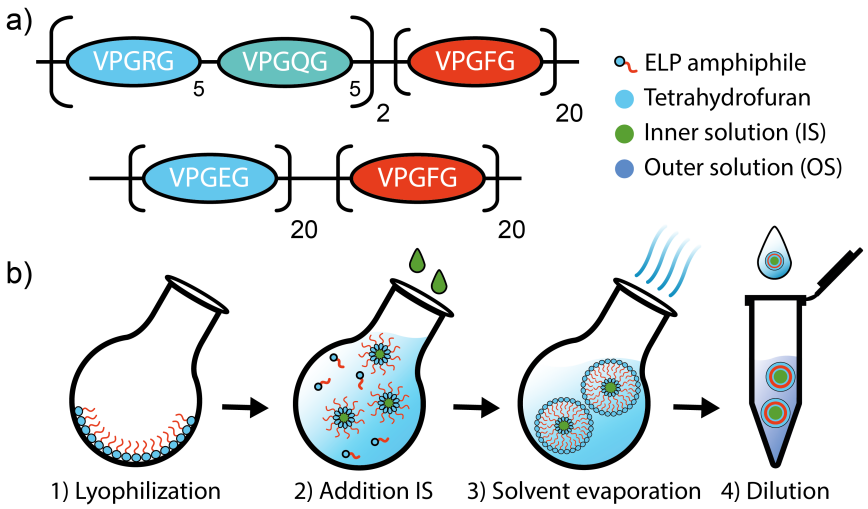

Figure 3.3.1: GUV formation protocol: *Schematic Overview of ELP components (a) and formation process of GUV using Solvent Evaporation Protocol (b).*

droplet identification and measurements were conducted using the Matlab code provided by Korbinian Kapsner. [201]

Streptavidin-Biotin interaction on membrane

Membrane compositions containing 1,2-dioleoyl-sn-glycero-3-phosphoethanolamine bound biotin (DOPE-Bio) were incubated with Streptavidin in a 1:1 ratio after GUV production for 10 min at RT. Streptavidin interacting molecules were added in the OS before mixing the two solutions.

3.4. *In Vitro* transcription

3.4.1. Fluorescent aptamer

Experiments involving active transcription of fluorescent RNA aptamers (dBroccoli, iMango-III) within the GUV or in the OS were composed as stated in table 3.4.1. The reactions were run under the microscope at 29°C.

Due to incubation times during the formation of the vesicles, two distinct species of vesicles were produced. Each vesicle species containing all reaction components but one. By omitting T7 RNA polymerase in one and the DNA template in the other vesicle species, the reaction is halted until mixing of the two groups directly before inserting them in the observation chamber.

3.4.2. pRNA Aptamer

For the production of the multivalent RNA aptamer (pRNA), the sample composition is stated in table 3.4.3. It was run at 37°C for 12 h in the thermocycler for subsequent purification.

Table 3.4.1: In vitro Transcription (IVT) of fluorescent RNA aptamer dBroccoli: *Composition encapsulated IVT solutions*

Component	**C_{Stock} (mM)**	**C_{sample} (mM)**	**Volume (µL)**
10xNEB	10	1	6
MgCl	1000	6	0.36
KCl	2000	25	0.75
DFHBI-1T	0.4	0.02	3
rNTPs	25	2	4.8
RNase Inhibitor murine (U/µL)	40	1	1.5
linear DNA template (µM)	10	0.2	1.6
T7 RNA polymerase (U/µL)	80	4	4
Sucrose+2% PEG-8000	3000	1500	40
H_2O_{nf}			fill to 80

Table 3.4.2: In vitro Transcription (IVT) of fluorescent RNA aptamer iMango-III: *Composition non-encapsulated IVT solutions*

Component	**C_{Stock} (mM)**	**C_{sample} (mM)**	**Volume (µL)**
10xNEB	10	1	6
MgCl	1000	6	0.36
KCl	2000	25	0.75
TO1-PEG3-Biotin	0.05	0.015	18
rNTPs	25	2	4.8
RNase Inhibitor murine (U/µL)	40	1	1.5
linear DNA template (µM)	10	0.1	0.8
T7 RNA polymerase (U/µL)	80	4	4
Sucrose+2% PEG-8000	3000	1500	40
H_2O_{nf}			fill to 80

Table 3.4.3: In vitro Transcription of multivalent pRNA aptamers: *Composition IVT solutions for pRNA aptamer for subsequent purification*

Component	**C_{Stock} (mM)**	**C_{sample} (mM)**	**Volume (µL)**
10xNEB	10	1	12
MgCl	1000	6	0.72
rNTPs	25	6	28.8
RNase Inhibitor murine (U/µL)	40	1	3
linear DNA template (µM)	0.724	0.1	16.57
T7 RNA polymerase(U/µL)	80	4	6
H_2O_{nf}			fill to 120

The used pRNA aptamers were purified using a commercial kit from Zymo Research (RNA Clean & Research Kit) and stored at -20°C.

3.5. Cell-free Gene Expression

For the encapsulation of the Cell-free Gene Expression (CFE) system in the ELP vesicles the same method as above was used, it is described in table 3.5.1.

Table 3.5.1: Cell-Free Expression of proteins: *Composition CFE solution encapsulated for in vesiculo protein expression*

Component	**C_{Stock} (mM)**	**C_{sample} (mM)**	**Volume (µL)**
CFE			28.5
Buffer solution			35.7
purified Plasmid template (µM)	0.1	0.005	5
RNase Inhibitor murine (U/µL)	40	1	2.5
T7 RNA polymerase(U/µL)	80	0.5	0.625
3M Sucrose+2% PEG-8000			fill to 100

The formed vesicles were transfered in the OS containing kanamycin and subsequently transfered in the described observation slides.

3.6. sAPEX2 Reconstitution

3.6.1. Production

The two parts of the split APEX2 enzyme N-AP and EX-C were expressed and purified according to the protocol mentioned in chapter 3.1. The purified enzymes were buffer exchanged using Amicon Ultra Centrifugal filters with a MW cutoff of 10 kDa and afterwards stored in 1xPBS at 4°C for 4 weeks.

3.6.2. Amplex Red Activity Assay

To estimate the activity of the split enzyme and the ratio of compnents necessary for the reaction, Amplex RED fluorescence measurements were conducted in different concentrations of the enzyme, heme, pRNA and H_2O_2. Aliquots of hemin and Amplex Red were prepared beforehand, stored at -80°C and only used once. Final concentrations for a single measurement are shown in table 3.6.1.

Table 3.6.1: sAPEX2 Amplex Red Assay: *Composition enzyme activity assay using Amplex Red*

Component	**C_{Stock} (mM)**	**C_{sample} (mM)**	**Volume (µL)**
Hemin chloride	0.6	0.0005	0.025
Amplex Red	20	0.05	0.075
KCl	2000	100	1.5
pRNA	0.0183	0.0005	0.82
N-AP	0.0152	0.00005	0.0987
EX-C	0.0505	0.00005	0.0297
H_2O_2	18	1	0.167
1xPBS			27.389

Addition of H_2O_2 is performed closely before the start of the measurement. The sample is mixed in a single well of an 384 well plate (ibidi GmbH) and afterwards centrifuged for 30 s at 300 rcf. The measurements were run in a FLUOstar Omega microplate reader while being incubated at 29°C.

Measurements containing GOX instead of H_2O_2 were conducted following the composition in table3.6.2.

Table 3.6.2: sAPEX2 Amplex Red Assay with GOX: *Composition enzyme activity assay using Amplex Red and glucose oxidase/glucose system*

Component	**C_{Stock} (mM)**	**C_{sample} (mM)**	**Volume (µL)**
Hemin chloride	0.6	0.0005	0.025
Amplex Red	20	0.05	0.075
KCl	2000	100	1.5
pRNA	0.0183	0.0005	0.82
N-AP	0.0152	0.00005	0.0987
EX-C	0.0505	0.00005	0.0297
Glucose	9000	300	1
Glucose oxidase (GOX)	0.00003	0.0000001	0.1
1xPBS			26.289

3.6.3. Biotinylation Assay

As the activity of sAPEX2 could be verified in the Amplex Red Assay, a different substrate was tested for further application. The ability to label proteins using biotinyl-tyramide was tested by incubating different proteins at RT like described in table 3.6.3. The aliquots of biotinyl-teramide were prepared beforehand and stored at -20°C and only used once.

Samples were taken after 2 min, 10 min, 1 h and 2 h and immediatly transfered into 5x quenching buffer.

The quenched samples were incubated on ice for 10 min and then transferred in 2x Laemmli Buffer. The samples were heated at 90°C for 5 min and then put on an SDS PAGE with 10% (BSA) and 15% (EF20) respectively. The samples were run at 110 mV for 10 min and then at 190 mV for 20 min (BSA) and 50 min (EF20) respectively. The used protein standard was PageRuler Plus Prestained Protein Ladder 10 - 250 kDa purchased from Thermo Scientific.

3.7. Western Blotting

The visualization of the biotinylation assays was conducted via western blotting using fluorescent Anti-Biotin antibodies (Biotin Polyclonal Antibody, DyLight 649, Thermo Fisher). The transfer of proteins from SDS-PAGE to Polyvinylidene fluoride

Table 3.6.3: sAPEX2 Biotinylation: *Composition biotinylation activity assay using BSA and EF20*

Component	C_{Stock} (mM)	C_{sample} (mM)	Volume (µL)
Hemin chloride	0.06	0.0005	1.25
Biotinyl-Teramide	5.503	0.05	1.363
KCl	2000	100	7.5
pRNA	0.0181	0.00025	2.066
N-AP	0.00152	0.00005	4.937
EX-C	0.00505	0.00005	1.484
BSA/EF20	0.15/1.74	0.0152/0.0421	15.152/3.63
H_2O_2	18	1	8.33
1xPBS			107.91/119.44

(PVDF) membranes was performed with a Semi-Dry-Blotter. Three layers of whatman filter paper were soaked in transfer buffer, while activating the PVDF membrane with 100% methanol for 15 seconds. The PVDF membrane was washed in transfer buffer and then placed on top of the soaked whatman filters on the Semi-Dry-Blotter. The Gels were placed on top of the PVDF membranes followed by another three layers of soaked whatman filters, before the lid was placed on top of the blotter. The transfer was run at 30 mV, 350 mA for 60-70 until the transfer was complete. The PVDF membranes were blocked for 1 h in 3% BSA in 1x phosphate buffered saline (PBS) while being shaken. Afterwards the membranes were washed 3 x 10 min in washing buffer. For the last step of visualization, the membranes were incubated with the antibody (1:5000 in blocking buffer, ≈ 0.1 µg/mL) for 1 h at RT in a dark box while being shaken. The results were visualized using a laser scanner (GE Typhoon FLA 9000 Gel Scanner).

3.8. Observation chambers

Observation chambers used for microscopy experiments were produced beforehand in one of two different ways. All experiments performed in chapter 4.1 and chapter 4.2 were conducted using silanized observation chambers composed of glass coverslides and parafilm. The larger glass coverslides were cleaned and coated with Trichloro-(1H,1H,2H,2H-perfluorooctyl)-silane using vapor phase depo-

sition. The individual chambers were separated with parafilm and a second coverslip was put on top. The parafilm was molten on a heating plate at 120°C bonding the separate glass coverslides. Experiments performed in chapter 4.4 were conducted using observation chambers composed of a hydrophobically coated glass slide with an rubber O-ring. The O-ring was fixed using epoxy glue. The makeshift chamber was sealed after the samples were filled in the O-ring using a second glass coverslide.

4. Results

The aim of this project is the creation of biocompatible vesicles with a membrane able to interact with external molecules, while encapsulating enzymatic reaction systems. One major milestone for this is the production of peptide and hybrid membrane vesicles. They are essential for the project as they define the designability of the tested membranes. Therefore, the basic properties of the vesicles are considered first, before the results of the formation of hybrid membrane vesicles are discussed. Next, the ability of the vesicles to interact with streptavidin and potential ligands in the sample can be verified. Further, the functionality of a multivalent RNA aptamer is validated using co-localization measurements of fluorescent proteins on the membrane surface. Additionally, the aptamer ability to trigger protein reconstitution is tested using a split enzyme.

The second goal of this thesis is to test and discuss the ability of peptide vesicles to encapsulate active processes. The *in vesiculo* transcription of an fluorescent RNA aptamer as well as the expression of an fluorescent protein using CFE are explained. As last milestone, the osmotically-driven process of vesicles growth observed during this project is thoroughly reviewed.

4.1. Size Distribution of Giant Unilamelar Vesicles

Throughout this thesis, vesicles were the main subject for experiments conducted. In the initial phase, the focus was set on the production of polypeptide vesicles and was later extended to the formation of lipid-polypeptide hybrid vesicles. The aim was to establish a basic reaction compartment with a functionalizable membrane which could be combined with active enzymatic reaction encapsulated within the vesicles.

The first step to characterize the resulting ELP vesicles is the examination of the size distribution of the formed vesicles. As it has already been shown in previous publications, ELPs possess the ability to form vesicles over a broad scope of diameters ranging from SUVs to GUVs. [99] [101] Therefore, initial measurements of ELP based vesicles included observation using transmission electron microscopy (TEM), dynamic light scattering (DLS) and light microscopy (LM) to cover all possible orders of magnitude.

The results depicted in Fig.4.1.1 show the polydisperse spectrum of vesicles formed using a modified solvent evaporation protocol. [202] Analysing the TEM micrographs of the ELP SVs depicted in Fig.4.1.1 a, a mean radius of 0.03 µm ±0.01 µm can be

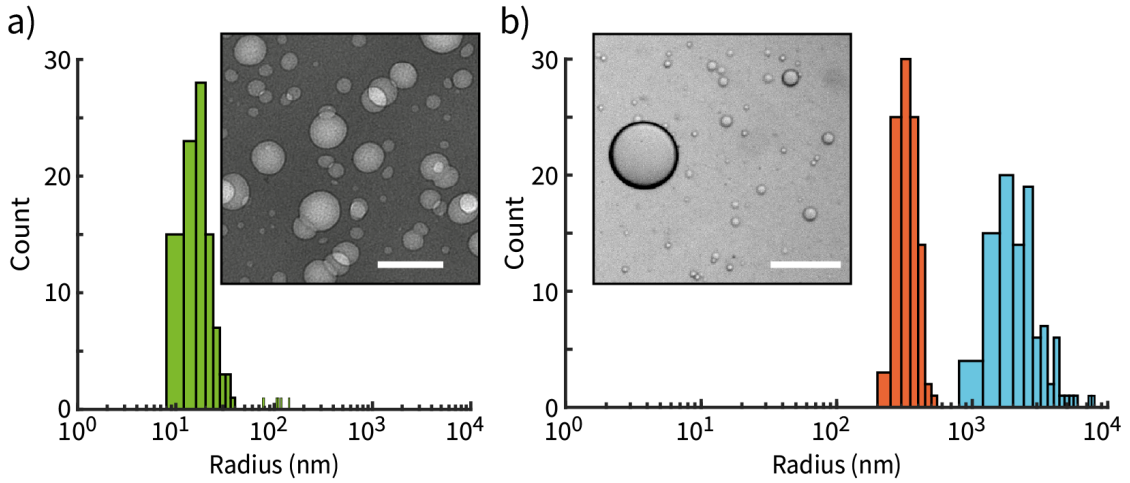

Figure 4.1.1: Size Distribution of ELP based vesicles: *Measurement of ELP vesicles over a broad size range using different analysis methods. a) Size distribution of ELP vesicles analyzed with TEM (green). Sample size: N=100. Inset: TEM image of ELP vesicles. Scale bar:100 nm. b) Size distributions of vesicles using DLS (orange) and LM (cyan). Sample sizes: N = 100. Inset: LM image of ELP vesicles. Scale bar:50 µm. Adapted from Frank et. al.* [102]

derived. The estimated uncertainty represents the standard deviation of the distribution. The size distribution of large and giant vesicles present in the samples made it necessary to use different observation methods due to resolution limits of DLS and LM. Using different observation methods allows to estimate the lower and upper size limits of the GVs depicted in Fig.4.1.1 b. Radii ranging between 200 nm and 10 µm can be observed in the sample. The presence of these two distinct populations might lie in two parallel occuring formation processes: While SVs are formed due to spontaneous formation upon water addition to the solved monomers, GVs might form due to the formation method itself, where the continous evaporation of solvent leads to bigger vesicles.

For further experimentation the produced vesicles had to be monitored for longer time intervals in solution, which is possible with light or fluorescence microscopes. With a diameter in the micron level, GUVs are better suited this mode of continuous observation than SUVs.

During this thesis, lipid, ELP, and hybrid vesicles were measured to examine different membrane compositions. All vesicles depicted in the histogram in Fig.4.1.2 were produced using the same solvent evaporation method described in chapter 3.3. The liposomes consisted of DOPS, DPPC, cholesterol, and DOPE-RhoB, while the hybrid vesicles replaced DPPC with EF20. The ELP vesicles were completely composed of EF20 ELPs.

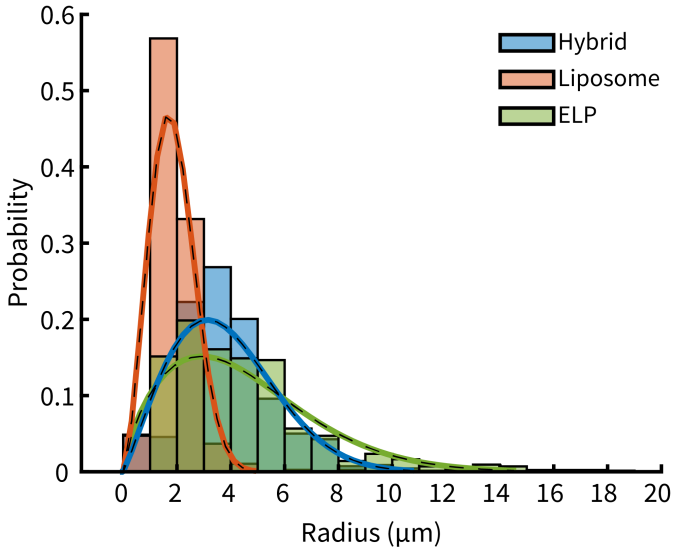

Figure 4.1.2: Size Distribution of GUVs: *Size Distribution of liposomes (orange), ELP vesicles (green) and hybrid vesicles (blue) produced using solvent evaporation vesicle formation. Data interpreted using a weibull probability distribution (colored lines). Sample sizes: Liposome N=380; Hybrid vesicle N=678; ELP vesicle N=423.*

Taking a look at Fig.4.1.2 shows the difference in size of the vesicles observed via LM. While the lipid vesicles (orange) show a comparatively narrow distribution with a radius median of ≈ 1.90 µm, hybrid (blue) and ELP (green) vesicles seem to allow a bigger variance in size. The median of the measured radii of ELP vesicles (3.88 µm) and hybrid vesicles (3.65 µm) show increased size in comparison to pure lipid vesicles. The data was evaluated using a weibull probability distribution of the vesicles radii measured in different areas of interest of the respective samples. Both distribution fits show the same trend where the peak is decreased and the distribution gets broader in comparison to the fit of the liposome distribution. This agrees with the histogram data (bars) shown in the same figure.

The results of the measurements point to the conclusion that the addition of polymers within the membrane increases the size of the vesicles. As the hybrid vesicles exhibit a similar size distribution as ELP vesicles, a potential explanation is the interstitial position of lipid molecules between ELPs as seen in Fig.2.2.2 b. [74]

With this, the ELPs can be expected to be one of the critical factors for the overall size of the vesicles. In literature, the formation process itself was also observed to highly influence the vesicle size. [55] [203] Addition of ELPs could potentially stabilize the lipid components during the formation process, as literature has shown formation of lipid vesicles with comparatively large durable radii. [204] Without the addition of ELPs, a majority of liposomes created with the solvent evaporation pro-

tocol used in this thesis are too instable if exceeding a specific diameter and burst before observation.

In addition to the observation of created vesicles with brightfield imaging, the introduction of fluorescently labeled monomers within the membrane provides the possibility to visualize the vesicle composition. The fluorescent components were mixed into non-modified membrane components, creating membranes observable under epifluorescence microscopy as seen in Fig.4.1.3. EF20-Atto488 and DOPE Lissamine Rhodamine B were mixed into the peptide and phospholipid mixtures repectively. The percentage of the fluorescent monomers within the whole membrane compostition is 0,0167% (75 nM) for 1,2-dioleoyl-sn-glycero-3-phosphoethanolamine-Lissamine-RhodamineB (DOPE-RhoB) and 1% (1,5 µM) for EF20-A488. Fluorescently labeled ELP were prepared using click chemistry following the protocols described in chapter 3.2.

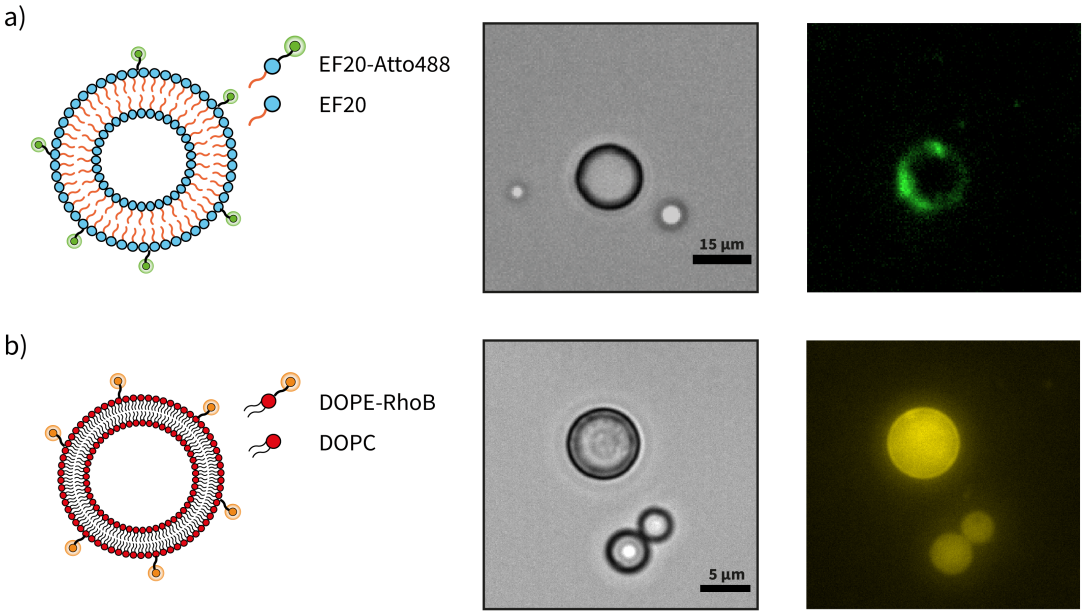

Figure 4.1.3: Fluorescence-labeled GUVs: *Fluorescently labeled membrane components integrated into vesicle membrane. a) EF20 monomers fluorescently labeled with Atto488 were mixed in non-labeled EF20 monomers for GUV formation. Scale bar represents 15 µm. b) Fluorescently labeled DOPE-RhoB monomers were added to DOPC mixture for GUV formation. Scale bar represents 5 µm.*

In Fig.4.1.3 a, it is visible that there is no completely homogeneous distribution of the fluorescently labeled ELPs in the membrane. Patches with an increased fluorescent signal exist, leading to the assumption of aggregates on the surface. After observing that the patches do not demix after 1 h within the membrane it can be deduced that the peptide membrane shows slow dynamics of its components. With respect to the monomer structure and size of the peptide vesicles, this assumption seems reasonable. [19]

The behavior of DOPE Liss Rhod within the phospholipid membrane shows a different picture. The fluorescent signal is, with exception of smaller patches, evenly distributed in the whole vesicle. In the microscopy image of Fig.4.1.3 b no distinct ring shape which would indicate the presence of labeled monomers only within the membrane can be observed. Here the inside of the vesicle also shows increased fluorescent signals. A potential explanation for this is the presence of residual solvent as well as smaller micelles containing labeled lipids within the lumen of the vesicle. The observations made using confocal microscopy 4.2.1 supports this potential explanation.

4.2. Functionalized Hybrid Membranes

One part of this thesis is the formation of reactive GUV membranes, which are able to interact with components in their immediate environment. The formation of hybrid membranes enables to combine different characteristics such as the fluidity of lipid membranes with the possibility to use the integrated ELPs as targets for modification. The major aim is to link an enzymatic mechanism to the surface of the vesicle membrane which is able to biotinylate surrounding ELP molecules integrated into the membrane. If achieved successfully, such a process results in a positive feedback loop leading to the accumulation of proteins on restricted regions on the surface of the vesicle and therefore changing the morphology of the GUV. [32]

In Fig.4.2.1 all necessary milestones are shown, that are verified over the course of the thesis, to enable the linkage of enzymatic mechanisms to the vesicle membranes. First, the binding ability of streptavidin to hybrid membranes has to be verified. For this, fluorescently labeled biotin probes are added as depicted in Fig.4.2.1 b. Biotinylated DOPE within the membranes serve as anchores for streptavidin on the vesicle surface. This interaction is used as initial platform to link even more complex constructs to the surface of the membrane. As this system had to be tested to the presence of external stimuli, the approach is to provide this signal by addition of an RNA aptamer structure which is able to interact with several different proteins at once (Fig.4.2.1 c). Once it is established that the RNA structure is able to maintain structure and interaction with binding proteins, the functionality of a split enzyme system can be tested *in vitro*. Using the split enzyme sAPEX2 brings the advantage that the presence of background activity of the system can be reduced while the co-localization of the split protein with membrane surface is controlled by the same RNA construct. If bound, the reconstituted enzyme can biotinylate surrounding peptides under consumption of biotinyl-tyramide and in turn provide new binding spots for streptavidin in solution as depicted in Fig.4.2.1 d.

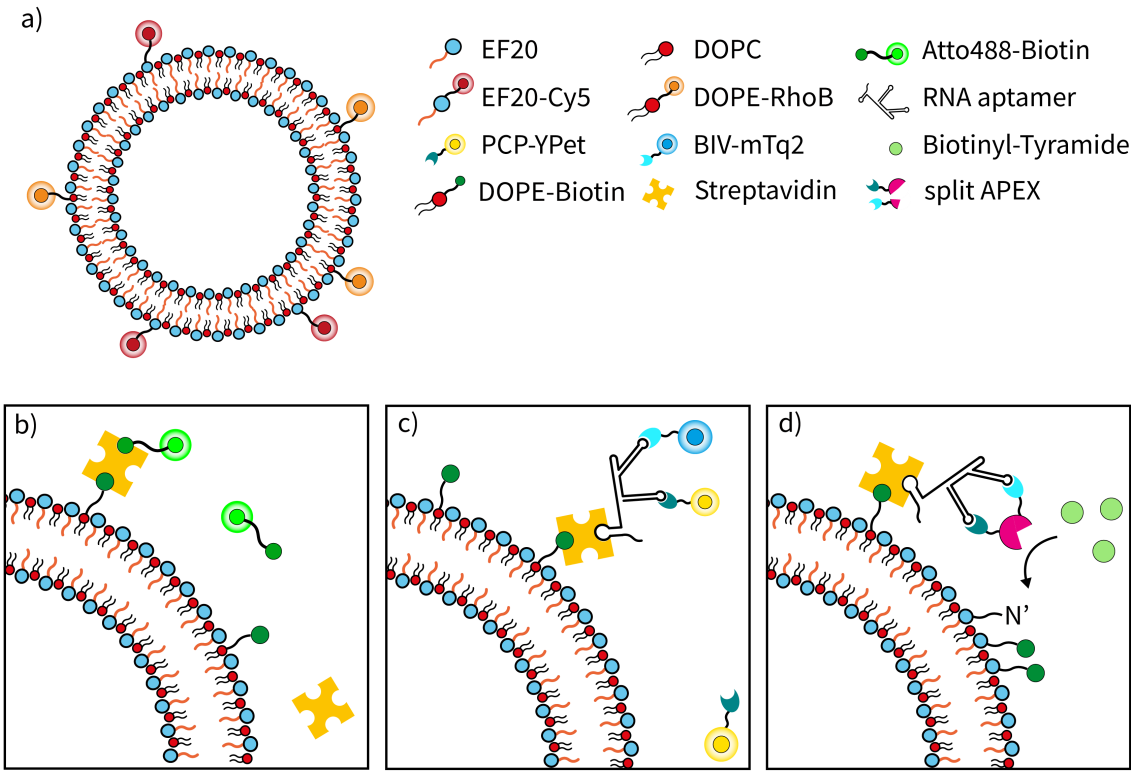

Figure 4.2.1: Interactions on Membrane Surface: *Schematic overview of components used in membrane interaction experiments. a) Hybrid membranes composed of DOPC/DOPE and EF20 ELPs containing fluorescently labeled monomers of each. b) Membranes containing biotinylated DOPE capable of binding free streptavidin, which in turn can interact with free Atto488-Biotin molecules in the OS. c) Biotinylated DOPE in the membrane binds free streptavidin. A specific RNA aptamer containing specific binding motives for streptavidin, PCP and BIV acts as a linker between bound streptavidin and fluorescent proteins modified with corresponding peptide tag. [158] d) Streptavidin bound to membrane by anchored DOPE-Bio interacts with multi-binding RNA aptamer. The components of the split peroxidase APEX2 contain the peptide tags, which enable the interaction with the RNA aptamer. Binding of the split components enables reconstitution of the enzyme, which facilitates the biotynilation of neighboring peptides by catalyzing the conversion of biotinyl-tyramide to biotinyl-phenol radicals. These radicals are able to interact with N-Termini of ELPs in membrane.*

The initial necessary step, is to ensure that lipids and ELPs are able to form stable GUVs, while still maintaining the ability to bind streptavidin. For this, mixtures of ELPs and lipids contaning fluorescently labeled amphiphiles as well as biotinylated amphiphiles are used to form GUVs. The resulting vesicles are observed using epifluorescence and confocal microscopy. It can be seen in Fig.4.2.2 that vesicles contaning ELPs and lipids show an increased signal on the membrane in both epifluorescence as well as in confocal microscopy micrographs. The distribution of fluorescent signal originating from fluorescently labeled ELPs (Atto488) is more uneven compared to the signal from lipids (RhodamineB) within the mem-

brane. This is not surprising, considering the fact that polymers with a high bending rigidity tend to incorporate lipids into gaps between them as already depicted in Fig.2.2.2 b. The signal of EF20-Cy5 as well as the signal of EF20-Atto488 shows brighter regions within the membrane which could point to distinct accumulations of peptides in these regions of the vesicle. Whether this is due to microdomain formation or aggregation of peptides outside of the membrane cannot be completly ascertained using fluorescence data alone.

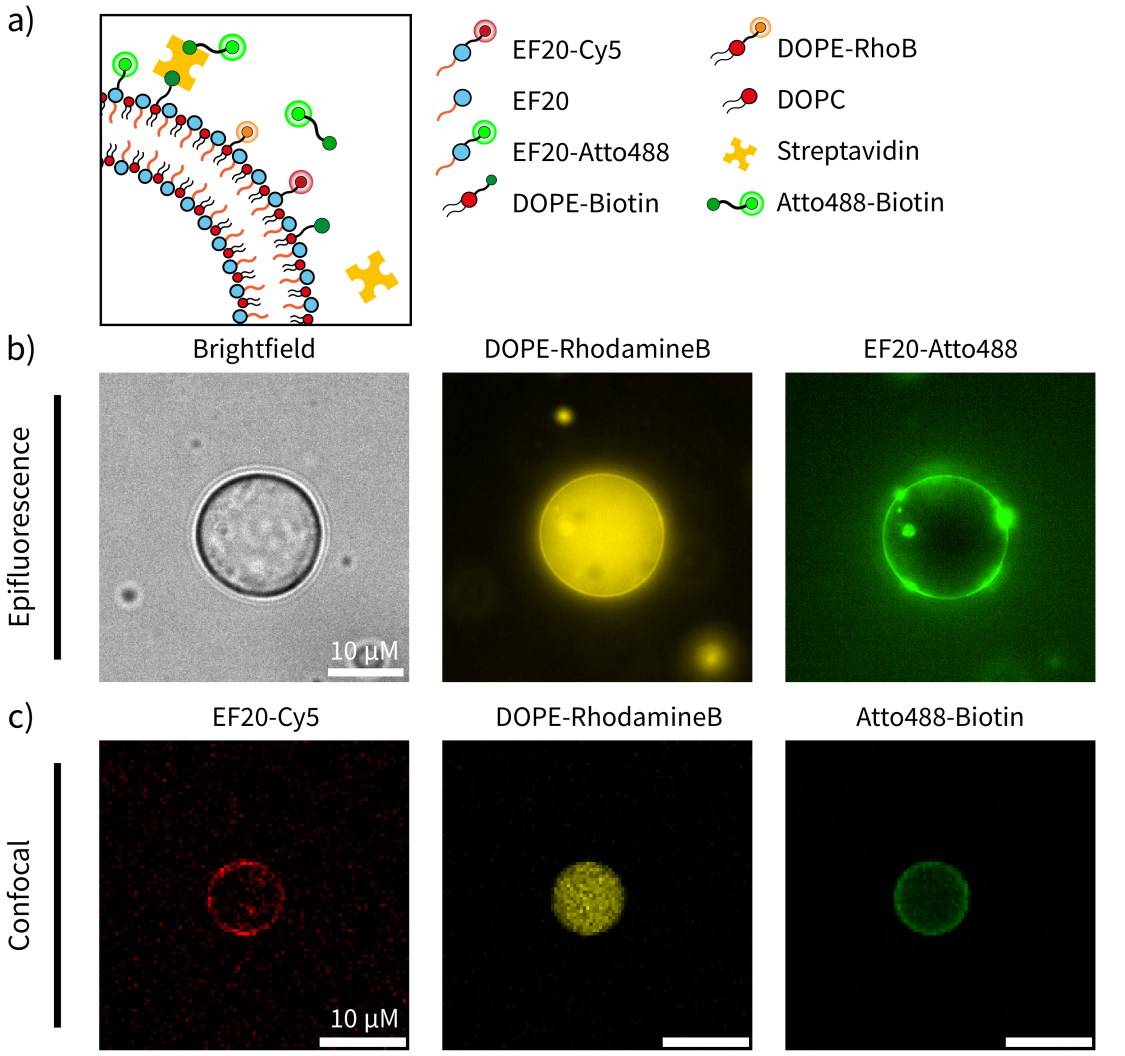

Figure 4.2.2: Hybrid Membrane: *Experiments to visualize the ability of ELPs and lipids to form hybrid membranes. a) A schematic overview of the formation of hybrid membranes interacting with streptavidin. b) Epifluorescence micrographs of hybrid vesicles composed of DOPE-RhodamineB and EF20-A488 showing brightfield and fluorescent images. Scale bar represents 10 µm. c) Confocal micrographs of hybrid vesicles composed of DOPC, DOPE-Biotin, DOPE-RhodamineB, EF20 and EF20-Cy5 showing fluorescent images. Streptavidin interaction on the membrane surface was visualized using Atto488-Biotin. Scale bar represents 10 µm.*

The fluorescent signal within the vesicle in the RhodamineB channel shows the presence of an increased amount of fluorescently labeled DOPE within the vesicle.

This correlates with observations of liposomes using the same solvent evporation protocol for vesicle formation. Nevertheless, the presence of labeled lipids can be observed in the increased fluorescence of the biotinylated Atto-488 dye on the membrane surface.

For all experiments conducted with biotinylated lipids, negative controls without streptavidin were observed. The negative controls showed only low fluorescence localized on the membrane compared to the surrounding medium as shown in Fig.A.1.1.

After establishing that vesicles composed of lipids and ELPs can be formed while binding streptavidin, next the implementation of RNA structures binding to the membrane is targeted. This is done in two different ways: In the first approach the ligand of a fluorescent aptamer is bound to streptavidin, in the other, a multimeric RNA aptamer binding streptavidin itself is utilized. [158]

The co-localization of two fluorescent proteins using a streptavidin binding RNA aptamer linked to an PCP and BIV binding domain is schematically depicted in Fig.4.2.3 a. For these experiments hybrid vesicles are formed and incubated at room temperature in a 1:1 ratio with streptavidin for 10 min to ensure that most biotinylated lipids are bound. A higher concentration of streptavidin bound to the membrane not only results in higher fluorescent membrane labeling, but also correlates to a lower concentration of free streptavidin binding the RNA aptamer in solution. The aptamer structure is isolated beforehand and added to the preformed vesicles to bind the membrane associated streptavidin. The used streptavidin to RNA ratio was 10:1. The inner and outer solution used are isotonic and contain optimal salt concentrations for the correct folding of RNA. Fluorescent proteins with a peptide tag that interacts with the RNA aptamer are added to the samples directly before transferring them into the observation slides. Both fluorescent proteins were at 0.2 µM for the measurements to ensure low background fluorescence.

As illustrated in the micrographs in Fig.4.2.3 the fluorescent signal gained from the respective channels of mTurquoise2 and YPET shows increased intensity alongside the vesicle membrane. All vesicles show intesities in comparable ranges, while the distribution differed between individual spots on the membrane surface. A potential explanation could be the different ratio of fluorescent protein to RNA due to the ability of YPET-PCP to bind as dimer. However, the steric hindrance exerted by two ≈29 kDa proteins could prevent the bininding of several proteins.

Negative controls without streptavidin show some degree of increased fluorescent signal on the membrane, but to a lesser extent as the samples containing

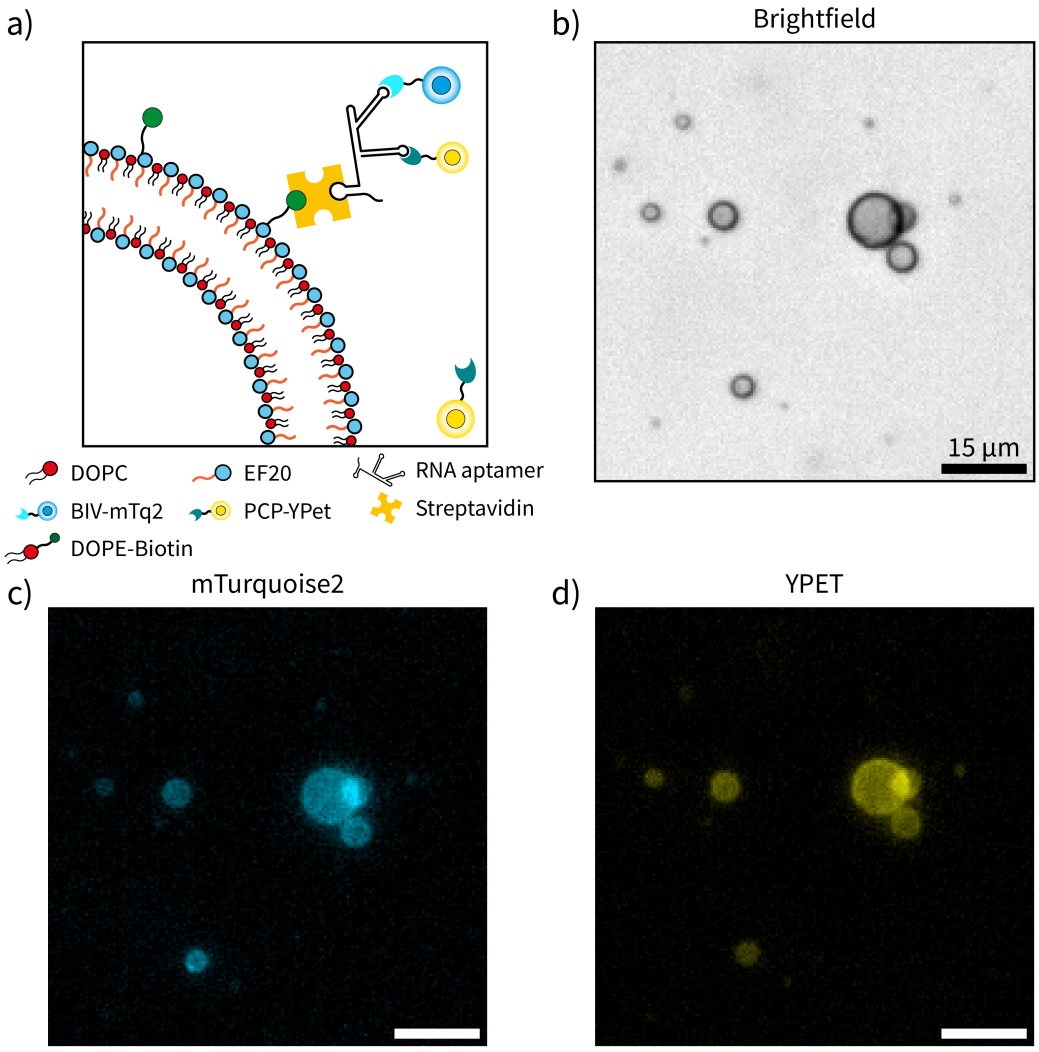

Figure 4.2.3: Co-Localization: *Co-localization of fluorescent proteins facilitated by a multifunctional RNA aptamer. a) Schematic overview over the mechanism to bind fluorescent proteins containing peptide tags to a hybrid membrane using a modular RNA aptamer. Micrographs of hybrid GUVs composed of DOPS, DOPE-Biotin, EF20 and cholesterol are depicted in brightfield (b), CFP (c) and YFP channel (d). The scales in the micrographs represent 15 µm. The background correction of the images was done with the BioVoxxel Toolbox plugin for Fiji.* [200]

both. Micrographs of vesicles without binding molecules are depicted in Fig.A.1.2. An explanation for the unspecific binding of fluorescent proteins could be the incomplete shielding of electrostatic forces which attract the surface charge of the proteins. Also the presence of residual solvent could be responsible for the aggregation of proteins on the membrane surface.

4.3. sAPEX2 Reconstitution

Verification of the functionality of the RNA aptamer on the membrane surface provides the basis for further protein interaction experiments. As mentioned in chapter 4.2 each component of the enzymatic system attached to the membrane surface has to be tested individually before combination. The next step is to identify an enzymatic system that provides localized activity combined with controllable activity.

For this, an optimized version of soybean ascorbate peroxidase (APEX2) is chosen to bind to the membrane. As mentioned in chapter 2.2.3, the enzyme is able to label proteins in its immediate proximity in the presence of its substrates and H_2O_2. Furthermore, the functionality of a split version of the enzyme as shown by Han et. al. enables the localized activity upon reconstitution. [156] This mechanism can be controlled with the same RNA aptamer used for the co-localization of PCP-YPET and BIV-mTurquoise2 as seen in Fig.4.2.3. Therefore, the N-Termini of both split enzymes are modified with the aforementioned peptide tags, BIV and PCP. Comparison of the RNA structures initially used for the reconstitution *in vivo* and the RNA aptamer used in this thesis show comparable distances between the individual binding sites.

Initial tests for the enzymatic activity are performed utilizing Amplex Red as substrate for sAPEX2 in the abscence of a membrane. The oxidative conversion of Amplex Red to the fluorescent product resorufin is a common reaction to identify oxidase activity *in vitro* and *in vivo*. [205] The presence of radicals produced by peroxidases catalyze this reaction. [206] The protocols used for the measurements are modified from the *in vivo* application due to the absence of cell membranes restricting availability of individual reaction components. For the measurements lower H_2O_2 concentrations are chosen due to the degradative effect on the protein and nucleic acid content within the sample. Additionally, glucose oxidase (GOX) and glucose are tested as alternative provider of H_2O_2. To ensure a low activity throughout the sample preparation, all components are kept on ice and H_2O_2 is added directly before measurement in a plate reader. The measurements were conducted at 37°C and all samples were tested as triplets.

The fluorescence measurements show an increase in fluorescence intensity in all samples (Fig.4.3.1 a). The data shown is already background corrected as the used H_2O_2 and heme concentrations lead to increases in fluorescence signal without enzymatic components within the sample. An inital steep increase in fluorescence can be seen within the first 20 min in all samples. This is also the case with

negative controls containing both parts of the split enzyme without RNA. Measurements performed with single split enzyme units confirmed the lack of enzymatic activity of a single unit, which would point to unspecific reconstitution of the split enzyme. Nevertheless, samples containing the aptamer showed roughly a three-fold increase in fluorescence compared to the negative controls.

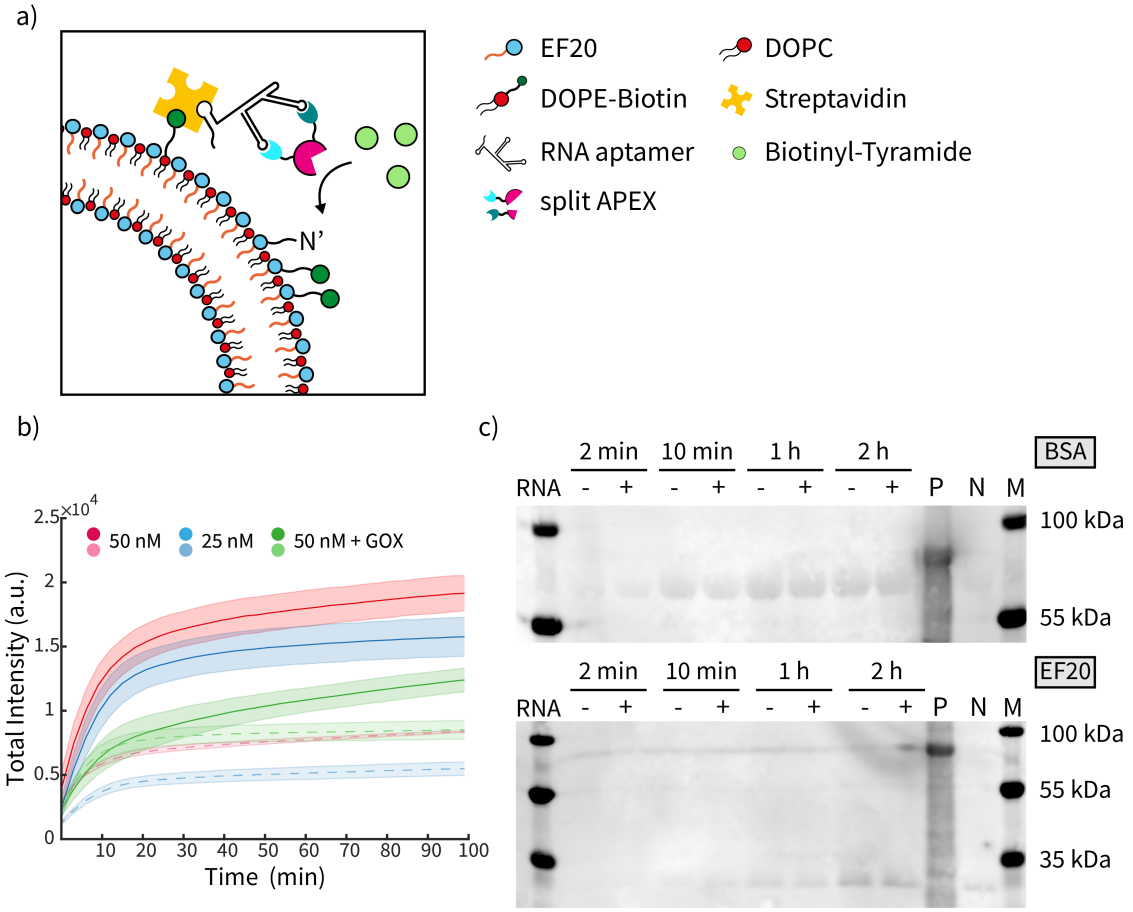

Figure 4.3.1: sAPEX2 reconstitution: *The RNA-dependent reconstitution and enzymatic activity of sAPEX2 using different substrates. a) Schematic overview of RNA-dependent biotinylation activity of reconstituted sAPEX2. The depiction describes activity on membrane surface while measurements were conducted in bulk. b) Fluorescence signal of resorufin over time using Amplex Red as substrate to visualize the RNA-dependent enzymatic activity of sAPEX2 in vitro. Measurements are conducted for 50 nM (red) and 25 nM (blue) of sAPEX2 as well as for 50 nM + 0.1 nM GOX (green). Samples with GOX contain 300 mM glucose instead of H_2O_2. All samples are measured in triplicates. The shaded area represents the standard deviation. Enzyme activity is measured with (solid lines) and without (dashed lines) RNA. c) Western blot of biotinylation assay of BSA and EF20 using 50 nM sAPEX2. Samples are taken after 2 min, 10 min, 1 h and 2 h of incubation at RT. Biotinylation reactions with RNA (+) and without RNA (-). Commercially available Biotin-BSA as positive control for the western blot (P). Negative controls of the proteins omitting RNA as well as enzymes to estimate the background activity of reagents (N). PageRuler Plus (Thermo Fisher Scientific) as protein standard (M).*

The samples containing GOX additionally showed further increase of fluorescence after 20 minutes of reaction time. This could point to the fact that the availability of H_2O_2 can be a restricting factor for the reaction. The fact that the negative control of the GOX sample shows no further increase, could be a sign for a more specific reaction of the enzyme with lower concentrations of H_2O_2 available in the sample.

After verification of the enzymatic activity of the split enzyme, their ability to label proteins is tested. As APEX can be used with a variety of different substrates, this promiscuity is used to catalyze the conversion of biotinyl tyramide to its phenyl radical. This highly reactive molecule is able to interact with primary and secondary amines in its vicinity.

The ability to biotinylate proteins using sAPEX2 is examined with BSA and EF20 ELPs, which can later serve as target within the membrane. For each protein a negative control omitting the RNA (-) as well as a control without split enzymes was prepared (N). Furthermore, a positive control for the detection method in form of commercially available biotinylated BSA was added onto the gel (M). The reaction mixtures were prepared and incubated at RT before taking samples after 2 min, 10 min, 1 h and 2 h. The reactions are quenched using 5 x quenching buffer containing antioxidants and stored on ice. The samples are analyzed via western blotting using Anti-Biotin antibody-fluorophore conjugates. Visualization of the bound antibodies is done using a fluorescence scanner.

The results of the biotinylation assay in Fig.4.3.1 c show the presence of biotinylated proteins in the gel. The very present band of the positive control (P) can be used as verification of correct binding of the anti-biotin antibody. The sizes of the bands roughly match the expected sizes of BSA (66.5 kDA) and EF20 (18.3 kDa). The positive control (P) runs slightly slower due to the fact that commercial Bio-BSA has a higher degree of labeling lying at 8-16 molecules per BSA molecule, increasing its size $\approx$ 2 - 4 kDa. In the western blot of EF20 a band can be seen roughly at the same size of the positive control in all samples. It is improbable that the band represents residual BSA in the samples as the biotynilated BSA samples in Fig.4.3.1 show a lower size compared to the positive control. As there is no increasing intensity over time it seems to be an artifact introduced during SDS-PAGE or western blotting. One explanation might be the contamination of the pockets during the loading process with low amounts of the positive control.

In the western blots it can be seen, that the absence of RNA does not impair the ability of sAPEX2 to label the protein. However, the increasing intensity of the

labeled proteins over time might indicate a enzymatically-driven process. This assumption is reinforced as samples without sAPEX2 which were incubated for 2 h, show weaker signals. Taking intensity signals and comparing them to the labeled BSA in the positive control show only a limited degree of labeling in the BSA samples. After correction of background activity (N) and background fluorescence of the western blot, the fluorescence of BSA after 2 h of incubation with pRNA + sAPEX2 amounts to $\approx$ 35.7% compared to the BSA-Biotin sample. For the EF20 samples a maximum intensity of $\approx$ 9% in comparison to BSA-Biotin was measured. This lower value can be partly explained by the lower amount of potential labeling sites in the ELP compared to the reported 8-16 biotins per molecule BSA in the commercial BSA sample.

Potential explanations for the unspecific activity observed in Amplex Red and biotinylation assays might be caused by the intended application: As sAPEX2 is optimized for use *in vivo*, lower specificity of the system might occur *in vitro*. Like mentioned before, protocols were adjusted to an *in vitro* setting for this thesis. Initial concentrations of heme, H_2O_2 and the used substrates were 6 - 10 fold lower compared to the original *in vivo* protocols. [156] The change of conditions in the surrounding medium could promote unspecific reconstitution of the split enzyme. Even low affinities between the split enzyme units could facilitate reconstitution on its own as it is normally used in dimerization assays. [207] Overall changes to the sample environment can influence the efficiency of the reaction. Factors like intracellular salt concentrations, [208] as well as the packing density within cells [149] can alter the labeling rates and have to be taken in account when using this method *in vitro*.

In summary, the data acquired in this thesis points to the possibility that the used labeling system also shows enzymatic activity in an *in vitro* setup. Further improvement and optimization of the reaction conditions could reduce background activity as well as unspecific binding events. As the implementation of GOX into the system has shown that multiple enzymatic systems are compatible, further improvement in this direction can be targeted for its application. Of these enzymatic systems, one could be repurposed in the future for the continous generation of RNA aptamers as discussed in chapter 4.4.1. This could be used for long-term experiments involving reconstitution of split enzymes and therefore regulating enzymatic activity. During all tests conducted, the amount of RNA nanostructure was not increased during the test runs. A continous synthesis of RNA structures could improve the number of the binding events. Such systems are tested in the second part of this thesis and are explained in more detail in the following chapters.

4.4. Encapsulation of Active Systems

The investigation of reaction compartments on a µm scale is an important component in the field of bottom-up synthetic biology. The creation of cell-like carriers with defined chemical and enzymatic reactions could enable the design of protocell structures.

4.4.1. In-vitro Transcription

One approach to test the capability of encapsulating active processes within the produced vesicles was the *in vitro* Transcription of the fluorescent RNA aptamer dBroccoli. The process is schematically depicted in Fig.4.4.1. Therefore, two distinct vesicle groups were mixed directly before the observation under the microscope to minimize unobserved RNA transcription. The reactions within the vesicles are started as soon as two vesicles containing the essential components, T7 RNA polymerase and DNA template, fuse on contact. These fusion events were promoted by the presence of the non-ionic surfactant Triton X-100 which was added to the OS for all experiments involving fusion events. A potential explanation for this lies in the slight destabilization of the peptide membrane by the interaction with the surfactant. Addition of DNase I in the surrounding medium prevented the expression of RNA aptamers outside of the vesicle and therefore minimized background flourescence.

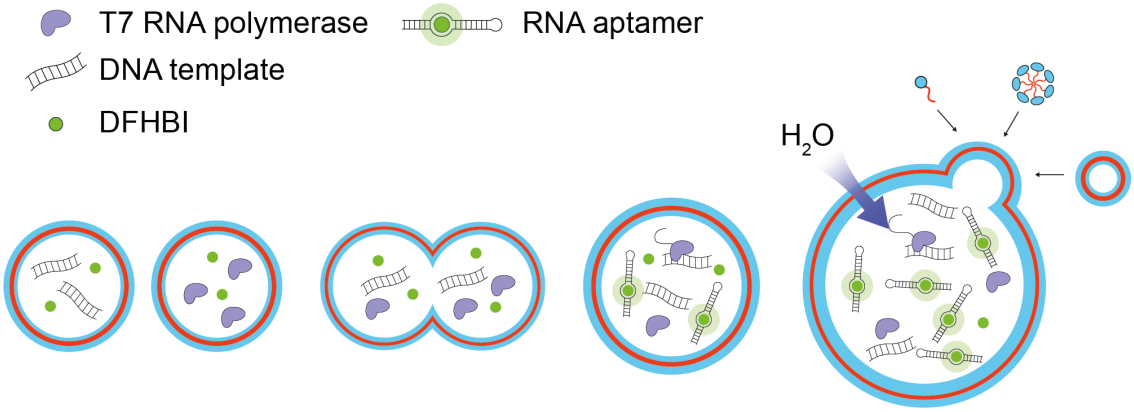

Figure 4.4.1: In vitro Transcription encapsulated in GUV: *Schematic overview of encapsulated IVT reaction separated in different vesicles omitting one key component (T7 RNAP or DNA template). Production of dBroccoli by T7 RNA polymerase enabled after fusion of vesicles. RNA aptamers produced by transcription interacts with DFHBI and leads to increase in fluorescent signal. Continous biopolymerization leads to increase in osmotic pressure within the vesicle. Influx of water in the vesicle paired with additional fusion of ELP monomers, micelles and vesicles with vesicle membrane. Growth of vesicles as result of ongoing enzymatic process within. Adapted from Frank et. al.* [102]

During the measurement of active processes within the ELP vesicles, the vesicles show different behaviour depending on the surrounding concentration of free ELPs in the solution. The observed vesicles resulted in mixed growth behaviors, in which some vesicles started to shrink at one point until they vanished completely out of the visible range of light microscopy. Others continued to grow as long as unbound ELPs were provided in the OS and the transcription of RNA aptamers continued as depicted in Fig.4.4.2. This biochemically driven growth can be traced back to the encapsulated polymerization process. The resulting changes in osmotic pressure as well as the integration of micelles, smaller vesicles and free ELPs promote the vesicle growth. The lack of incorporable material leads to shrinking and even bursting vesicles over time.

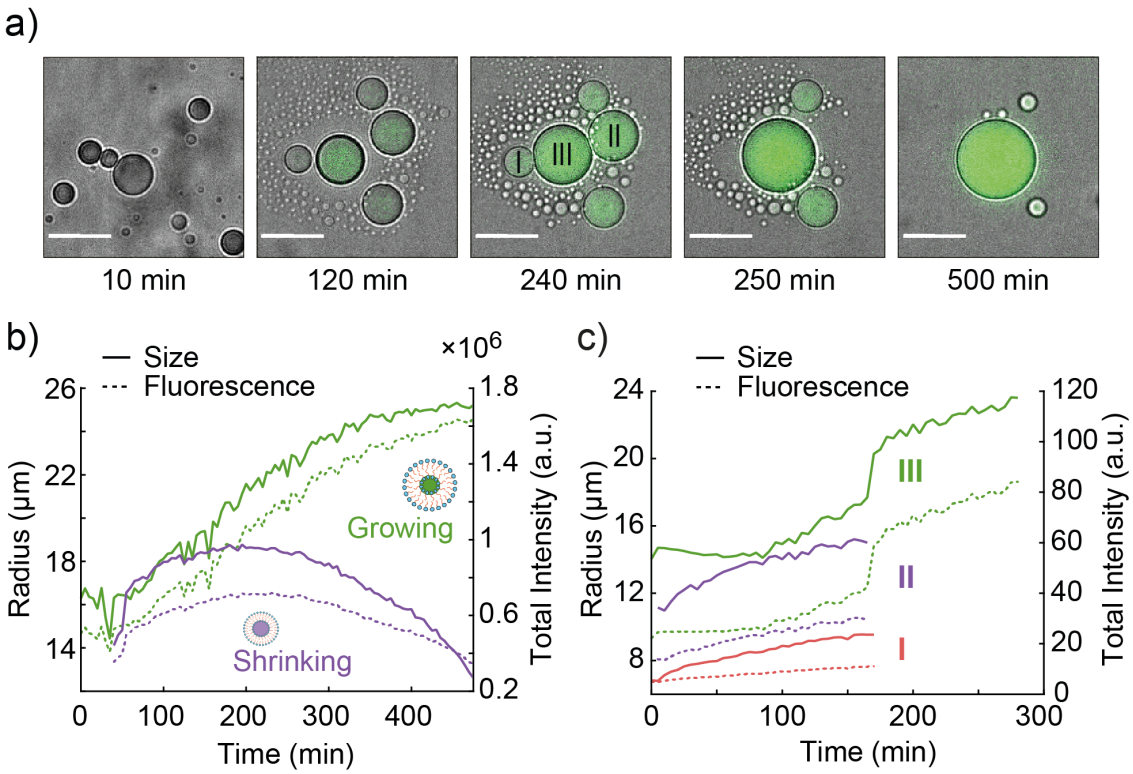

Figure 4.4.2: Transcription-driven growth of GUV: *Transcription dependent growth of ELP vesicles. a) Time series of LM images (composite of brightfield and fluorescence channels) of growing ELP vesicles. Scale bars:40 µm. b) Typical timetraces for vesicle radius (solid lines) and fluorescence intensity(dashed lines) of continuously growing vesicles (green)and growth followed by shrinkage (purple). c) Exemplary time traces for vesicle radius (solid) and fluorescence (dashed) of fusing vesicles (I–III) in- dicatedinb). Afterthe fusion of II and III, the combined (II+III) fuse with I. Adapted from Frank et. al.* [102]

Due to the high polydispersity achieved during the formation process using the solvent evaporation method, different quantities of the essential transcription components within the vesicles were to be expected. Therefore a broad distribution of transcription rates and fluorescent intensities were expected throughout the

reaction. [209] The active transcription of RNA within the vesicles was observed over the course of several hours.

Within this time period not only the shrinking and growing of the individual vesicles was measured, but also the appearance of 'satellite' vesicles can be seen in Fig.4.4.2 a. These smaller structures were appearing in the near vincinity of the active vesicles after some incubation time. Compared to the originally monitored GUVs, these vesicles showed lower fluorescent intensity increases, which nonetheless indicated the presence of an active IVT system within the vesicles. Therefore, an active exchange between the IS of the observed vesicles and the newly forming 'satellite' vesicles must occur in form of budding. These spontaneous budding events, might be induced by surfactants or interactions of the swelling membrane with the hydrophobic glass slide. [210]

Looking at the whole of the micrograph in Fig.4.4.2 a brings up another potential cause for these 'satellite' vesicles. This would align with our initial assumption considering the connection between active polymerization reactions, changes in osmotic pressure and swelling of the vesicles. [211] Smaller vesicles seem to pop up not exclusively around bigger GUVs but rarely also appear without any other objects in its immediate surroundings. This could point to the explanation of SVs under the resolution limit of the light microscope, swelling into an observable level. Fusion events due to gradual sedimentation of vesicles within the solution might accompany this observation. The instability of the peptide membrane caused by continous growth and surfactants in solution however might be a potential reason why an increased number of smaller vesicles is observed in the vincinity of the GUVs. Due to the instability of the membrane surface, monomers get available for the surrounding 'satellites' and therefore promotes their growth much more compared with vesicles out in the open. To rule out the fact that fusion events and accumulation of ELPs within the already existing GUVs, the same experimental settings were chosen for an experiment lacking the active components encapsulated within. The presence of surplus peptides within the OS does not promote the growth of the vesicles on its own. (Fig.A.1.4)

The GUV's dependency of available membrane material to support continous growth becomes apparent when looking at Fig.4.4.2 b showing the comparison between two similar vesicles with different positions inside of the chamber. Comparing the growing (green) and the shrinking (purple) vesicle shows the correlation between the overall fluorescence intensity and the size of the vesicle. While continous increase of fluorescence promotes the growth of the vesicle in one case, no substantial increase in fluorescence can be seen in the shrinking vesicle. The fluorescence was measured for the exact vesicle area for each frame. Next to active

transcription also fusion events further promote the rapid growth of the vesicles. Looking at Fig.4.4.2 c, the sizes and fluorescent intensities of three depicted vesicles in Fig.4.4.2 b are compared. Analyzing the final fluorescent intensities within the vesicle, the radius as well as the volume of the remaining vesicle shows a discrepancy between the measured and the theoretical values. As the abrupt increase in size and fluorescent intensity of vesicle III after 240 min does not account for the sum of vesicles I and II some loss of material occured. (Figure S9) The remaining surplus membrane components might either be distributed to the outer solution in form of smaller vesicles or micelles or might as well be incorporated in a multilamellar membrane structure.

The complex connection between the individual processes of RNA polymerization, the growth of the membrane surface either by fusion events or incorporation of free ELPs and the influx of water are the driving forces for the observed growth of the vesicles. Looking at the linear fashion in which the fluorescent intensities increases alongside the vesicle volume, as seen in Fig.4.4.3 a indicates that the RNA concentrations within the vesicle stays constant. This in turn speaks for the ability of the vesicle membranes to withstand the influx of water which is induced by the osmotic pressure changes of the newly synthesized polyelectrolytes. [211] [212] [213] This water uptake has to be fast enough to compensate the RNA transcription rate throughout the reaction time, which suggests a certain permeability of the ELP monomers for water molecules. [88] Although the global trend of the observed vesicles tends to show the linear correlation between the growing vesicles and the increasing number of RNA molecules within the vesicle, exceptions can be seen as well. The inset in Fig.4.4.3 a shows the alternating trends of individual vesicles, where growth phases may alternate with shrinking phases. Looking at the form of the curve shows that shrinkage as well as a halt in the production of fluorescent aptamer molecules take place simultaneously. The potential explanation lies in the lack of free ELP molecules as well as a lack of essential components for the transcription reaction within. The growth phases are only restarted after supply of further components via vesicle fusion.

The availability of membrane components overall seems to be a crucial factor for the behavior of the vesicles throughout the observation time. Looking the depicted vesicles in Fig.4.4.3 c and their relative trends in Fig.4.4.3 b, growth seems to be connected to their immideate surroundings. In this case the supply of ELPs as well as 'fuel' for the transcription reaction is ensured by the amount of 'satellite' vesicles surrounding the main vesicle in the middle. Considering the size of the T7 RNA polymerase and the charged nature of the rNTPs, one has to assume that the provision of these essential components can only be achieved by fusion. While

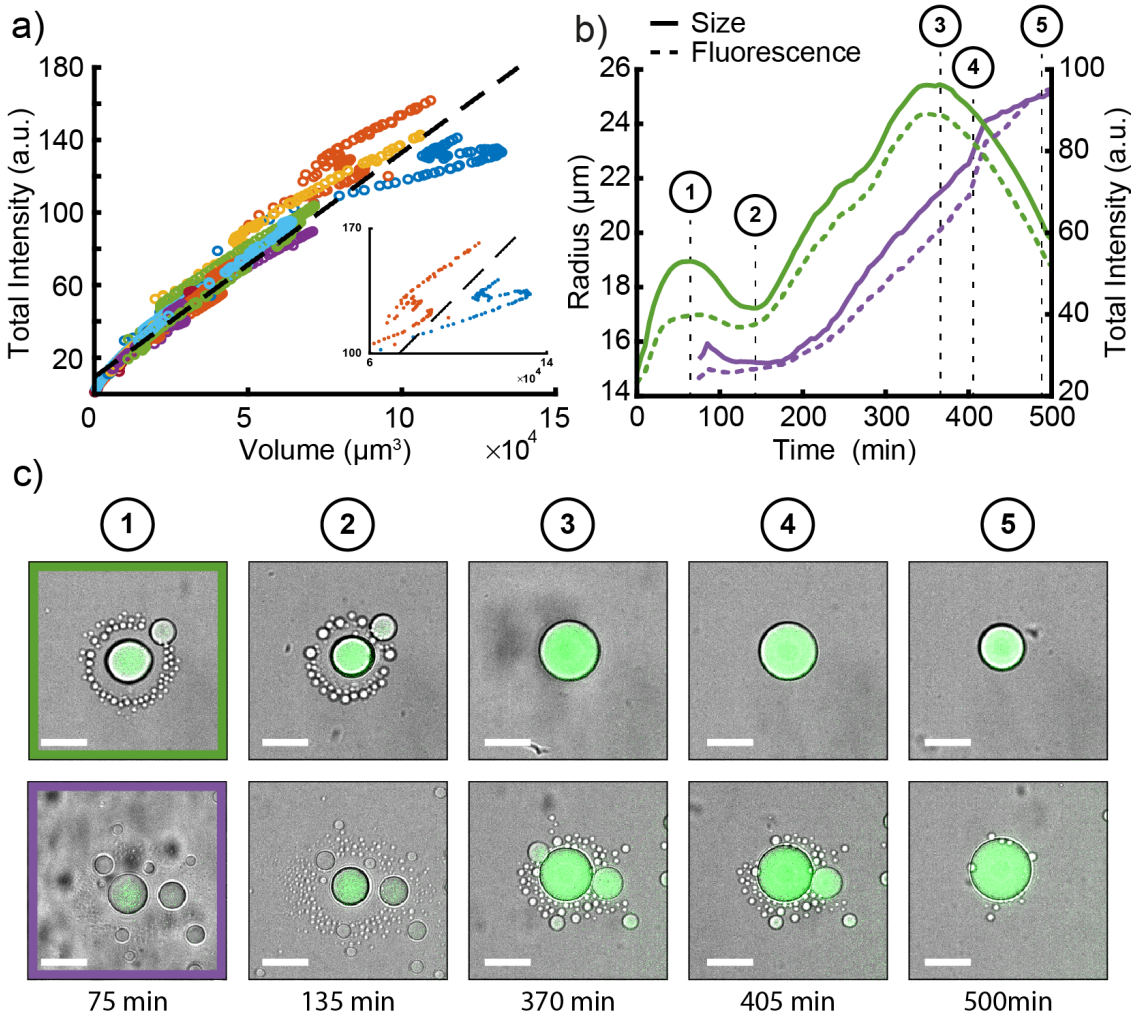

Figure 4.4.3: ELP dependent Growth *Growing behavior of ELP vesicles in correlation to ELPs in immediate proximity a) Representative plots of total vesicle fluorescence intensity vs. vesicle volume over a time course of 500 min. The different colors indicate different vesicles (N=20). The dashed line shows a linear fit to all 20 vesicles (see SupportingInformation). Inset: intensity vs. volume of two exemplary vesicles showing growth, shrinkage and re-occuring growth. b)Typical time traces for vesicle radius (solid lines)and fluorescence intensity (dashed lines) of agrowing vesicle (purple) and avesicle showing alternatinggrowth and shrinking phases (green). For all curves a 4-point moving averagefilter was used. Numbers 1–5 indicate the corresponding LM images. c) Time series of LM images (composite of brightfield and fluorescence channels). The green and purple frame indicate the corresponding trace in b). Data analysis started after t=75 min due to ongoing sedimentation, which impaired the image analysis. Scale bars:40 mm. Adapted from Frank et. al.* [102]

the smaller vesicles disappear over time the bigger central vesicles grow until their supplies are exhausted. As soon as this is the case the overall increase in size and fluorescence is halted and promptly reversed to shrinkage of the vesicle until it completely vanishes at some point This change of growing behavior can be seen at several points for one vesicle (green), where an initial halt in RNA transcription

correlates with the hold in growth (1). Afterwards the vesicle shrinks until it starts to absorb the surrounding 'satellites' to deliver substrates for the continuation of the transcription reaction (2-3). As soon as the reservoirs in form of 'satellite' vesicles are used up a decline in fluorescence and size can be observed (4). This exemplifies the correlation between the necessity of active transcription, presence of ELPs and the resulting growth of vesicles.

The ability of ELP vesicles to accomodate *in vitro* transcription reactions is a first step towards the formation of reaction compartments in the micron scale. Their ability to withstand increased osmotic pressures while actively producing properly folded RNA aptamer structures enables the integration of further reaction systems. In addition to the desired interacction between newly formed RNA structure and the functionalized membrane, other complex reaction systems were implemented within ELP vesicles.

4.4.2. Cell-free Gene Expression

The initial focus to encapsulate active processes was not only in the transcription of RNA aptamers, but also the expression of proteins within the preformed peptide vesicles as already shown within SUVs. [99] For this a plasmid encoding the yellow fluorescent protein YPET, was encapsulated alongside a *in vitro* protein expression system, which is based on an *E.coli BL21 rosetta* cell extract. [186] The addition of kanamycin into the isotonic OS prevented the proper expression of the fluorescent protein outside of the vesicles, due to non-encapsulated CFE mix. Vesicles prepared with the solvent evaporation method and actively producing YPET were observed for 24 h using a closed observation slide as described in chapter 3.8. The images depicted in Fig.4.4.4 a were taken after 15 min (left) and 24 h (right) respectively.

Looking at Fig.4.4.4 and Fig.4.4.3 shows the comparable behavior of the vesicles containing CFE to the described IVT reactions, where the increase in fluorescent intensity is accompanied by the growth of the overall diameter of the vesicles over time as seen in Fig.A.1.6 and Fig.A.1.8. Comparing the initial sizes of the vesicles at the beginning of the measurement shows an overall increased size. A potential explanation for this lies in the high viscosity of the used CFE reaction mix, containing 2% PEG-8000 in contrast to the IVT reactions without any crowding agents present. Additionally, the amount of proteins present in CFE systems would also increase this effect. The presence of crowding agents in liposomes shows an increased efficiency in encapsulation, this behavior could also have an effect on the encapsulation rate of the CFE reaction mix in ELP vesicles. [214] As the whole CFE

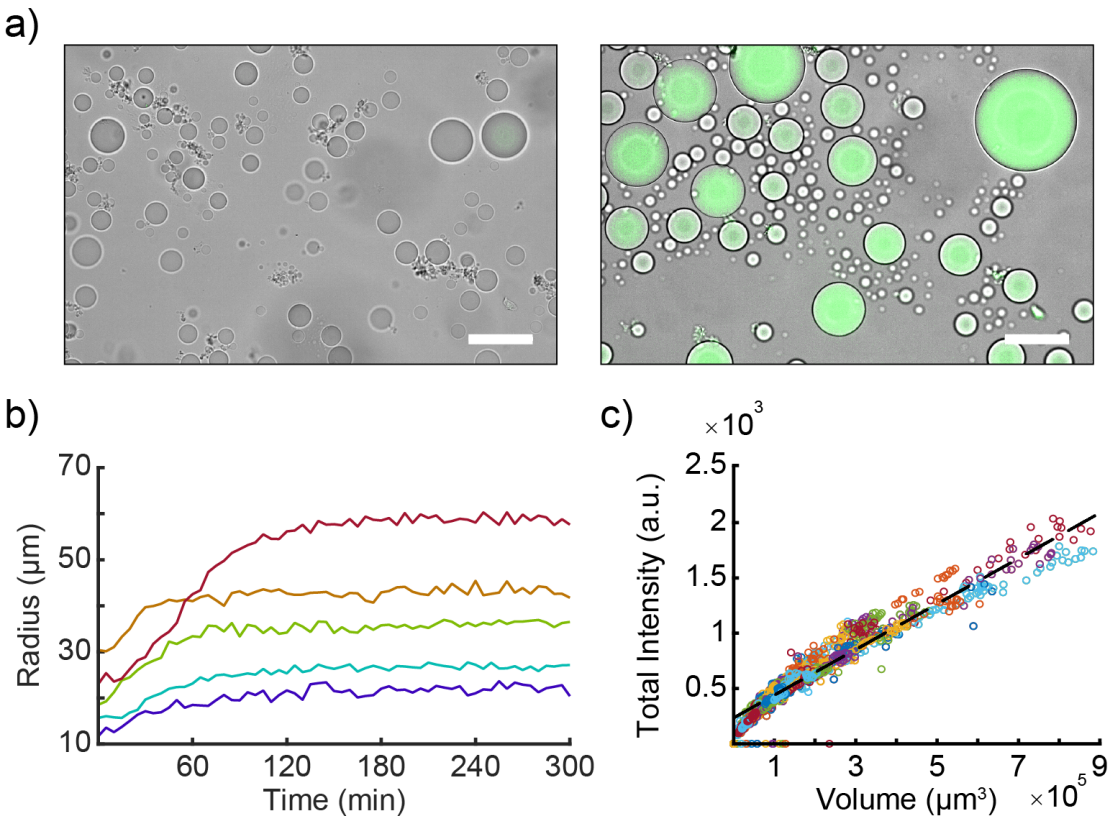

Figure 4.4.4: Cell-free gene expression: *a) Microscopy images (composite images of brightfield and fluorescence channel) of vesicles containing CFE after 15 min (left) and 24 h(right). The fluorescence is produced by the active expression of YPet. Scale bars:50 mm. b) Exemplary radius vs. time traces of vesicles expressing YPet. c) Fluorescence intensity vs. volume scatter plot of 77 vesicles expressing YPet over the course of 3 h. The dashed line shows a linear fit to all 77 vesicles. Adapted from Frank et. al.* [102]

reaction solution was pre-mixed before the encapsulation process, the observation was started with a degree of YPet already expressed within the vesicles. This was confirmed by bulk measurements in a plate reader, where the fluorescent intensity levels were already increased after the handling time of roughly 45 min of encapsulation and microscopy setup. (Fig.A.1.10)

The *in vesiculo* expression of fluorescent proteins appears to show a linear correlation between the intensity levels and the overall volume of the individual compartement which is depicted in Fig.4.4.4 c. This behavior is comparable to the observations made for the encapsulated IVT reactions in Fig.4.4.3 a. This in turn also speaks for the hypothesis of the connection between the accumulation of biopolymers and osmotically driven growth of the whole vesicle. Keeping in mind the complexity introduced by CFE, different dynamics in the changes of osmotic pressures were expected due to the multitude of different biochemical reactions within the GUV. This shows in the low numbers of shrinking vesicles over the time

scale of 15 h, where the vesicles enter a plateau phase after roughly 2 h in both size and fluorescent intensity depicted in Fig.A.1.8. The overall exhaustion of essential reagents like tRNA or nucleotides within the vesicles leads to a diminished production of bioploymers and therefore a decreased influx of water. Looking at these different behaviors of the vesicles with encapsulated enzymatic reaction systems, shows that a potential factor for the stability of the vesicles is not only the availability of ELPs but also the complexity of reactions contributing to the osmotic pressure differences.

The encapsulation of CFE reaction systems within peptide-based vesicles shows the possibility of gene expression within these artificial compartments. The stability of the ELP membrane seems to withstand the stress exerted by the differences in osmotic pressure between the inside and the outside of the vesicle. By verifying the ability to express proteins within a stable compartment could lead to even more detailed interaction networks. The implementation of continous production of membrane monomers within, which was already demonstrated at a nm scale, [99] could provide a way to promote membrane interactions. This way we could approach a responsive cell-like compartment step by step where individual components of the systems were tested inside of ELP vesicles or on the surface of lipid, ELP or hybrid membranes.

5. Conclusion and Outlook

5.1. Conclusion

During this work, one major goal was the creation of cell-sized vesicles capable of interacting with their environment. For this behavior several intermediate steps leading to more complex interactions were made. First, the compatibility of polypeptides and phospholipids to form stable vesicle membranes was ascertained, before streptavidin interaction with these hybrid membranes was proven. Molecular fluorescent biotin probes were localized on the membrane surface with streptavidin as linker molecule. Additionally, the interaction of a specific multivalent RNA aptamer enabled the co-localization of two separate fluorescent molecules on the vesicle membrane.

With the same RNA aptamer structure the split peroxidase sAPEX2 was reconstituted, which provided switchable enzyme activity. The reconstituted split enzyme was able to catalyze the conversion of Amplex Red to resorufin as well as the biotinylation of BSA and ELP monomers used to form hybrid membranes. Here, still some optimization needs to be done in respect to switchability of the enzymatic activity and reduction of unspecific reactions. Furthermore, final measurements combining the enzymatic system with the formed hybrid vesicles have to to be conducted.

The second part of the project was the encapsulation of active enzymatic reaction mimicking essential cellular processes within biocompatible ELP vesicles. These essential processes included the active transcription of RNA and the expression of YPET using CFE. The encapsulation of these cell-derived mechanisms shows the potential of the polypeptide vesicles in respect to the creation of artificial cells. Further, substantial growth of vesicles in prescence of active processes within was shown in time lapse microscopy. As possible reason of the vesicle growth, the increase of osmotic pressure due to bio-polymerization of nucleic acids and polypeptides leading to an increased influx of water was detected. In case of IVT experiments the growth process was influenced by the concentration of ELP vesicles and monomers within the sample. The growth behavior changed in case of monomer depletion and led to shrinkage and eventually to disappearance. The stability the ELP membranes displayed during this dynamic process was vital for the process.

5.2. Outlook

Over the course of this thesis, several subprojects have been initiated, but acquired data did not as yet allow to conclusively verify all stated functionalities. Within the following section, an overview over all data collected from these subprojects are given and brief resumes are drawn.

Membrane Interactions with Nucleic Acids

The compatibility of IVT activity with modified membrane components was tested by production of a fluorescent aptamer with a biotinylated ligand as depicted in Fig.5.2.1 a. For this system Mango-III was transcribed in the outer solution of the vesicle while its ligand biotinylated thiazole orange 1 (TO1) was bound at the membrane surface. [215] Initial tests showed increased fluorescence on the membrane surface, but could not provide further increase over time. Negative controls conducted with the biotinylated ligand alone showed no increased fluorescence on the membrane surface as depicted in Fig.A.1.12. From this it can be derived, that in-vitro transcriptions can in general be applied in the vicinity of membrane bound nucleic acids. With this, all individual components for the colocalization of split-enzymes with *in-vitro* transcribed pRNA on hybrid membranes were shown. In future experiments, the complete setup can be tested and all necessary negative controls performed. This process could provide an addition to the project discussed in chapter 4.2 where the on site transcription of the RNA aptamer provides new functionalities.

As several publications have shown the ability to bind DNA nanostructures on liposome surfaces, the compatibility of these structures and hybrid membranes was tested. [216] Brick-shaped nanostructures (5 MDa) containing biotinylated and fluorescently labeled staple strands (Atto633) available in the lab were bound to the membrane surface via streptavidin-biotin interactions. [217] The schematic draft of this interaction and the microscopy image of initial experiments with DNA nanostructures on the membrane surface are depicted in 5.2.1 b. The combination of DNA scaffold structures with hybrid membranes could pose a valid approach to produce cortex-like properties in artificial compartments. [218]

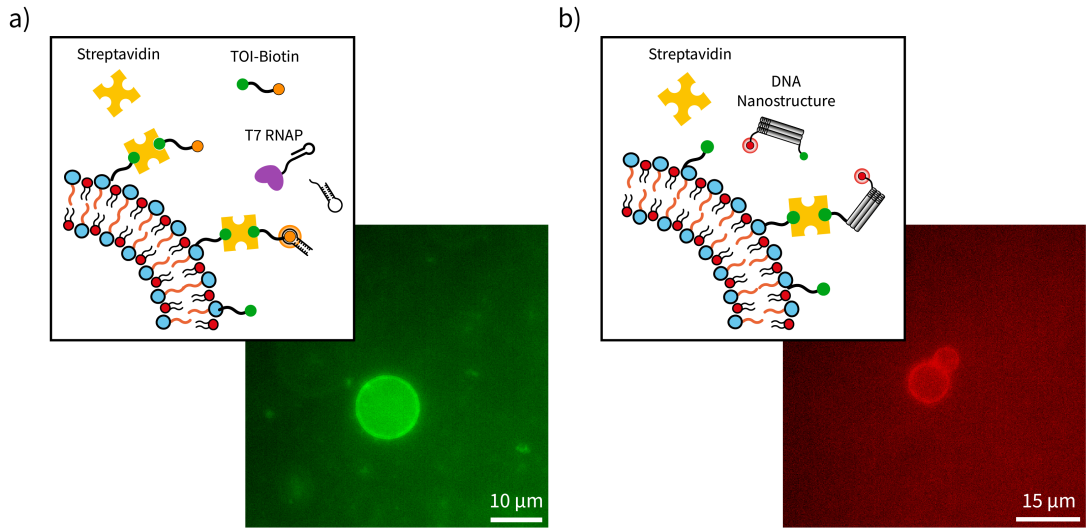

Figure 5.2.1: Membrane Interactions: *a) Schematic overview of labeling process using IVT with Mango-III. Micrograph of vesicle in GFP channel 10 min after start of IVT reaction. Scale bar: 10 µm b) Schematic overview of surface binding of biotinylated DNA nanostructures. Micrograph of vesicle in Cy5 channel after incubation with streptavidin and biotinylated DNA nanostructure. Scale bar: 15 µm.*

Deformation of Vesicles in Electric Fields

Deformation of hybrid and ELP membranes in electric fields was tested to assess the changes of material properties to external stimuli. While for hybrid membranes applied direct current (DC) fields result in no observable deformaion due to extreme induced solvent flux (data not shown), the alternating current (AC) induced deformation can be observed clearly as depicted in Fig.5.2.2 a. [219]

In contrast, ELP vesicles shown in Fig.5.2.2 b present an even more pronounced deformation in an applied DC field, but do not visibly react with deformation to an applied AC field (data not shown). While hybrid membranes only showed elongation up to a certain degree, ELP vesicles presented budding in DC fields with increasing voltage.

These initial results are pointing towards the potential of further study of phase behavior and membrane properties of ELPs. [220] [221]

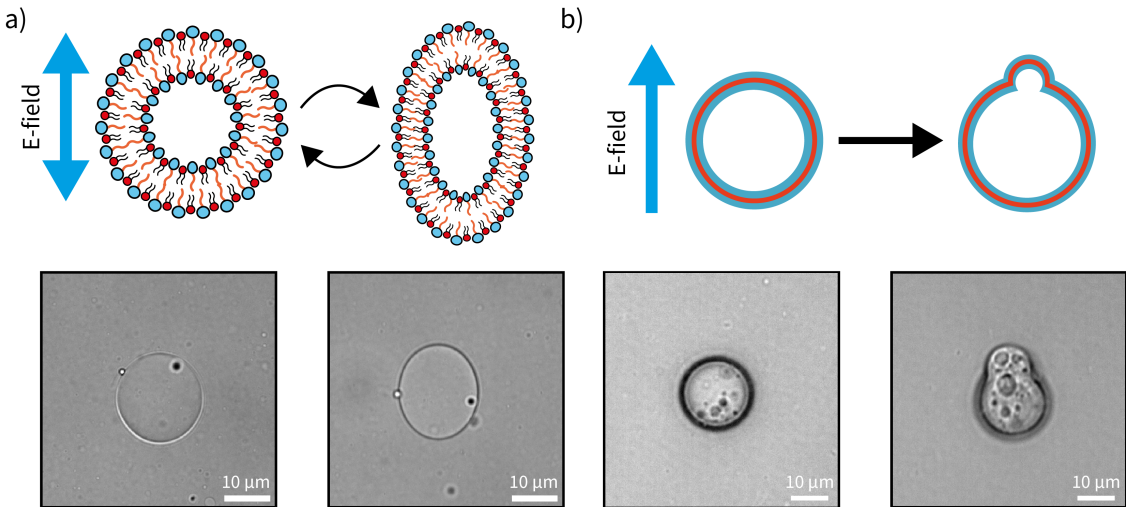

Figure 5.2.2: Deformation in Electric Fields: *Schematic behavior of hybrid (a) and ELP (b) vesicles in electric fields. Micrographs of vesicles in nuclease free water in an alternating current at a voltage of 500 V (a) and direct current (d) fields, showing different degrees of deformation. Scale bar: 10 µm.*

Versatility of Vesicle Applications

Summarizing, it can be said that the vesicles produced during this thesis provide a wide range of beneficial characteristics for applications in synthetic biology. These range from increased stability of polypeptide vesicles to the potential of self-modification using RNA mediated split enzyme reconstitution. As the necessity for novel material properties rises in different fields like drug delivery, there is an increasing interest in responsive and biocompatible systems. [31] [222] Composite materials like ELP-lipid vesicle membranes can provide much needed designability alongside biocompatibility and might play a major role in future drug development.

Publications

During the course of this thesis one publication centered around the production of ELP-based vesicles was published and contributions to two further publications were made:

Growth of Giant Peptide Vesicles Driven by Compartmentalized Transcription–Translation Activity

Thomas Frank, Kilian Vogele, Aurore Dupin, Friedrich C. Simmel, and Tobias Pirzer,
Chemistry - A European Journal, Wiley, Volume 26, Issue 72 (2020) ISSN:1521-3765; DOI:10.1002/CHEM.202003366 under licence CC BY 4.0

In Vesiculo Synthesis of Peptide Membrane Precursors for Autonomous Vesicle Growth

Kilian Vogele,**Thomas Frank**, Lukas Gasser, Marisa A. Goetzfried, Mathias W. Hackl, Stephan A. Sieber, Friedrich C. Simmel, and Tobias Pirzer,
Journal of Visualized Experiments (148), (2019) ISSN:1940087X; DOI:10.3791/59831

Towards synthetic cells using peptide-based reaction compartments

Kilian Vogele,**Thomas Frank**, Lukas Gasser, Marisa A. Goetzfried, Mathias W. Hackl, Stephan A. Sieber, Friedrich C. Simmel, and Tobias Pirzer,
Nature Communications, Springer US, 9, 3862 (2018) ISSN:20411723; DOI:10.1038/s41467-018-06379-8

List of Figures

2.1.1 Packing Parameters 17
2.1.2 Overview Lipids 20
2.1.3 Overview Liposome Polymersome 23
2.2.1 Phase Separation 29
2.2.2 Phase Separation in hybrid membranes 30
2.2.3 This Caption is in Table of Figures 34
2.3.1 Gene Regulation 37
2.4.1 Overview CFE 41
3.3.1 GUV formation protocol 46
4.1.1 Size Distribution of ELP based vesicles 54
4.1.2 Size Distribution of GUVs 55
4.1.3 Fluorescence-labeled GUVs 56
4.2.1 Interactions on Membrane Surface 58
4.2.2 Hybrid Membrane 59
4.2.3 Co-Localization 61
4.3.1 sAPEX2 reconstitution 63
4.4.1 *In vitro* Transcription encapsulated in GUV 66
4.4.2 Transcription-driven growth of GUV 67
4.4.3 ELP dependent Growth 70
4.4.4 Cell-free gene expression 72
5.2.1 Membrane Interactions 77
5.2.2 Deformation in Electric Fields 78
A.1.1 Negative Control Biotin-Streptavidin Binding 109
A.1.2 Negative Control Co-Localization 110
A.1.3 Size DLS 110
A.1.4 Negative Control Size 111
A.1.5 Plate Reader IVT 111
A.1.6 Vesicle Growth IVT 112

A.1.7 Fusion Growth IVT 112
A.1.8 Vesicle Growth CFE 113
A.1.9 Scatter Plot Growth CFE 114
A.1.10 Plate Reader CFE 114
A.1.11 Negative Control DNA Nanostructure Binding 115
A.1.12 Thiazol-Orange 1 Fluorescence 115

List of Tables

3.4.1 In vitro Transcription (IVT) of fluorescent RNA aptamer dBroccoli 47
3.4.2 In vitro Transcription (IVT) of fluorescent RNA aptamer iMango-III 47
3.4.3 In vitro Transcription of multivalent pRNA aptamers 48
3.5.1 Cell-Free Expression of proteins 48
3.6.1 sAPEX2 Amplex Red Assay 49
3.6.2 sAPEX2 Amplex Red Assay with GOX 50
3.6.3 sAPEX2 Biotinylation 51
A.2.1 Composition Lysis Buffer 116
A.2.2 Composition Washing Buffer 116
A.2.3 Composition Elution Buffer 116
A.2.4 Composition Gel Filtration Buffer 116
A.2.5 Composition 5xQuenching Buffer 117
A.2.6 Composition Transfer Buffer (Western Blot) 117
A.3.1 Templates RNA Aptamers 117
A.3.3 Plasmids Protein Expression 118
A.4.1 Composition Liposomes 123
A.4.3 Composition ELP Vesicles 123
A.4.5 Composition Hybrid Vesicles 123

Glossary

E. coli	*Escherichia coli*
APEX	Ascorbate Peroxidase
Bio-AMP	Biotinoyl-adenylate monophosphate
Bio-ID	Biotin Identification
CFE	Cell-free Gene Expression
CuAAC	Cu(I)-catalyzed azide alkyne Huisgen cycloaddition
DNA	Deoxyribonucleic Acid
DOPE	1,2-dioleoyl-sn-glycero-3-phosphoethanolamine
DOPS	1,2-dioleoyl-sn-glycero-3-phospho-L-serine
EDTA	Ethylenediaminetetraacetic Acid
EX-C	C-terminal split enzyme of sAPEX2
GFP	Green Fluorescent Protein
GHUV	Giant Hybrid Unilamellar Vesicles
HRP	Horseradish Peroxidase
IMAC	Immobilized Metal Affinity Chromatography
IPTG	Isopropyl β-D-1-thiogalactopyranoside
IS	Inner Solution
IVT	In vitro Transcription
L_d	liquid-disordered phase
L_o	liquid-ordered phase
LB	Lysogeny Broth
LCST	Lower Critical Solution Temperature
mRNA	messenger RNA
MW	Molecular Weight
N-AP	N-terminal split enzyme of sAPEX2
NHS	N-Hydroxysuccinimide
PBS	Phosphate-buffered saline
PEG	Polyethylene Glycol
PVDF	Polyvinylidene Fluoride
RhoB	Lissamine rhodamine B
RT	Room Temperature
RNA	Ribonucleic Acid

SDS-PAGE	Sodium Dodecyl Sulfate Polyacrylamide Gel Electrophoresis
SEC	Size Exclusion
SELEX	Systematic Evolution of Ligands by Exponential Enrichment
TEM	Transmission Electron Microscopy
TCEP	Tris-(2-carboxyethyl)-phosphine
THF	Tetrahydrofuran
THPTA	Tris(3-hydroxypropyltriazolylmethyl)amine

Bibliography

[1] Michael Cuffe et al. *Cell*. 2022.

[2] Francis Crick. "Central Dogma of Molecular Biology". In: *Nature 1970 227:5258* 227.5258 (1970), pp. 561–563. ISSN: 1476-4687. DOI: 10.1038/227561a0.

[3] Alison C. Lloyd. "XThe regulation of cell size". In: *Cell* 154.6 (Sept. 2013), p. 1194. ISSN: 10974172. DOI: 10.1016/j.cell.2013.08.053.

[4] Nimrat Chatterjee and Graham C. Walker. "Mechanisms of DNA damage, repair, and mutagenesis". In: *Environmental and Molecular Mutagenesis* 58.5 (June 2017), pp. 235–263. ISSN: 1098-2280. DOI: 10.1002/EM.22087.

[5] Aubrey D. N. J. de Grey and Michael J. Rae. "Cellular Repair Processes". In: *Encyclopedia of Gerontology and Population Aging* (2021), pp. 877–887. DOI: 10.1007/978-3-030-22009-9_436.

[6] Jonathan M.W. Slack. "Metaplasia and transdifferentiation: from pure biology to the clinic". In: *Nature Reviews Molecular Cell Biology 2007 8:5* 8.5 (Mar. 2007), pp. 369–378. ISSN: 1471-0080. DOI: 10.1038/nrm2146.

[7] J. M. W. (Jonathan Michael Wyndham) Slack. "Essential developmental biology". In: (2006), p. 365.

[8] Paul D Boyer. "THE ATP SYNTHASE-A SPLENDID MOLECULAR MACHINE". In: *Annu. Rev. Biochem* 66 (1997), pp. 717–766.

[9] Kristen L. Pierce, Richard T. Premont, and Robert J. Lefkowitz. "Seven-transmembrane receptors". In: *Nature Reviews Molecular Cell Biology* 3.9 (Sept. 2002), pp. 639–650. ISSN: 1471-0080. DOI: 10.1038/nrm908.

[10] Cameron C. Scott, Fabrizio Vacca, and Jean Gruenberg. "Endosome maturation, transport and functions". In: *Seminars in Cell & Developmental Biology* 31 (July 2014), pp. 2–10. ISSN: 1084-9521. DOI: 10.1016/J.SEMCDB.2014.03.034.

[11] Ying Wang et al. "B Cell Development and Maturation". In: *Advances in Experimental Medicine and Biology* 1254 (2020), pp. 1–22. ISSN: 22148019. DOI: 10.1007/978-981-15-3532-1_1/COVER.

[12] Guillaume Salbreux, Guillaume Charras, and Ewa Paluch. "Actin cortex mechanics and cellular morphogenesis". In: *Trends in Cell Biology* 22.10 (Oct. 2012), pp. 536–545. ISSN: 0962-8924. DOI: 10.1016/J.TCB.2012.07.001.

[13] András Kapus and Paul Janmey. "Plasma Membrane-Cortical Cytoskeleton Interactions: A Cell Biology Approach with Biophysical Considerations". In: *Compr Physiol* 3 (2013), pp. 1231–1281. DOI: 10.1002/cphy.c120015.

[14] Y. Nakaseko and M. Yanagida. “Cytoskeleton in the cell cycle”. In: *Nature 2001 412:6844* 412.6844 (July 2001), pp. 291–292. ISSN: 1476-4687. DOI: 10.1038/35085684.

[15] Graham Warren. “MEMBRANE PARTITIONING DURING CELL DIVISION”. In: *Annual Review of Biochemistry* 62.1 (June 1993), pp. 323–348. ISSN: 0066-4154. DOI: 10.1146/annurev.bi.62.070193.001543.

[16] Jon Holy and Ed Perkins. “Structure and function of the nucleus and cell organelles”. In: *Bioinformatics for Systems Biology*. Vol. 9781597454. Humana Press Inc., 2009, pp. 3–31. ISBN: 9781597454407. DOI: 10.1007/978-1-59745-440-7_1/COVER.

[17] Martin Lowe. “Structural organization of the Golgi apparatus”. In: *Current Opinion in Cell Biology* 23.1 (Feb. 2011), pp. 85–93. ISSN: 0955-0674. DOI: 10.1016/J.CEB.2010.10.004.

[18] Dianne S. Schwarz and Michael D. Blower. “The endoplasmic reticulum: structure, function and response to cellular signaling”. In: *Cellular and Molecular Life Sciences 2015 73:1* 73.1 (Oct. 2015), pp. 79–94. ISSN: 1420-9071. DOI: 10.1007/S00018-015-2052-6.

[19] Emeline Rideau et al. “Liposomes and polymersomes: a comparative review towards cell mimicking”. In: *Chemical Society Reviews* (2018). ISSN: 10897550. DOI: 10.1063/1.4892631.

[20] J-F Le Meins et al. “Hybrid polymer/lipid vesicles: state of the art and future perspectives”. In: *Materials Today* 16 (2013). DOI: 10.1016/j.mattod.2013.09.002.

[21] Yashar Bashirzadeh and Allen P. Liu. “Encapsulation of the cytoskeleton: towards mimicking the mechanics of a cell”. In: *Soft Matter* 15.42 (Oct. 2019), pp. 8425–8436. ISSN: 1744-6848. DOI: 10.1039/C9SM01669D.

[22] Vincent Delatour et al. “Arp2/3 Controls the Motile Behavior of N-WASP-Functionalized GUVs and Modulates N-WASP Surface Distribution by Mediating Transient Links with Actin Filaments”. In: *Biophysical Journal* 94.12 (June 2008), pp. 4890–4905. ISSN: 0006-3495. DOI: 10.1529/BIOPHYSJ.107.118653.

[23] Eunhee Cho and Yuan Lu. “Compartmentalizing cell-free systems: Toward creating life-like artificial cells and beyond”. In: *ACS Synthetic Biology* 9.11 (Nov. 2020), pp. 2881–2901. ISSN: 21615063. DOI: 10.1021/ACSSYNBIO.0C00433/ASSET/IMAGES/LARGE/SB0C00433_0005.JPEG.

[24] Simon Kretschmer et al. “Synthetic cell division via membrane-transforming molecular assemblies”. In: *BMC Biology 2019 17:1* 17.1 (May 2019), pp. 1–10. ISSN: 1741-7007. DOI: 10.1186/S12915-019-0665-1.

[25] Roberto J. Brea et al. “In Situ Reconstitution of the Adenosine A2A Receptor in Spontaneously Formed Synthetic Liposomes”. In: *Journal of the American Chemical Society* 139.10 (Mar. 2017), pp. 3607–3610. ISSN: 15205126. DOI: 10.1021/JACS.6B12830/SUPPL_FILE/JA6B12830_SI_001.PDF.

[26] Qiang Yan and Yue Zhao. “Block copolymer self-assembly controlled by the “green” gas stimulus of carbon dioxide”. In: *Chemical Communications* 50.79 (Sept. 2014), pp. 11631–11641. ISSN: 1364-548X. DOI: 10.1039/C4CC03412K.

[27] Carina I.C. Crucho. “Stimuli-Responsive Polymeric Nanoparticles for Nanomedicine”. In: *ChemMedChem* 10.1 (Jan. 2015), pp. 24–38. ISSN: 1860-7187. DOI: 10.1002/CMDC.201402290.

[28] Marzieh Mohammadi et al. “Hybrid Vesicular Drug Delivery Systems for Cancer Therapeutics”. In: *Advanced Functional Materials* 28.36 (Sept. 2018), p. 1802136. ISSN: 1616-3028. DOI: 10.1002/ADFM.201802136.

[29] Vincenzo De Leo et al. “Recent Advancements in Polymer/Liposome Assembly for Drug Delivery: From Surface Modifications to Hybrid Vesicles”. In: *Polymers 2021, Vol. 13, Page 1027* 13.7 (Mar. 2021), p. 1027. ISSN: 2073-4360. DOI: 10.3390/POLYM13071027.

[30] Hailong Che and Jan C.M. Van Hest. “Stimuli-responsive polymersomes and nanoreactors”. In: *Journal of Materials Chemistry B* 4.27 (July 2016), pp. 4632–4647. ISSN: 2050-7518. DOI: 10.1039/C6TB01163B.

[31] José Carlos Rodríguez-Cabello et al. “Elastin-like polypeptides in drug delivery”. In: *Advanced Drug Delivery Reviews* 97 (Feb. 2016), pp. 85–100. ISSN: 0169-409X. DOI: 10.1016/J.ADDR.2015.12.007.

[32] Jeanne C. Stachowiak et al. “Membrane bending by protein–protein crowding”. In: *Nature Cell Biology 2012 14:9* 14.9 (Aug. 2012), pp. 944–949. ISSN: 1476-4679. DOI: 10.1038/ncb2561.

[33] Reinhard Lipowsky. “Remodeling of Membrane Shape and Topology by Curvature Elasticity and Membrane Tension”. In: *Advanced Biology* 6.1 (2022). ISSN: 27010198. DOI: 10.1002/adbi.202101020.

[34] BY E Gorter and F Grendel. “ON BIMOLECULAR LAYERS OF LIPOIDS ON THE CHROMO-CYTES OF THE BLOOD”. In: ().

[35] Jérome Garin et al. “The Phagosome ProteomeInsight into Phagosome Functions”. In: *Journal of Cell Biology* 152.1 (Jan. 2001), pp. 165–180. ISSN: 0021-9525. DOI: 10.1083/JCB.152.1.165.

[36] Vojo Deretic. “Autophagosome and phagosome”. In: *Methods in Molecular Biology* 445 (2008), pp. 1–9. ISSN: 10643745. DOI: 10.1007/978-1-59745-157-4_1/FIGURES/1_3_978-1-59745-157-4.

[37] Jacob N. Israelachvili. *Soft and Biological Structures*. 2011, pp. 535–576. ISBN: 9780123751829. DOI: 10.1016/b978-0-12-375182-9.10020-x.

[38] Dennis E. Discher and Fariyal Ahmed. “POLYMERSOMES”. In: *Annual Review of Biomedical Engineering* 8 (July 2006), pp. 323–341. ISSN: 15239829. DOI: 10.1146/ANNUREV.BIOENG.8.061505.095838.

[39] Aldo Jesorka and Owe Orwar. “Liposomes: Technologies and Analytical Applications”. In: (). DOI: 10.1146/annurev.anchem.1.031207.112747.

[40] Rona Chandrawati and Frank Caruso. “Biomimetic liposome- and polymersome-based multicompartmentalized assemblies”. In: *Langmuir* 28.39 (Oct. 2012), pp. 13798–13807. ISSN: 07437463. DOI: 10.1021/LA301958V/ASSET/IMAGES/LARGE/LA-2012-01958V_0006.JPEG.

[41] Martin Loose, Karsten Kruse, and Petra Schwille. “Protein Self-Organization:Lessons from the Min System”. In: *Annu. Rev. Biophys* 40 (2011), pp. 315–336. DOI: 10.1146/annurev-biophys-042910-155332.

[42] Eoin Fahy et al. “A comprehensive classification system for lipids1”. In: *Journal of Lipid Research* 46.5 (May 2005), pp. 839–861. ISSN: 0022-2275. DOI: 10.1194/JLR.E400004-JLR200.

[43] Kai Simons and Winchil L.C. Vaz. “Model systems, lipid rafts, and cell membranes”. In: *Annual Review of Biophysics and Biomolecular Structure* 33 (2004), pp. 269–295. ISSN: 10568700. DOI: 10.1146/annurev.biophys.32.110601.141803.

[44] Marek Cebecauer et al. “Membrane Lipid Nanodomains”. In: *Chemical Reviews* 118.23 (2018), pp. 11259–11297. ISSN: 15206890. DOI: 10.1021/acs.chemrev.8b00322.

[45] Andrea Alessandrini and Paolo Facci. “Phase transitions in supported lipid bilayers studied by AFM”. In: *Soft Matter* 10.37 (2014), pp. 7145–7164. ISSN: 17446848. DOI: 10.1039/c4sm01104j.

[46] John S. Allhusen and John C. Conboy. “The ins and outs of lipid flip-flop”. In: *Accounts of Chemical Research* 50.1 (Jan. 2017), pp. 58–65. ISSN: 15204898. DOI: 10.1021/ACS.ACCOUNTS.6B00435/ASSET/IMAGES/MEDIUM/AR-2016-00435K_0011.GIF.

[47] Muhammad Jan Akhunzada et al. “Interplay between lipid lateral diffusion, dye concentration and membrane permeability unveiled by a combined spectroscopic and computational study of a model lipid bilayer”. In: *Scientific Reports 2019 9:1* 9.1 (Feb. 2019), pp. 1–12. ISSN: 2045-2322. DOI: 10.1038/s41598-018-37814-x.

[48] Angus I. Lamond. “Swimming lessons”. In: *Nature 2002 417:6887* 417.6887 (May 2002), pp. 383–383. ISSN: 1476-4687. DOI: 10.1038/417383a.

[49] Aditya G. Kohli et al. “Designer lipids for drug delivery: From heads to tails”. In: *Journal of Controlled Release* 190 (Sept. 2014), pp. 274–287. ISSN: 0168-3659. DOI: 10.1016/J.JCONREL.2014.04.047.

[50] Cornelia G. Palivan et al. “Bioinspired polymer vesicles and membranes for biological and medical applications”. In: *Chemical Society Reviews* 45.2 (2016), pp. 377–411. ISSN: 14604744. DOI: 10.1039/c5cs00569h.

[51] Caterina LoPresti et al. “Polymersomes: nature inspired nanometer sized compartments”. In: *Journal of Materials Chemistry* 19.22 (June 2009), pp. 3576–3590. ISSN: 1364-5501. DOI: 10.1039/B818869F.

[52] Cornelia G. Palivan et al. “Protein–polymer nanoreactors for medical applications”. In: *Chemical Society Reviews* 41.7 (Mar. 2012), pp. 2800–2823. ISSN: 1460-4744. DOI: 10.1039/C1CS15240H.

[53] Chuanlong Li et al. “Self-assembly and functionalization of alternating copolymer vesicles”. In: *Polymer Chemistry* 8.32 (Aug. 2017), pp. 4688–4695. ISSN: 1759-9962. DOI: 10.1039/C7PY00908A.

[54] Dan Wu et al. “Alternating polymer vesicles”. In: *Soft Matter* 4.5 (Apr. 2008), pp. 1066–1071. ISSN: 1744-6848. DOI: 10.1039/B715608A.

[55] Matthias Schulz and Wolfgang H. Binder. “Mixed hybrid lipid/polymer vesicles as a novel membrane platform”. In: *Macromolecular Rapid Communications* 36.23 (Dec. 2015), pp. 2031–2041. ISSN: 15213927. DOI: 10.1002/MARC.201500344.

[56] Fabian Itel et al. “Molecular organization and dynamics in polymersome membranes: A lateral diffusion study”. In: *Macromolecules* 47.21 (2014), pp. 7588–7596. ISSN: 15205835. DOI: 10.1021/ma5015403.

[57] Thomas Smart et al. “Block copolymer nanostructures”. In: *Nano Today* 3.3-4 (June 2008), pp. 38–46. ISSN: 1748-0132. DOI: 10.1016/S1748-0132(08)70043-4.

[58] Harry Bermudez et al. “Molecular weight dependence of polymersome membrane structure, elasticity, and stability”. In: *Macromolecules* 35.21 (2002), pp. 8203–8208. ISSN: 00249297. DOI: 10.1021/ma020669l.

[59] Goundla Srinivas, Dennis E. Discher, and Michael L. Klein. “Self-assembly and properties of diblock copolymers by coarse-grain molecular dynamics”. In: *Nature Materials 2004 3:9* 3.9 (Aug. 2004), pp. 638–644. ISSN: 1476-4660. DOI: 10.1038/nmat1185.

[60] Ludwig Klermund and Kathrin Castiglione. “Polymersomes as nanoreactors for preparative biocatalytic applications: current challenges and future perspectives”. In: *Bioprocess and Biosystems Engineering 2018 41:9* 41.9 (May 2018), pp. 1233–1246. ISSN: 1615-7605. DOI: 10.1007/S00449-018-1953-9.

[61] Regina Bleul, Raphael Thiermann, and Michael Maskos. “Techniques To Control Polymersome Size”. In: (2015). DOI: 10.1021/acs.macromol.5b01500.

[62] Tamuka Chidanguro and Yoan C. Simon. “Bent out of shape: towards non-spherical polymersome morphologies”. In: *Polymer International* 70.7 (July 2021), pp. 951–957. ISSN: 10970126. DOI: 10.1002/PI.6203.

[63] Giulio Biroli and Juan P. Garrahan. “Perspective: The glass transition”. In: *The Journal of Chemical Physics* 138.12 (Mar. 2013), 12A301. ISSN: 0021-9606. DOI: 10.1063/1.4795539.

[64] R Dimova et al. “Hyperviscous diblock copolymer vesicles”. In: *The European Physical Journal E* 7.3 (2002), pp. 241–250. ISSN: 1292-8941. DOI: 10.1140/epje/i200101032.

[65] H Bermú Dez, D A Hammer, and D E Discher. “Effect of Bilayer Thickness on Membrane Bending Rigidity”. In: (2004). DOI: 10.1021/la035497f.

[66] Giuseppe Battaglia and Anthony J. Ryan. “Bilayers and interdigitation in block copolymer vesicles”. In: *Journal of the American Chemical Society* 127.24 (June 2005), pp. 8757–8764. ISSN: 00027863. DOI: 10.1021/JA050742Y/ASSET/IMAGES/MEDIUM/JA050742YN00001.GIF.

[67] Manish Kumar et al. “Highly permeable polymeric membranes based on the incorporation of the functional water channel protein Aquaporin Z”. In: *Proceedings of the National Academy of Sciences of the United States of America* 104.52 (Dec. 2007), pp. 20719–20724. ISSN: 00278424. DOI: 10.1073/PNAS.0708762104/ASSET/F0D41687-55E7-44A3-8F0C-7AEC11DEE0B0/ASSETS/GRAPHIC/ZPQ05207-8662-M01.JPEG.

[68] Kamal Kumar Upadhyay et al. “The in vivo behavior and antitumor activity of doxorubicin-loaded poly(γ-benzyl l-glutamate)-block-hyaluronan polymersomes in Ehrlich ascites tumor-bearing BalB/c mice”. In: *Nanomedicine: Nanotechnology, Biology, and Medicine* 8.1 (Jan. 2012), pp. 71–80. ISSN: 1549-9634. DOI: 10.1016/j.nano.2011.05.008.

[69] Hyun Ouk Kim et al. “A biodegradable polymersome containing Bcl-xL siRNA and doxorubicin as a dual delivery vehicle for a synergistic anticancer effect”. In: *Macromolecular Bioscience* 13.6 (June 2013), pp. 745–754. ISSN: 16165187. DOI: 10.1002/mabi.201200448.

[70] Alisha J. Miller et al. “Probing and Tuning the Permeability of Polymersomes”. In: *ACS Central Science* 7.1 (2021), pp. 30–38. ISSN: 23747951. DOI: 10.1021/acscentsci.0c01196.

[71] Lei Wang et al. “Acid-Disintegratable Polymersomes of pH-Responsive Amphiphilic Diblock Copolymers for Intracellular Drug Delivery”. In: *Macromolecules* 48.19 (2015), pp. 7262–7272. ISSN: 15205835. DOI: 10.1021/acs.macromol.5b01709.

[72] Hugo Oliveira et al. “Magnetic field triggered drug release from polymersomes for cancer therapeutics”. In: *Journal of Controlled Release* 169.3 (Aug. 2013), pp. 165–170. ISSN: 18734995. DOI: 10.1016/j.jconrel.2013.01.013.

[73] Dennis M Vriezema et al. “Positional assembly of enzymes in polymersome nanoreactors for cascade reactions”. In: *Angewandte Chemie - International Edition* 46.39 (2007), pp. 7378–7382. ISSN: 14337851. DOI: 10.1002/anie.200701125.

[74] Paul A Beales et al. “Durable vesicles for reconstitution of membrane proteins in biotechnology”. In: (2017). DOI: 10.1042/BST20160019.

[75] Dan W. Urry. “On the molecular mechanisms of elastin coacervation and coacervate calcification”. In: *Faraday Discussions of the Chemical Society* 61.0 (Jan. 1976), pp. 205–212. ISSN: 0301-7249. DOI: 10.1039/DC9766100205.

[76] Dan E. Meyer and Ashutosh Chilkoti. “Quantification of the effects of chain length and concentration on the thermal behavior of elastin-like polypeptides”. In: *Biomacromolecules* 5.3 (May 2004), pp. 846–851. ISSN: 15257797. DOI: 10.1021/BM034215N/SUPPL_FILE/BM034215NSI20031125_032417.PDF.

[77] Nan K. Li et al. “Sequence Directionality Dramatically Affects LCST Behavior of Elastin-Like Polypeptides”. In: *Biomacromolecules* 19.7 (July 2018), pp. 2496–2505. ISSN: 15264602. DOI: 10.1021/ACS.BIOMAC.8B00099/ASSET/IMAGES/LARGE/BM-2018-00099C_0006.JPEG.

[78] Dan W. Urry. “Physical chemistry of biological free energy transduction as demonstrated by elastic protein-based polymers”. In: *Journal of Physical Chemistry B* 101.51 (Dec. 1997), pp. 11007–11028. ISSN: 15206106. DOI: 10.1021/JP972167T/ASSET/IMAGES/LARGE/JP972167TF00016.JPEG.

[79] Javier Reguera et al. “Effect of NaCl on the exothermic and endothermic components of the inverse temperature transition of a model elastin-like polymer”. In: *Biomacromolecules* 8.2 (Feb. 2007), pp. 354–358. ISSN: 15257797. DOI: 10.1021/BM060936L/ASSET/IMAGES/MEDIUM/BM060936LN00001.GIF.

[80] J. Andrew MacKay et al. “Quantitative model of the phase behavior of recombinant pH-responsive elastin-like polypeptides”. In: *Biomacromolecules* 11.11 (Nov. 2010), pp. 2873–2879. ISSN: 15264602. DOI: 10.1021/BM100571J/SUPPL_FILE/BM100571J_SI_001.PDF.

[81] Alessandra Girotti et al. “Influence of the molecular weight on the inverse temperature transition of a model genetically engineered elastin-like pH-responsive polymer”. In: *Macromolecules* 37.9 (May 2004), pp. 3396–3400. ISSN: 00249297. DOI: 10.1021/MA035603K/ASSET/IMAGES/LARGE/MA035603KF00007.JPEG.

[82] K. Trabbic-Carlson et al. “Effect of protein fusion on the transition temperature of an environmentally responsive elastin-like polypeptide: a role for surface hydrophobicity?” In: *Protein Engineering, Design and Selection* 17.1 (Jan. 2004), pp. 57–66. ISSN: 1741-0126. DOI: 10.1093/PROTEIN/GZH006.

[83] Younhee Cho et al. “Effects of hofmeister anions on the phase transition temperature of elastin-like polypeptides”. In: *Journal of Physical Chemistry B* 112.44 (Nov. 2008), pp. 13765–13771. ISSN: 15206106. DOI: 10.1021/JP8062977/SUPPL_FILE/JP8062977_SI_001.PDF.

[84] C. M. Venkatachalam and D. W. Urry. “Development of a Linear Helical Conformation from Its Cyclic Correlate. β-Spiral Model of the Elastin Poly(pentapeptide) (VPGVG)n”. In: *Macromolecules* 14.5 (1981), pp. 1225–1229. ISSN: 15205835. DOI: 10.1021/MA50006A017/ASSET/MA50006A017.FP.PNG_V03.

[85] Dan W. Urry. “Entropic elastic processes in protein mechanisms. I. Elastic structure due to an inverse temperature transition and elasticity due to internal chain dynamics”. In: *Journal of Protein Chemistry 1988 7:1* 7.1 (Feb. 1988), pp. 1–34. ISSN: 1875-8355. DOI: 10.1007/BF01025411.

[86] X. L. Yao and M. Hong. “Structure Distribution in an Elastin-Mimetic Peptide (VPGVG)3 Investigated by Solid-State NMR”. In: *Journal of the American Chemical Society* 126.13 (Apr. 2004), pp. 4199–4210. ISSN: 00027863. DOI: 10.1021/JA036686N/ASSET/IMAGES/MEDIUM/JA036686NN00001.GIF.

[87] Peter C. Groß, Wulff Possart, and Michael Zeppezauer. “An Alternative Structure Model for the Polypentapeptide in Elastin”. In: *Zeitschrift fur Naturforschung - Section C Journal of Biosciences* 58.11-12 (Dec. 2003), pp. 873–878. ISSN: 09395075. DOI: 10.1515/ZNC-2003-11-1223/MACHINEREADABLECITATION/RIS.

[88] Nan K. Li, Yuxin Xie, and Yaroslava G. Yingling. “Insights into Structure and Aggregation Behavior of Elastin-like Polypeptide Coacervates: All-Atom Molecular Dynamics Simulations”. In: *Journal of Physical Chemistry B* 125.30 (Aug. 2021), pp. 8627–8635. ISSN: 15205207. DOI: 10.1021/ACS.JPCB.1C02822/SUPPL_FILE/JP1C02822_SI_002.WMV.

[89] Ali Ghoorchian, James T. Cole, and Nolan B. Holland. “Thermoreversible micelle formation using a three-armed star elastin-like polypeptide”. In: *Macromolecules* 43.9 (May 2010), pp. 4340–4345. ISSN: 00249297. DOI: 10.1021/MA100285V/ASSET/IMAGES/MEDIUM/MA-2010-00285V_0008.GIF.

[90] Yue Zhang et al. “Modeling the Early Stages of Phase Separation in Disordered Elastin-like Proteins”. In: *Biophysical Journal* 114.7 (Apr. 2018), pp. 1563–1578. ISSN: 15420086. DOI: 10.1016/J.BPJ.2018.01.045/ATTACHMENT/14626C0F-D422-444C-87A4-6DD73050F71F/MMC1.PDF.

[91] Sarah R. Macewan and Ashutosh Chilkoti. “Applications of elastin-like polypeptides in drug delivery”. In: *Journal of Controlled Release* 190 (Sept. 2014), pp. 314–330. ISSN: 0168-3659. DOI: 10.1016/J.JCONREL.2014.06.028.

[92] Dana L. Nettles, Ashutosh Chilkoti, and Lori A. Setton. “Applications of elastin-like polypeptides in tissue engineering”. In: *Advanced Drug Delivery Reviews* 62.15 (Dec. 2010), pp. 1479–1485. ISSN: 0169-409X. DOI: 10.1016/J.ADDR.2010.04.002.

[93] Agnes Yeboah et al. “Elastin-like polypeptides: A strategic fusion partner for biologics”. In: *Biotechnology and Bioengineering* 113.8 (Aug. 2016), pp. 1617–1627. ISSN: 1097-0290. DOI: 10.1002/BIT.25998.

[94] Xin Ge et al. “Self-cleavable stimulus responsive tags for protein purification without chromatography”. In: *Journal of the American Chemical Society* 127.32 (Aug. 2005), pp. 11228–11229. ISSN: 00027863. DOI: 10.1021/JA0531125/SUPPL_FILE/JA0531125SI20050707_110644.PDF.

[95] Helmut Schlaad. “Solution Properties of Polypeptide-based Copolymers”. In: *Adv Polym Sci*. Vol. 202. 2006, pp. 53–73. DOI: 10.1007/12_082.

[96] Vusala Ibrahimova et al. “Thermosensitive Vesicles from Chemically Encoded Lipid-Grafted Elastin-like Polypeptides”. In: *Angewandte Chemie International Edition* 60.27 (June 2021), pp. 15036–15040. ISSN: 1521-3773. DOI: 10.1002/ANIE.202102807.

[97] Hwankyu Lee, Hyun Ryoung Kim, and Jae Chan Park. “Dynamics and stability of lipid bilayers modulated by thermosensitive polypeptides, cholesterols, and PEGylated lipids”. In: *Physical Chemistry Chemical Physics* 16.8 (Jan. 2014), pp. 3763–3770. ISSN: 1463-9084. DOI: 10.1039/C3CP52639A.

[98] Matthias C. Huber et al. “Designer amphiphilic proteins as building blocks for the intracellular formation of organelle-like compartments”. In: *Nature Materials 2014 14:1* 14.1 (Nov. 2014), pp. 125–132. ISSN: 1476-4660. DOI: 10.1038/nmat4118.

[99] Kilian Vogele et al. “Towards synthetic cells using peptide-based reaction compartments”. In: *Nature Communications* 9.1 (2018), pp. 1–7. ISSN: 20411723. DOI: 10.1038/s41467-018-06379-8.

[100] Tobias Pirzer et al. “In vesiculo synthesis of peptide membrane precursors for autonomous vesicle growth”. In: *Journal of Visualized Experiments* 2019.148 (June 2019). ISSN: 1940087X. DOI: 10.3791/59831.

[101] Andreas Schreiber et al. “Self-Assembly Toolbox of Tailored Supramolecular Architectures Based on an Amphiphilic Protein Library”. In: *Small* 15.30 (July 2019), p. 1900163. ISSN: 1613-6829. DOI: 10.1002/SMLL.201900163.

[102] Thomas Frank et al. “Growth of Giant Peptide Vesicles Driven by Compartmentalized Transcription–Translation Activity”. In: *Chemistry – A European Journal* 26.72 (Dec. 2020), pp. 17356–17360. ISSN: 1521-3765. DOI: 10.1002/CHEM.202003366.

[103] Yoo Kyung Go and Cecilia Leal. “Polymer-Lipid Hybrid Materials”. In: *Chemical Reviews* 121.22 (2021), pp. 13996–14030. ISSN: 15206890. DOI: 10.1021/acs.chemrev.1c00755.

[104] Tomoki Nishimura et al. “Substrate-Sorting Nanoreactors Based on Permeable Peptide Polymer Vesicles and Hybrid Liposomes with Synthetic Macromolecular Channels”. In: *Journal of the American Chemical Society* 142.1 (Jan. 2020), pp. 154–161. ISSN: 15205126. DOI: 10.1021/JACS.9B08598/SUPPL_FILE/JA9B08598_SI_001.PDF.

[105] Natassa Pippa et al. “PEO-b-PCL–DPPC chimeric nanocarriers: self-assembly aspects in aqueous and biological media and drug incorporation”. In: *Soft Matter* 9.15 (Mar. 2013), pp. 4073–4082. ISSN: 1744-6848. DOI: 10.1039/C3SM27447K.

[106] Johannes Thoma et al. “Membrane protein distribution in composite polymer–lipid thin films”. In: *Chemical Communications* 48.70 (Aug. 2012), pp. 8811–8813. ISSN: 1364-548X. DOI: 10.1039/C2CC32851H.

[107] / Langmuir et al. “Giant Phospholipid/Block Copolymer Hybrid Vesicles: Mixing Behavior and Domain Formation”. In: *Langmuir* 27.1 (2011), pp. 1–6. DOI: 10.1021/la103428g.

[108] Martin Fauquignon, Emmanuel Ibarboure, and Jean François Le Meins. “Membrane reinforcement in giant hybrid polymer lipid vesicles achieved by controlling the polymer architecture”. In: *Soft Matter* 17.1 (Jan. 2021), pp. 83–89. ISSN: 17446848. DOI: 10.1039/D0SM01581D.

[109] Charles M. Hansen. *Hansen solubility parameters: A user’s handbook: Second edition*. 2007, pp. 1–519. ISBN: 9781420006834. DOI: 10.1201/9781420006834.

[110] S. J. Singer and Garth L. Nicolson. “The Fluid Mosaic Model of the Structure of Cell Membranes”. In: *Science* 175.4023 (Feb. 1972), pp. 720–731. ISSN: 00368075. DOI: 10.1126/SCIENCE.175.4023.720.

[111] Donald W. Hilgemann et al. “On the existence of endocytosis driven by membrane phase separations”. In: *Biochimica et Biophysica Acta - Biomembranes* 1862.1 (Jan. 2020). ISSN: 18792642. DOI: 10.1016/J.BBAMEM.2019.06.006.

[112] Joseph Y. Ong and Jorge Z. Torres. “Phase Separation in Cell Division”. In: *Molecular Cell* 80.1 (Oct. 2020), pp. 9–20. ISSN: 1097-2765. DOI: 10.1016/J.MOLCEL.2020.08.007.

[113] Yan G. Zhao and Hong Zhang. “Phase Separation in Membrane Biology: The Interplay between Membrane-Bound Organelles and Membraneless Condensates”. In: *Developmental Cell* 55.1 (Oct. 2020), pp. 30–44. ISSN: 18781551. DOI: 10.1016/J.DEVCEL.2020.06.033.

[114] Bodil Westerlund and J. Peter Slotte. “How the molecular features of glycosphingolipids affect domain formation in fluid membranes”. In: *Biochimica et Biophysica Acta - Biomembranes* 1788.1 (Jan. 2009), pp. 194–201. ISSN: 00052736. DOI: 10.1016/J.BBAMEM.2008.11.010.

[115] Jacopo Frallicciardi et al. “Membrane thickness, lipid phase and sterol type are determining factors in the permeability of membranes to small solutes”. In: *Nature Communications 2022 13:1* 13.1 (Mar. 2022), pp. 1–12. ISSN: 2041-1723. DOI: 10.1038/s41467-022-29272-x.

[116] Sarah L Veatch and Sarah L Keller. “Seeing spots: Complex phase behavior in simple membranes”. In: (2005). DOI: 10.1016/j.bbamcr.2005.06.010.

[117] Ruthven N.A.H. Lewis and Ronald N. McElhaney. “Membrane lipid phase transitions and phase organization studied by Fourier transform infrared spectroscopy”. In: *Biochimica et Biophysica Acta - Biomembranes* 1828.10 (2013), pp. 2347–2358. ISSN: 00052736. DOI: 10.1016/J.BBAMEM.2012.10.018.

[118] Marc Eeman and Magali Deleu. “From biological membranes to biomimetic model membranes”. In: *Biotechnology, Agronomy, Society and Environment* 14.4 (2010), pp. 719–736. ISSN: 17804507.

[119] Deborah A. Brown and Erwin London. “Structure and function of sphingolipid- and cholesterol-rich membrane rafts”. In: *Journal of Biological Chemistry* 275.23 (June 2000), pp. 17221–17224. ISSN: 00219258. DOI: 10.1074/jbc.R000005200.

[120] Ruby May A. Sullan et al. “Cholesterol-dependent nanomechanical stability of phase-segregated multicomponent lipid bilayers”. In: *Biophysical Journal* 99.2 (July 2010), pp. 507–516. ISSN: 15420086. DOI: 10.1016/J.BPJ.2010.04.044.

[121] Thi Phuong Tuyen Dao et al. “Modulation of phase separation at the micron scale and nanoscale in giant polymer/lipid hybrid unilamellar vesicles (GHUVs)”. In: *Soft Matter* 13.3 (Jan. 2017), pp. 627–637. ISSN: 1744-6848. DOI: 10.1039/C6SM01625A.

[122] Jin Nam, T. Kyle Vanderlick, and Paul A. Beales. “Formation and dissolution of phospholipid domains with varying textures in hybrid lipo-polymersomes”. In: *Soft Matter* 8.30 (July 2012), pp. 7982–7988. ISSN: 1744-6848. DOI: 10.1039/C2SM25646K.

[123] Matthias Schulz et al. “Lateral surface engineering of hybrid lipid–BCP vesicles and selective nanoparticle embedding”. In: *Soft Matter* 10.6 (Jan. 2014), pp. 831–839. ISSN: 1744-6848. DOI: 10.1039/C3SM52040D.

[124] Martin Fauquignon, Emmanuel Ibarboure, and Jean François Le Meins. “Hybrid polymer/lipid vesicles: Influence of polymer architecture and molar mass on line tension”. In: *Biophysical Journal* 121.1 (Jan. 2022), pp. 61–67. ISSN: 0006-3495. DOI: 10.1016/J.BPJ.2021.12.005.

[125] Maud Chemin et al. “Hybrid polymer/lipid vesicles: Fine control of the lipid and polymer distribution in the binary membrane”. In: *Soft Matter* 8.10 (2012), pp. 2867–2874. ISSN: 1744683X. DOI: 10.1039/c2sm07188f.

[126] C. Dimova, R. Marques. “The Giant Vesicle Book”. In: *The Giant Vesicle Book* (Nov. 2019). DOI: 10.1201/9781315152516.

[127] A. M. Whited and A. Johs. “The interactions of peripheral membrane proteins with biological membranes”. In: *Chemistry and Physics of Lipids* 192 (2015), pp. 51–59. ISSN: 18732941. DOI: 10.1016/j.chemphyslip.2015.07.015.

[128] Mark A. Lemmon. “Membrane recognition by phospholipid-binding domains”. In: *Nature Reviews Molecular Cell Biology 2008 9:2* 9.2 (Feb. 2008), pp. 99–111. ISSN: 1471-0080. DOI: 10.1038/nrm2328.

[129] Anna Mulgrew-Nesbitt et al. “The role of electrostatics in protein–membrane interactions”. In: *Biochimica et Biophysica Acta (BBA) - Molecular and Cell Biology of Lipids* 1761.8 (Aug. 2006), pp. 812–826. ISSN: 1388-1981. DOI: 10.1016/J.BBALIP.2006.07.002.

[130] Felix Campelo, Harvey T. McMahon, and Michael M. Kozlov. “The hydrophobic insertion mechanism of membrane curvature generation by proteins”. In: *Biophysical Journal* 95.5 (Sept. 2008), pp. 2325–2339. ISSN: 15420086. DOI: 10.1529/biophysj.108.133173.

[131] Marija Backovic, Theodore S. Jardetzky, and Richard Longnecker. “Hydrophobic Residues That Form Putative Fusion Loops of Epstein-Barr Virus Glycoprotein B Are Critical for Fusion Activity”. In: *Journal of Virology* 81.17 (Sept. 2007), pp. 9596–9600. ISSN: 0022-538X. DOI: 10.1128/JVI.00758-07/ASSET/67A9EE4D-C774-45B3-BD69-66FB03CCB996/ASSETS/GRAPHIC/ZJV0170795130004.JPEG.

[132] Marissa J. Nadolski and Maurine E. Linder. “Protein lipidation”. In: *The FEBS Journal* 274.20 (Oct. 2007), pp. 5202–5210. ISSN: 1742-4658. DOI: 10.1111/J.1742-4658.2007.06056.X.

[133] Bettina Zens, Justyna Sawa-Makarska, and Sascha Martens. “In vitro systems for Atg8 lipidation”. In: *Methods* 75 (Mar. 2015), pp. 37–43. ISSN: 1046-2023. DOI: 10.1016/J.YMETH.2014.11.004.

[134] Hong Jiang et al. “Protein Lipidation: Occurrence, Mechanisms, Biological Functions, and Enabling Technologies”. In: *Chemical Reviews* 118.3 (Feb. 2018), pp. 919–988. ISSN: 15206890. DOI: 10.1021/ACS.CHEMREV.6B00750/ASSET/IMAGES/MEDIUM/CR-2016-00750Z_0049.GIF.

[135] Daniel M. Rosenbaum, Søren G.F. Rasmussen, and Brian K. Kobilka. “The structure and function of G-protein-coupled receptors”. In: *Nature 2009 459:7245* 459.7245 (May 2009), pp. 356–363. ISSN: 1476-4687. DOI: 10.1038/nature08144.

[136] Hiroyuki Mori and Koreaki Ito. “The Sec protein-translocation pathway”. In: *Trends in Microbiology* 9.10 (Oct. 2001), pp. 494–500. ISSN: 0966842X. DOI: 10.1016/S0966-842X(01)02174-6.

[137] Jeffrey A. Nye and Jay T. Groves. “Kinetic control of histidine-tagged protein surface density on supported lipid bilayers”. In: *Langmuir* 24.8 (Apr. 2008), pp. 4145–4149. ISSN: 07437463. DOI: 10.1021/LA703788H/ASSET/IMAGES/LARGE/LA703788HF00004.JPEG.

[138] Camila Fabiano de Freitas et al. ““Biotin-targeted mixed liposomes: A smart strategy for selective release of a photosensitizer agent in cancer cells””. In: *Materials Science and Engineering: C* 104 (Nov. 2019), p. 109923. ISSN: 0928-4931. DOI: 10.1016/J.MSEC.2019.109923.

[139] Pieta K. Mattila and Pekka Lappalainen. “Filopodia: molecular architecture and cellular functions”. In: *Nature Reviews Molecular Cell Biology 2008 9:6* 9.6 (May 2008), pp. 446–454. ISSN: 1471-0080. DOI: 10.1038/nrm2406.

[140] Tatyana M. Svitkina et al. “Mechanism of filopodia initiation by reorganization of a dendritic network”. In: *Journal of Cell Biology* 160.3 (Feb. 2003), pp. 409–421. ISSN: 0021-9525. DOI: 10.1083/JCB.200210174.

[141] Allen P. Liu et al. “Membrane-induced bundling of actin filaments”. In: *Nature Physics* 4.10 (Oct. 2008), pp. 789–793. ISSN: 1745-2473. DOI: 10.1038/nphys1071.

[142] Marco Faini et al. “Vesicle coats: structure, function, and general principles of assembly”. In: *Trends in Cell Biology* 23.6 (June 2013), pp. 279–288. ISSN: 0962-8924. DOI: 10.1016/J.TCB.2013.01.005.

[143] Michael M. Lacy et al. “Molecular mechanisms of force production in clathrin-mediated endocytosis”. In: *FEBS Letters* 592.21 (Nov. 2018), pp. 3586–3605. ISSN: 1873-3468. DOI: 10.1002/1873-3468.13192.

[144] Michael M. Kozlov et al. “Mechanisms shaping cell membranes”. In: *Current Opinion in Cell Biology* 29.1 (Aug. 2014), pp. 53–60. ISSN: 0955-0674. DOI: 10.1016/J.CEB.2014.03.006.

[145] Guillaume Drin and Bruno Antonny. “Amphipathic helices and membrane curvature”. In: *FEBS Letters* 584.9 (May 2010), pp. 1840–1847. ISSN: 1873-3468. DOI: 10.1016/J.FEBSLET.2009.10.022.

[146] Tom Kirchhausen. “Bending membranes”. In: *Nature Cell Biology 2012 14:9* 14.9 (Sept. 2012), pp. 906–908. ISSN: 1476-4679. DOI: 10.1038/ncb2570.

[147] Wei Qin et al. “Deciphering molecular interactions by proximity labeling”. In: *Nature Methods 2021 18:2* 18.2 (Jan. 2021), pp. 133–143. ISSN: 1548-7105. DOI: 10.1038/s41592-020-01010-5.

[148] Dae In Kim et al. “An improved smaller biotin ligase for BioID proximity labeling”. In: *Molecular Biology of the Cell* 27.8 (Apr. 2016), pp. 1188–1196. ISSN: 19394586. DOI: 10.1091/MBC.E15-12-0844/ASSET/IMAGES/LARGE/MBC-27-1188-G004.JPEG.

[149] Victoria Hung et al. “Spatially resolved proteomic mapping in living cells with the engineered peroxidase APEX2”. In: *Nature Protocols 2016 11:3* 11.3 (Feb. 2016), pp. 456–475. ISSN: 1750-2799. DOI: 10.1038/nprot.2016.018.

[150] Dae In Kim et al. “Probing nuclear pore complex architecture with proximity-dependent biotinylation”. In: *Proceedings of the National Academy of Sciences of the United States of America* 111.24 (June 2014), E2453–E2461. ISSN: 10916490. DOI: 10.1073/PNAS.1406459111/SUPPL_FILE/PNAS.1406459111.SD03.XLSX.

[151] Hyun Woo Rhee et al. “Proteomic mapping of mitochondria in living cells via spatially restricted enzymatic tagging”. In: *Science* 339.6125 (Mar. 2013), pp. 1328–1331. ISSN: 10959203. DOI: 10.1126/SCIENCE.1230593/SUPPL_FILE/RHEE_SUPPSS2.REVISION.1.XLSX.

[152] Kyle J. Roux et al. “A promiscuous biotin ligase fusion protein identifies proximal and interacting proteins in mammalian cells”. In: *Journal of Cell Biology* 196.6 (Mar. 2012), pp. 801–810. ISSN: 0021-9525. DOI: 10.1083/JCB.201112098.

[153] Tess C. Branon et al. “Efficient proximity labeling in living cells and organisms with TurboID”. In: *Nature Biotechnology 2018 36:9* 36.9 (Oct. 2018), pp. 880–887. ISSN: 1546-1696. DOI: 10.1038/nbt.4201.

[154] Kelvin F. Cho et al. “Proximity labeling in mammalian cells with TurboID and split-TurboID”. In: *Nature Protocols 2020 15:12* 15.12 (Nov. 2020), pp. 3971–3999. ISSN: 1750-2799. DOI: 10.1038/s41596-020-0399-0.

[155] Stephanie S. Lam et al. “Directed evolution of APEX2 for electron microscopy and proximity labeling”. In: *Nature Methods* 12.1 (2014), pp. 51–54. ISSN: 15487105. DOI: 10.1038/nmeth.3179.

[156] Yisu Han et al. “Directed Evolution of Split APEX2 Peroxidase”. In: *ACS Chemical Biology* 14.4 (2019), pp. 619–635. ISSN: 15548937. DOI: 10.1021/acschembio.8b00919.

[157] Jeffrey D. Martell et al. “A split horseradish peroxidase for the detection of intercellular protein–protein interactions and sensitive visualization of synapses”. In: *Nature Biotechnology 2016 34:7* 34.7 (May 2016), pp. 774–780. ISSN: 1546-1696. DOI: 10.1038/nbt.3563.

[158] Matthaeus Schwarz-Schilling et al. “Optimized Assembly of a Multifunctional RNA-Protein Nanostructure in a Cell-Free Gene Expression System”. In: *Nano Letters* 18.4 (Apr. 2018), pp. 2650–2657. ISSN: 15306992. DOI: 10.1021/ACS.NANOLETT.8B00526/SUPPL_FILE/NL8B00526_SI_001.PDF.

[159] Samuel W. Schaffter and Elizabeth A. Strychalski. “Cotranscriptionally encoded RNA strand displacement circuits”. In: *Science Advances* 8.12 (Mar. 2022), p. 4354. ISSN: 23752548. DOI: 10.1126/SCIADV.ABL4354/SUPPL_FILE/SCIADV.ABL4354_SM.PDF.

[160] Bertrand Beckert and Benoît Masquida. “Synthesis of RNA by In Vitro Transcription BT - RNA: Methods and Protocols”. In: *Methods in molecular biology (Clifton, N.J.)* Vol. 703. Humana Press, 2011, pp. 29–41. ISBN: 978-1-59745-248-9.

[161] John F. Milligan and Olke C. Uhlenbeck. “[5] Synthesis of small RNAs using T7 RNA polymerase”. In: *Methods in Enzymology* 180.C (Jan. 1989), pp. 51–62. ISSN: 0076-6879. DOI: 10.1016/0076-6879(89)80091-6.

[162] Susanne Brakmann and Sandra Grzeszik. “An Error-Prone T7 RNA Polymerase Mutant Generated by Directed Evolution”. In: *ChemBioChem* 2.3 (Mar. 2001), pp. 212–219. ISSN: 1439-4227. DOI: https://doi.org/10.1002/1439-7633(20010302)2:3<212::AID-CBIC212>3.0.CO;2-R.

[163] Adam J. Meyer, Jared W. Ellefson, and Andrew D. Ellington. “Directed Evolution of a Panel of Orthogonal T7 RNA Polymerase Variants for in Vivo or in Vitro Synthetic Circuitry”. In: *ACS Synthetic Biology* 4.10 (Oct. 2015), pp. 1070–1076. ISSN: 21615063. DOI: 10.1021/SB500299C/SUPPL_FILE/SB500299C_SI_001.PDF.

[164] Ramesh Padmanabhan, Subha Narayan Sarcar, and Dennis L. Miller. “Promoter Length Affects the Initiation of T7 RNA Polymerase In Vitro: New Insights into Promoter/Polymerase Co-evolution”. In: *Journal of Molecular Evolution* 88.2 (Mar. 2020), pp. 179–193. ISSN: 14321432. DOI: 10.1007/S00239-019-09922-3/FIGURES/13.

[165] G. Zubay, D. Schwartz, and J. Beckwith. “Mechanism of Activation of Catabolite-Sensitive Genes: A Positive Control System*”. In: *Proceedings of the National Academy of Sciences* 66.1 (May 1970), pp. 104–110. ISSN: 00278424. DOI: 10.1073/PNAS.66.1.104.

[166] François Jacob and Jacques Monod. “Genetic regulatory mechanisms in the synthesis of proteins”. In: *Journal of Molecular Biology* 3.3 (June 1961), pp. 318–356. ISSN: 0022-2836. DOI: 10.1016/S0022-2836(61)80072-7.

[167] Jaidip Chatterjee, Carol M. Miyamoto, and Edward A. Meighen. “Autoregulation of luxR: the Vibrio harveyi lux-operon activator functions as a repressor”. In: *Molecular Microbiology* 20.2 (Apr. 1996), pp. 415–425. ISSN: 1365-2958. DOI: 10.1111/J.1365-2958.1996.TB02628.X.

[168] Yun Kang, Mike S. Son, and Tung T. Hoang. “One step engineering of T7-expression strains for protein production: Increasing the host-range of the T7-expression system”. In: *Protein Expression and Purification* 55.2 (Oct. 2007), pp. 325–333. ISSN: 1046-5928. DOI: 10.1016/J.PEP.2007.06.014.

[169] Pascal J. Lopez et al. “On the mechanism of inhibition of phage T7 RNA polymerase by lac repressor”. In: *Journal of Molecular Biology* 276.5 (Mar. 1998), pp. 861–875. ISSN: 0022-2836. DOI: 10.1006/JMBI.1997.1576.

[170] Nico Mertens, Erik Remaut, and Walter Fiers. “Tight Transcriptional Control Mechanism Ensures Stable High-Level Expression from T7 Promoter-Based Expression Plasmids”. In: *Bio/Technology 1995 13:2* 13.2 (1995), pp. 175–179. ISSN: 1546-1696. DOI: 10.1038/nbt0295-175.

[171] Liping Du, Seth Villarreal, and Anthony C. Forster. “Multigene expression in vivo: Supremacy of large versus small terminators for T7 RNA polymerase”. In: *Biotechnology and Bioengineering* 109.4 (Apr. 2012), pp. 1043–1050. ISSN: 00063592. DOI: 10.1002/BIT.24379.

[172] Muthukumar Ramanathan, Douglas F. Porter, and Paul A. Khavari. “Methods to study RNA–protein interactions”. In: *Nature Methods 2019 16:3* 16.3 (Feb. 2019), pp. 225–234. ISSN: 1548-7105. DOI: 10.1038/s41592-019-0330-1.

[173] Isabel Sola et al. “RNA-RNA and RNA-protein interactions in coronavirus replication and transcription”. In: *http://dx.doi.org/10.4161/rna.8.2.14991* 8.2 (Mar. 2011), pp. 237–248. ISSN: 1547-6286. DOI: 10.4161/RNA.8.2.14991.

[174] Mingqi Xie and Martin Fussenegger. “Designing cell function: assembly of synthetic gene circuits for cell biology applications”. In: *Nature Reviews Molecular Cell Biology 2018 19:8* 19.8 (June 2018), pp. 507–525. ISSN: 1471-0080. DOI: 10.1038/s41580-018-0024-z.

[175] Chee Huat Linus Eng et al. “Profiling the transcriptome with RNA SPOTs”. In: *Nature Methods 2017 14:12* 14.12 (Nov. 2017), pp. 1153–1155. ISSN: 1548-7105. DOI: 10.1038/nmeth.4500.

[176] Amin Espah Borujeni et al. “Automated physics-based design of synthetic riboswitches from diverse RNA aptamers”. In: *Nucleic Acids Research* 44.1 (Jan. 2016), pp. 1–13. ISSN: 0305-1048. DOI: 10.1093/NAR/GKV1289.

[177] Laurène Bastet et al. “New insights into riboswitch regulation mechanisms”. In: *Molecular Microbiology* 80.5 (June 2011), pp. 1148–1154. ISSN: 1365-2958. DOI: 10.1111/J.1365-2958.2011.07654.X.

[178] Matthew R. Dunn, Randi M. Jimenez, and John C. Chaput. “Analysis of aptamer discovery and technology”. In: *Nature Reviews Chemistry* 1.10 (2017). ISSN: 23973358. DOI: 10.1038/S41570-017-0076.

[179] Jeffrey A. Chao et al. “Structural basis for the coevolution of a viral RNA–protein complex”. In: *Nature Structural & Molecular Biology 2008 15:1* 15.1 (Dec. 2007), pp. 103–105. ISSN: 1545-9985. DOI: 10.1038/nsmb1327.

[180] Joseph D. Puglisi et al. “Solution Structure of a Bovine Immunodeficiency Virus Tat-TAR Peptide-RNA Complex”. In: *Science* 270.5239 (Nov. 1995), pp. 1200–1203. ISSN: 00368075. DOI: 10.1126/SCIENCE.270.5239.1200.

[181] H. Ulrich. “RNA aptamers: From basic science towards therapy”. In: *Handbook of Experimental Pharmacology* 173 (2006), pp. 305–326. ISSN: 18650325. DOI: 10.1007/3-540-27262-3_15/COVER.

[182] Jonathan Ouellet. “RNA fluorescence with light-Up aptamers”. In: *Frontiers in Chemistry* 4.JUN (2016), pp. 1–12. ISSN: 22962646. DOI: 10.3389/fchem.2016.00029.

[183] Anthony D. Keefe, Supriya Pai, and Andrew Ellington. “Aptamers as therapeutics”. In: *Nature Reviews Drug Discovery 2010 9:7* 9.7 (July 2010), pp. 537–550. ISSN: 1474-1784. DOI: 10.1038/nrd3141.

[184] Geoffrey Zubay. “IN VITRO SYNTHESIS OF PROTEIN IN MICROBIAL SYSTEMS”. In: *Annual Review of Genetics* 7 (1973).

[185] David Garenne et al. “Cell-free gene expression”. In: *Nature Reviews Methods Primers* 1.1 (2021). ISSN: 26628449. DOI: 10.1038/s43586-021-00046-x.

[186] Zachary Z. Sun et al. “Protocols for implementing an Escherichia coli based TX-TL cell-free expression system for synthetic biology”. In: *Journal of Visualized Experiments* 79 (Sept. 2013). ISSN: 1940087X. DOI: 10.3791/50762.

[187] Nicole E. Gregorio, Max Z. Levine, and Javin P. Oza. “A User’s Guide to Cell-Free Protein Synthesis”. In: *Methods and Protocols 2019, Vol. 2, Page 24* 2.1 (Mar. 2019), p. 24. ISSN: 2409-9279. DOI: 10.3390/MPS2010024.

[188] David Garenne and Vincent Noireaux. “Cell-free transcription–translation: engineering biology from the nanometer to the millimeter scale”. In: *Current Opinion in Biotechnology* 58.Figure 1 (2019), pp. 19–27. ISSN: 18790429. DOI: 10.1016/j.copbio.2018.10.007.

[189] Yiren Xu et al. “Production of bispecific antibodies in "knobs-into-holes" using a cell-free expression system”. In: *mAbs* 7.1 (Jan. 2015), pp. 231–242. ISSN: 19420870. DOI: 10.4161/19420862.2015.989013/SUPPL_FILE/KMAB_A_989013_SM4977.ZIP.

[190] Jonghyeon Shin, Paul Jardine, and Vincent Noireaux. “Genome replication, synthesis, and assembly of the bacteriophage T7 in a single cell-Free reaction”. In: *ACS Synthetic Biology* 1.9 (Sept. 2012), pp. 408–413. ISSN: 21615063. DOI: 10.1021/SB300049P/SUPPL_FILE/SB300049P_SI_001.PDF.

[191] Mark Rustad et al. “Cell-free TXTL synthesis of infectious bacteriophage T4 in a single test tube reaction”. In: *Synthetic Biology* 3.1 (Jan. 2018). ISSN: 23977000. DOI: 10.1093/SYNBIO/YSY002.

[192] Vincent Noireaux and Albert Libchaber. “A vesicle bioreactor as a step toward an artificial cell assembly”. In: *Proceedings of the National Academy of Sciences of the United States of America* 101.51 (Dec. 2004), pp. 17669–17674. ISSN: 00278424. DOI: 10.1073/PNAS.0408236101/ASSET/B958CF02-C4D0-4C24-BE44-E1870B851521/ASSETS/GRAPHIC/ZPQ0510467490007.JPEG.

[193] Nan Nan Deng et al. “Microfluidic assembly of monodisperse vesosomes as artificial cell models”. In: *Journal of the American Chemical Society* 139.2 (Jan. 2017), pp. 587–590. ISSN: 15205126. DOI: 10.1021/JACS.6B10977/SUPPL_FILE/JA6B10977_SI_006.AVI.

[194] Takumi Furusato et al. “De Novo Synthesis of Basal Bacterial Cell Division Proteins FtsZ, FtsA, and ZipA Inside Giant Vesicles”. In: *ACS Synthetic Biology* 7.4 (Apr. 2018), pp. 953–961. ISSN: 21615063. DOI: 10.1021/ACSSYNBIO.7B00350/SUPPL_FILE/SB7B00350_SI_001.PDF.

[195] Vincent Noireaux, Yusuke T. Maeda, and Albert Libchaber. “Development of an artificial cell, from self-organization to computation and self-reproduction”. In: *Proceedings of the National Academy of Sciences of the United States of America* 108.9 (Mar. 2011), pp. 3473–3480. ISSN: 00278424. DOI: 10.1073/PNAS.1017075108/ASSET/EBFE0302-3BF1-417F-A87A-D6F90F058BC9/ASSETS/GRAPHIC/PNAS.1017075108FIG5.JPEG.

[196] Sagardip Majumder et al. “Cell-sized mechanosensitive and biosensing compartment programmed with DNA”. In: *Chemical Communications* 53.53 (June 2017), pp. 7349–7352. ISSN: 1364-548X. DOI: 10.1039/C7CC03455E.

[197] Samuel Berhanu, Takuya Ueda, and Yutetsu Kuruma. “Artificial photosynthetic cell producing energy for protein synthesis”. In: *Nature Communications 2019 10:1* 10.1 (Mar. 2019), pp. 1–10. ISSN: 2041-1723. DOI: 10.1038/s41467-019-09147-4.

[198] T. Y. Dora Tang et al. “Fatty acid membrane assembly on coacervate microdroplets as a step towards a hybrid protocell model”. In: *Nature Chemistry 2014 6:6* 6.6 (Apr. 2014), pp. 527–533. ISSN: 1755-4349. DOI: 10.1038/nchem.1921.

[199] Lukas Aufinger and Friedrich C. Simmel. “Künstliche, gelbasierte Organellen für die räumliche Organisation von zellfreien Genexpressionsreaktionen”. In: *Angewandte Chemie* 130.52 (Dec. 2018), pp. 17491–17495. ISSN: 1521-3757. DOI: 10.1002/ANGE.201809374.

[200] Jan Brocher. *biovoxxel/BioVoxxel-Toolbox: BioVoxxel Toolbox*. Feb. 2022. DOI: 10.5281/ZENODO.5986130.

[201] Korbinian Kapsner and Friedrich C. Simmel. “Partitioning Variability of a Compartmentalized in Vitro Transcriptional Thresholding Circuit”. In: *ACS Synthetic Biology* 4.10 (Oct. 2015), pp. 1136–1143. ISSN: 21615063. DOI: 10.1021/ACSSYNBIO.5B00051/SUPPL_FILE/SB5B00051_SI_001.PDF.

[202] Hana Robson Marsden, Luca Gabrielli, and Alexander Kros. “Rapid preparation of polymersomes by a water addition/ solvent evaporation method”. In: *Polymer Chemistry* 1.9 (Oct. 2010), pp. 1512–1518. ISSN: 17599954. DOI: 10.1039/C0PY00172D.

[203] J. F. Le Meins, O. Sandre, and S. Lecommandoux. “Recent trends in the tuning of polymersomes’ membrane properties”. In: *The European Physical Journal E 2011 34:2* 34.2 (Feb. 2011), pp. 1–17. ISSN: 1292-895X. DOI: 10.1140/EPJE/I2011-11014-Y.

[204] Nelson F. Morales-Penningston et al. “GUV preparation and imaging: Minimizing artifacts”. In: *Biochimica et Biophysica Acta - Biomembranes* 1798.7 (2010), pp. 1324–1332. ISSN: 00052736. DOI: 10.1016/j.bbamem.2010.03.011.

[205] Vladimir Mishin et al. “Application of the Amplex red/horseradish peroxidase assay to measure hydrogen peroxide generation by recombinant microsomal enzymes”. In: *Free Radical Biology and Medicine* 48.11 (June 2010), pp. 1485–1491. ISSN: 0891-5849. DOI: 10.1016/J.FREERADBIOMED.2010.02.030.

[206] Dawid Debski et al. “Mechanism of oxidative conversion of Amplex® Red to resorufin: Pulse radiolysis and enzymatic studies”. In: *Free Radical Biology and Medicine* 95 (June 2016), pp. 323–332. ISSN: 0891-5849. DOI: 10.1016/J.FREERADBIOMED.2016.03.027.

[207] Sujan S. Shekhawat and Indraneel Ghosh. “Split-protein systems: beyond binary protein–protein interactions”. In: *Current Opinion in Chemical Biology* 15.6 (Dec. 2011), pp. 789–797. ISSN: 1367-5931. DOI: 10.1016/J.CBPA.2011.10.014.

[208] Kathleen A Leamy et al. “Bridging the gap between in vitro and in vivo RNA folding”. In: (2016). DOI: 10.1017/S003358351600007X.

[209] Maximilian Weitz et al. “Diversity in the dynamical behaviour of a compartmentalized programmable biochemical oscillator”. In: *Nature Chemistry 2014 6:4* 6.4 (Feb. 2014), pp. 295–302. ISSN: 1755-4349. DOI: 10.1038/nchem.1869.

[210] Ling Miao et al. “Budding transitions of fluid-bilayer vesicles: The effect of area-difference elasticity”. In: *Physical Review E* 49.6 (June 1994), p. 5389. ISSN: 1063651X. DOI: 10.1103/PhysRevE.49.5389.

[211] Irene A. Chen, Richard W. Roberts, and Jack W. Szostak. “The emergence of competition between model protocells”. In: *Science* 305.5689 (Sept. 2004), pp. 1474–1476. ISSN: 00368075. DOI: 10.1126/SCIENCE.1100757/SUPPL_FILE/CHEN.SOM.PDF.

[212] Andrey V. Dobrynin, Ralph H. Colby, and Michael Rubinstein. “Scaling Theory of Polyelectrolyte Solutions”. In: *Macromolecules* 28.6 (Nov. 1995), pp. 1859–1871. ISSN: 15205835. DOI: 10.1021/MA00110A021/ASSET/MA00110A021.FP.PNG_V03.

[213] E. Raspaud, M. Da Conceiçao, and F. Livolant. “Do Free DNA Counterions Control the Osmotic Pressure?” In: *Physical Review Letters* 84.11 (Mar. 2000), p. 2533. ISSN: 10797114. DOI: 10.1103/PhysRevLett.84.2533.

[214] Lisa M. Dominak et al. “Polymeric crowding agents improve passive biomacromolecule encapsulation in lipid vesicles”. In: *Langmuir* 26.16 (Aug. 2010), pp. 13195–13200. ISSN: 07437463. DOI: 10.1021/LA101903R/SUPPL_FILE/LA101903R_SI_001.PDF.

[215] Robert J. Trachman et al. “Structure and functional reselection of the Mango-III fluorogenic RNA aptamer”. In: *Nature Chemical Biology* 15.5 (2019), pp. 472–479. ISSN: 15524469. DOI: 10.1038/s41589-019-0267-9.

[216] Martin Langecker et al. “DNA nanostructures interacting with lipid bilayer membranes”. In: *Accounts of Chemical Research* 47.6 (June 2014), pp. 1807–1815. ISSN: 15204898. DOI: 10.1021/AR500051R/ASSET/IMAGES/MEDIUM/AR-2014-00051R_0007.GIF.

[217] Yash Bogawat et al. “Tunable 2D diffusion of DNA nanostructures on lipid membranes”. In: *Biophysical Journal* 121.24 (Dec. 2022), pp. 4810–4818. ISSN: 0006-3495. DOI: 10.1016/J.BPJ.2022.10.015.

[218] Kevin Jahnke et al. “Bottom-Up Assembly of Synthetic Cells with a DNA Cytoskeleton”. In: *ACS Nano* 16 (2021), pp. 7233–7241. ISSN: 1936086X. DOI: 10.1021/ACSNANO.1C10703/SUPPL_FILE/NN1C10703_SI_008.MP4.

[219] Rumiana Dimova et al. “Vesicles in electric fields: Some novel aspects of membrane behavior”. In: *Soft Matter* 5.17 (2009), pp. 3201–3212. ISSN: 1744683X. DOI: 10.1039/b901963d.

[220] Rumiana Dimova and Karin A. Riske. “Using electric fields to assess membrane material properties in giant unilamellar vesicles”. In: *The Giant Vesicle Book*. CRC Press, Nov. 2019, pp. 347–364. ISBN: 9781315152516. DOI: 10.1201/9781315152516-15.

[221] Paul F. Salipante et al. “Electrodeformation method for measuring the capacitance of bilayer membranes”. In: *Soft Matter* 8.14 (Mar. 2012), pp. 3810–3816. ISSN: 1744-6848. DOI: 10.1039/C2SM07105C.

[222] Michael A Luzuriaga et al. “Enhanced Stability and Controlled Delivery of MOF-Encapsulated Vaccines and Their Immunogenic Response In Vivo”. In: (2019). DOI: 10.1021/acsami.8b20504.

A. Appendix

All additional experimental data and documentations can be found in this chapter.

A.1. Additional Data

Following figures and sections present additional experimental data completing the data presented in chapter 4. The data shown is partly taken from the publications of Frank et. al. [102]

A.1.1. Membrane Interaction

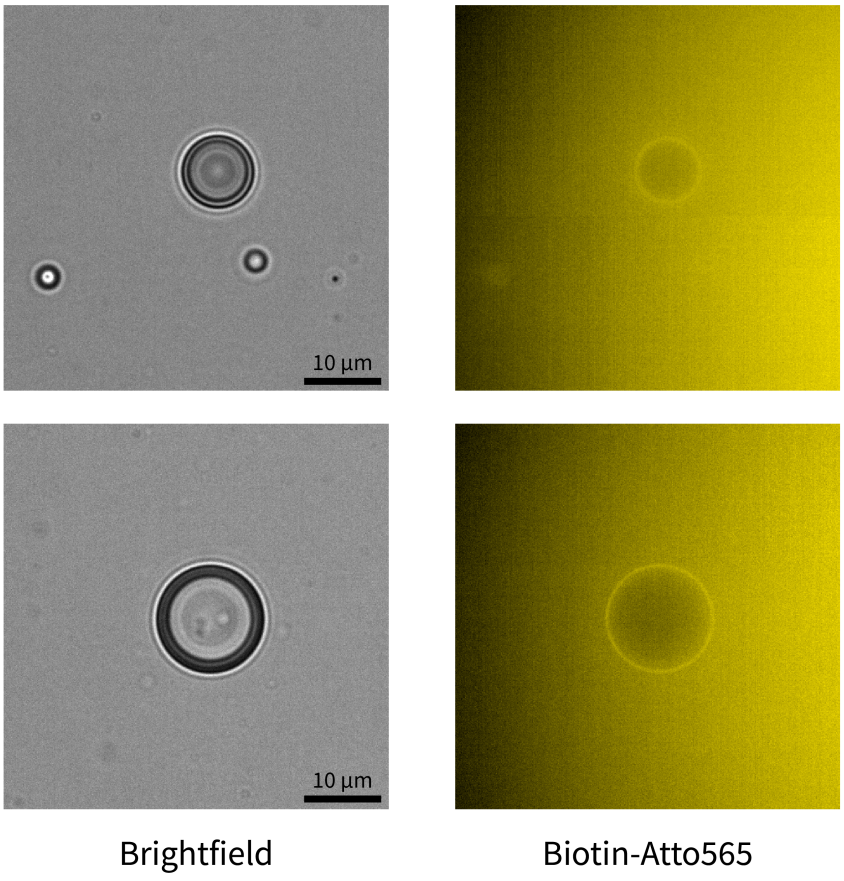

Figure A.1.1: Negative Control Biotin-Streptavidin Binding: *Micrographs of hybrid vesicles without streptavidin. Only low interaction between Biotin-Atto565 and vesicle membrane.*

A.1.2. Vesicle Size

As a control we also observed ELP vesicles containing only 3 M sucrose in water, whereas the outer solution contained only 3 M glucose in solution; there were ELPs provided in the outer solution. Figure S4 shows the vesicle radius vs. time traces of

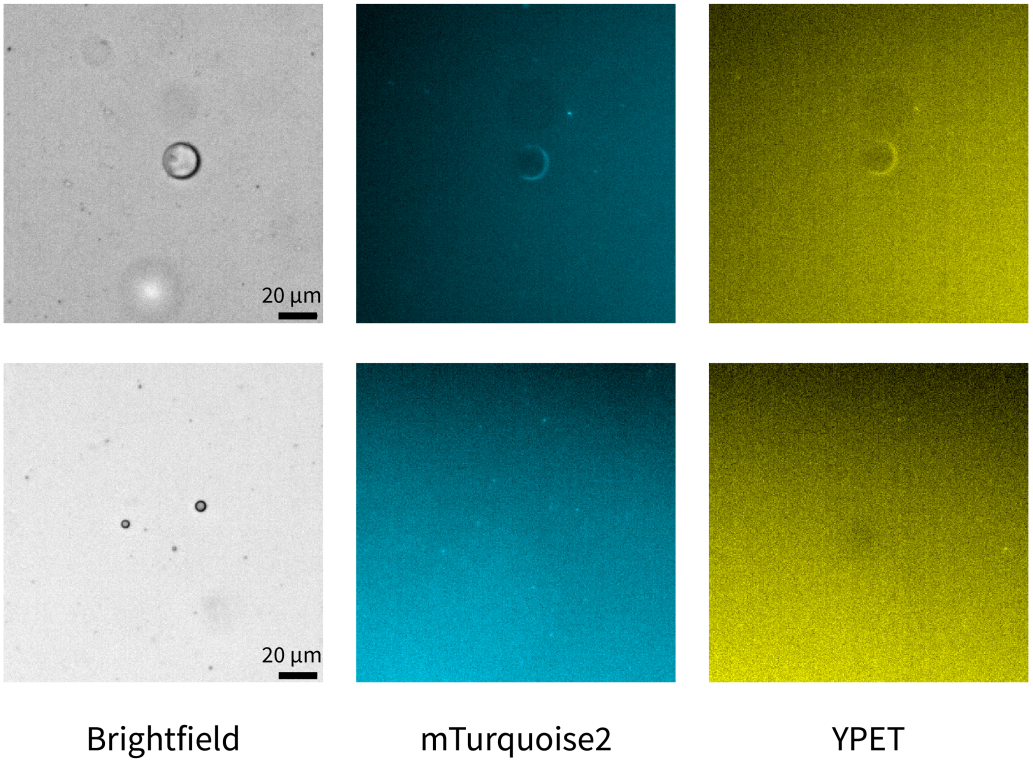

Figure A.1.2: Negative Control Co-Localization: *Micrographs of hybrid vesicles without streptavidin in solution with pRNA, BIV-mTurquoise2 and PCP-YPET. Very low interaction of fluorescent proteins and membrane observable.*

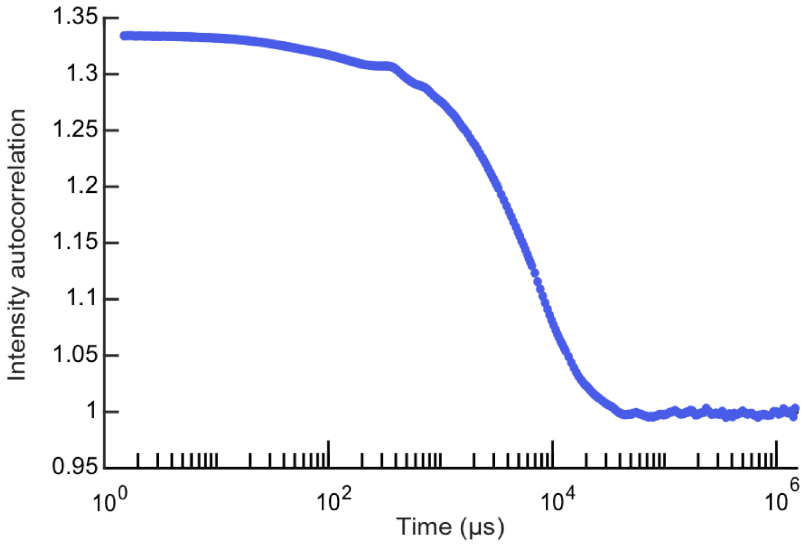

Figure A.1.3: Size DLS: *Autocorrelation function of ELP vesicles measured with DLS*

38 vesicles. The apparent initial increase in size can be explained through the on-going sedimentation of the vesicles. The latter can also be observed in long- term measurements. The automated droplet tracking algorithm covers only a small area

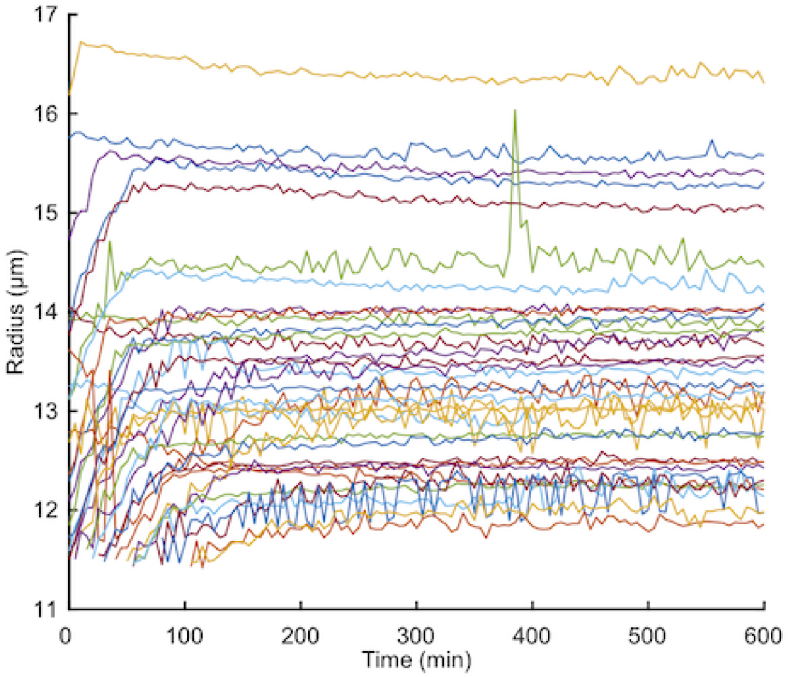

Figure A.1.4: Negative Control Size: *Vesicle radius over a time period of 10 h. Sample size N=38.*

of the vesicle outside of the focal plane, which grows when the vesicles sediment into the focal plane. Looking at vesicles with a larger radius, the opposite effect resulting from the same behavior is observable. After about 100 min most of the vesicles have a constant size after they settled on the surface of the glass slide.

A.1.3. In vitro Transcription (IVT)

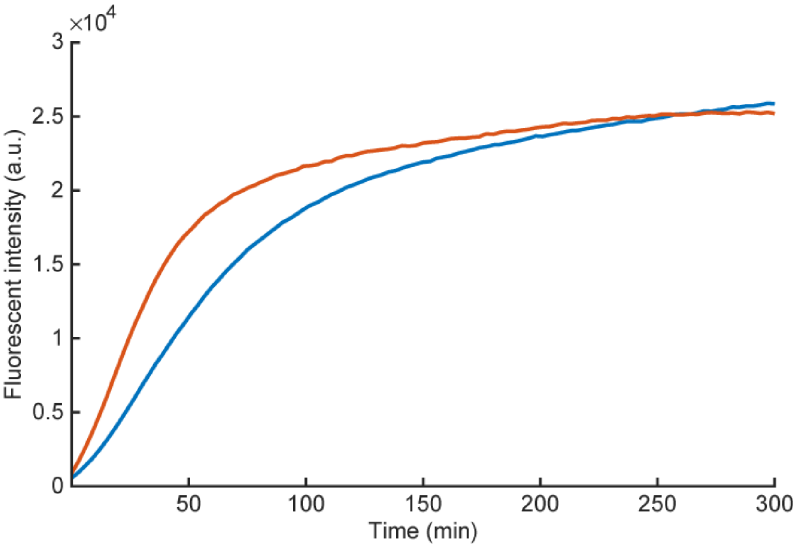

Figure A.1.5: Plate Reader IVT: *Duplicate plate reader measurement of IVT reaction mix with dBroccoli template used in microscopy experiments.*

The TX reaction mix used for encapsulation was measured in bulk as well to estimate the active time of transcription. Figure A.1.5 shows two time-traces of the measured aptamer fluorescence in bulk. The samples were measured with excitation using a filter 485 +/-6 nm and an emission filter of 520 +/-17 nm.

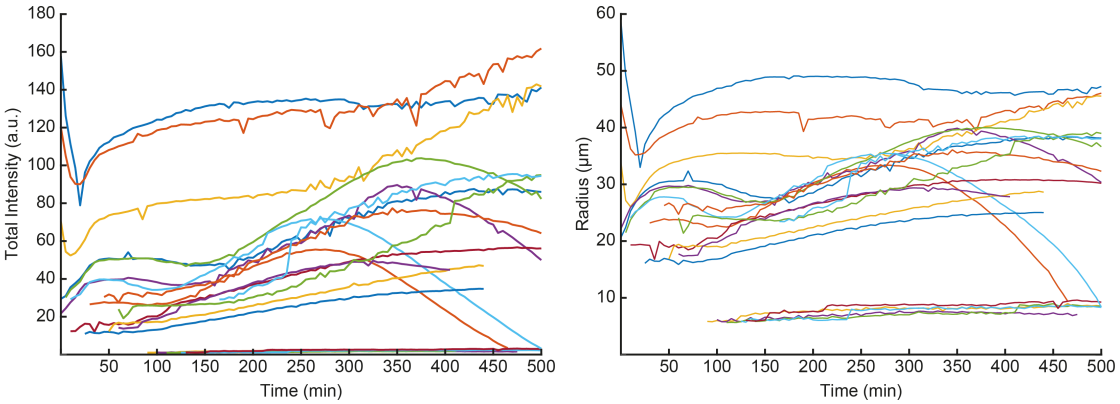

Figure A.1.6: Vesicle Growth IVT: *Measurement of fluorescence (left) and radius (right) of IVT mix encapsulated in ELP vesicles. Color coding indicates the same vesicle. Sample size N=20.*

Figure A.1.6 shows the fluorescence intensities and the radii of 20 vesicles containing an active RNA polymerization process. ELP amphiphiles were provided in the outer solution. For excitation an LED lamp and an excitation filter at 470 +/-20 nm were used, whereas emission was observed at 531 +/-13 nm.

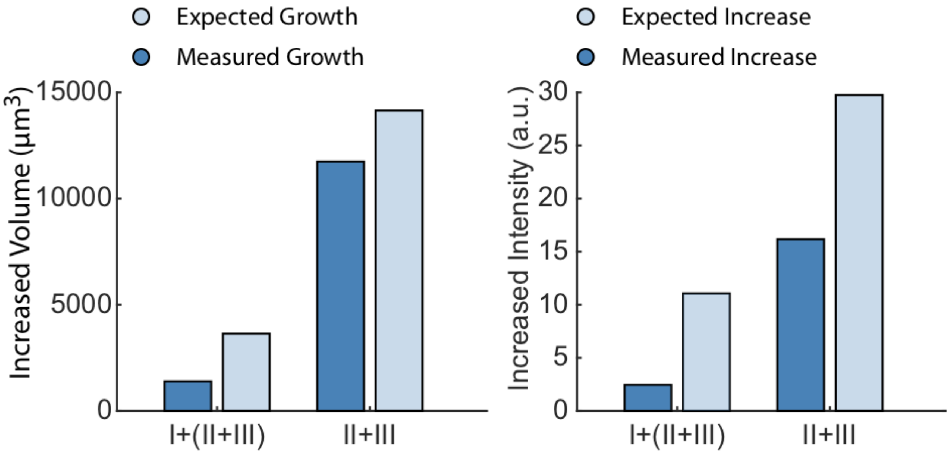

Figure A.1.7: Fusion Growth IVT: *Comparison of measured (dark blue) and expected (light blue) values after fusion events observed during long-term TX measurements. Bars represent the volume (left) or fluorescence (right) difference between the values after and before fusion. Abscissa numbering refers to vesicles depicted in Fig.4.4.2.*

Depending on the observed vesicle a stationary or decreasing trend can be seen in fluorescent intensity and vesicle size. Very small vesicles only show small changes

in fluorescence and size within the observation time. Depending on the observed vesicle, initial increase in size and fluorescence can either be seen continuing until the end of the measurement or individual vesicles start to shrink after a certain time.

Measurement of fused vesicles has shown that neither the expected volume nor the fluorescent intensity adds up after fusion of the observed vesicles (Fig. A.1.7). The expected values (light blue) surpass the measured values (dark blue) in both cases of the observed fusion events. Similar values were measured for several more fusion events.

A.1.4. Cell free gene expression (CFE)

Vesicles encapsulating an CFE reaction mix were measured at 29 °C for 900 min. ELP amphiphiles were provided in the outer solution.

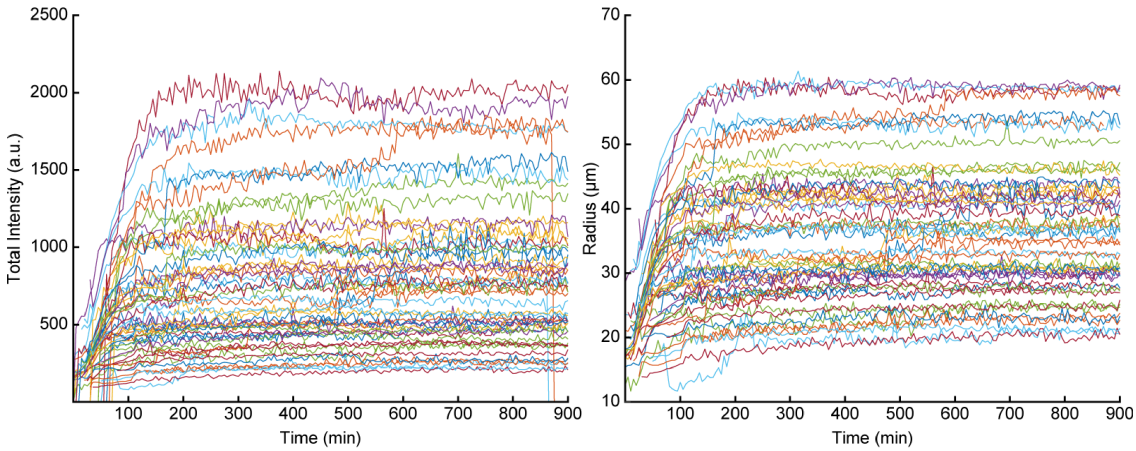

Figure A.1.8: Vesicle Growth CFE: *Increasing fluorescent intensity (left) and vesicles radius (right) for 900 min. Color coding indicates the same vesicle. Sample size N=77.*

For excitation an LED lamp and an excitation filter (470 +/-20 nm) were used, whereas emission was observed 531 $\pm$ 13 nm.

All vesicles show an initial increase in size as well as in fluorescent intensity up to roughly 160 min after the measurement was started. Until the end of the measurement all vesicles show no further change in size and fluorescence.

The dashed line is a linear fit to all values of the 77 observed vesicles. On a first approximation fluorescence intensity and volume are linearly correlated. Some vesicles appear in clusters, which can be explained by nearly constant values in fluorescence and volume after about 160 min.

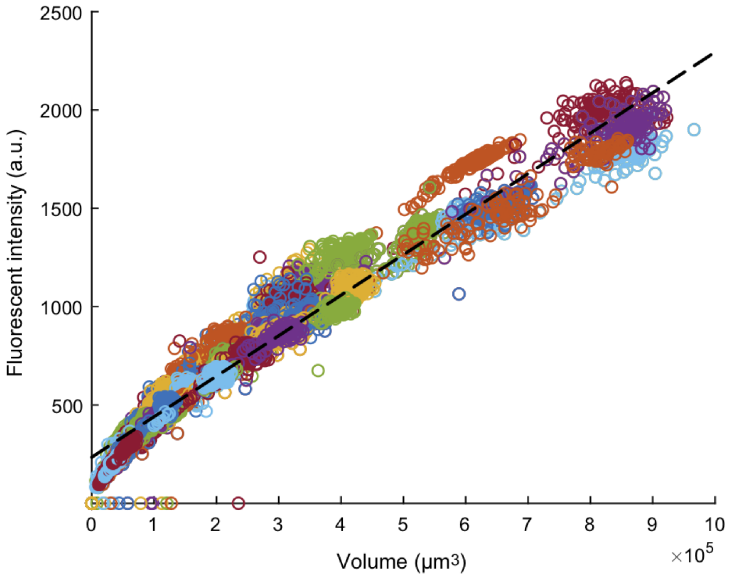

Figure A.1.9: Scatter Plot Growth CFE: *Scatter plot of fluorescent intensity vs. vesicle volume. Individual vesicles measured over a time period of 900 min. Each color represents an individual vesicle. Sample size N=77.*

The synthesis activity of the encapsulated cell free gene expression reaction was measured using fluorescence plate reader measurements. Figure A.1.10 shows a biological triplicate at 37 °C for 24h. The initial decrease in fluorescence can be explained by the consumption of NADH which shows auto fluorescence within the observed wavelengths. For excitation a filter of 497 +/-15 nm was used, whereas emission was observed at 540 +/-20 nm.

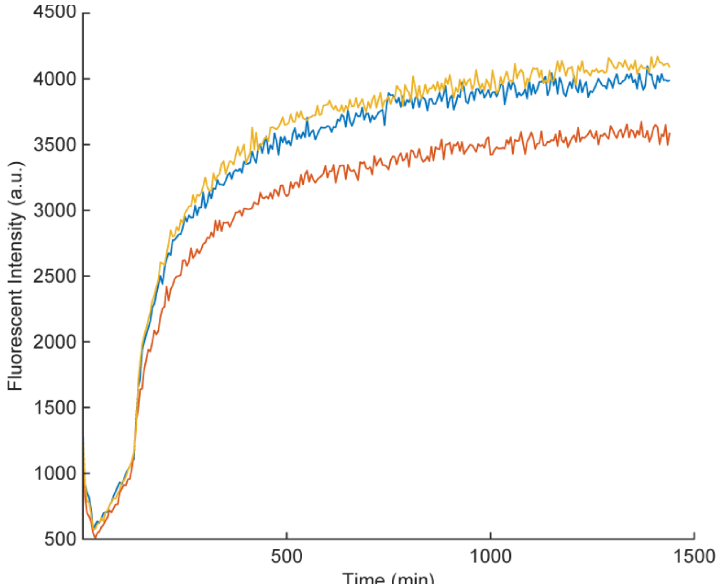

Figure A.1.10: Plate Reader CFE: *Measurement of YPet synthesis in a plate reader for 24 h. The shown curves represent triplicate measurement with identical composition.*

A.1.5. Outlook

Here additional data is shown on the correct functionality of the tested components in chapter 5. The specificity of binding events between tested components and membrane surface was monitored.

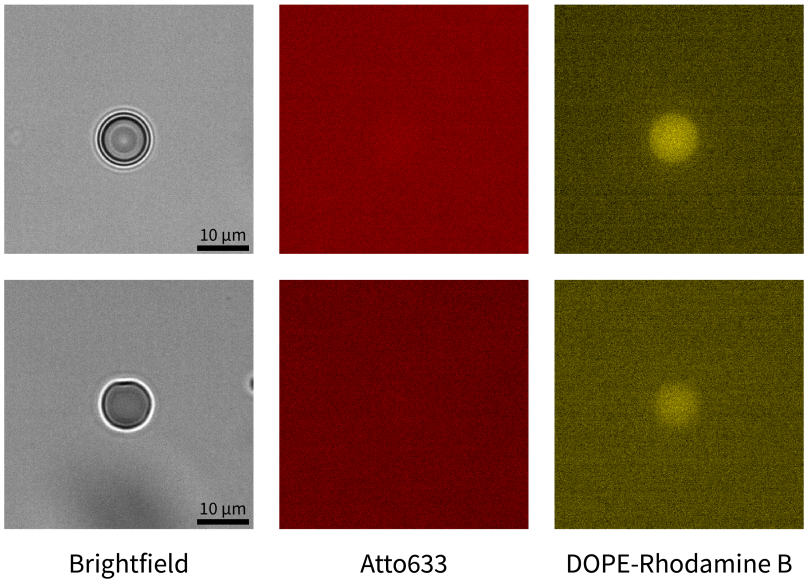

Figure A.1.11: Negative Control DNA Nanostructure Binding: *Micrographs of lacking interaction of fluorescently labeled DNA nanostructures and hybrid membrane omitting streptavidin. Atto633 channel (red) portrays DNA nanostructure and Rhodamine B channel (yellow) visualizes the lipid components of the hybrid membrane.*

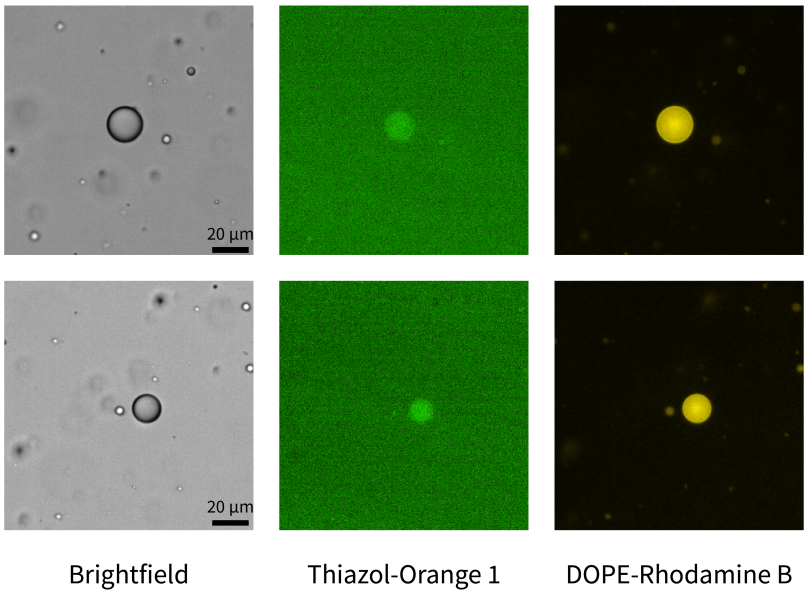

Figure A.1.12: Thiazol-Orange 1 Fluorescence: *Micrographs of fluorescent ligand Thiazol-Orange 1 (green) and vesicle membrane without IVT reactions shows lower fluorescence. Rhodamine B channel (yellow) visualizes the lipid components of the hybrid membrane.*

A.2. Buffer Composition

Table A.2.1: Composition Lysis Buffer

Component	C_{sample} (mM)	Molecular Weight (g/mol)
Lysozyme (mg/mL)	1	
PMSF	1	174.19
Benzamidin	1	120.15
DNase I (U)	0.5	
1xPBS		

Table A.2.2: Composition Washing Buffer

Component	C_{sample} (mM)	Molecular Weight (g/mol)
NaCl	300	58.44
Tris	50	121.14
Imidazol	20	68.08
H_2O_{dd}		

Table A.2.3: Composition Elution Buffer

Component	C_{sample} (mM)	Molecular Weight (g/mol)
NaCl	300	58.44
Tris	50	121.14
Imidazol	500	68.08
H_2O_{dd}		

Table A.2.4: Composition Gel Filtration Buffer

Component	C_{sample} (mM)	Molecular Weight (g/mol)
NaCl	200	58.44
Tris	100	121.14
DTT	2	154.25
EDTA	2	292.24
H_2O_{dd}		

Table A.2.5: Composition 5xQuenching Buffer

Component	C_{sample} (mM)	Molecular Weight (g/mol)
Trolox	25	250.29
Sodium Ascorbate	50	198.1
Sodium Azide	50	65.01
1xPBS		

Table A.2.6: Composition Transfer Buffer (Western Blot)

Component	C_{sample} (mM)	Molecular Weight (g/mol)
Tris	25	121.14
Glycine	190	75.07
Methanol (%)	20	
H_2O_{dd}		

A.3. DNA templates

Cloned constructs are only depicted as sequence within the multiple cloning site of commercially available DNA plasmids. Each construct sequence start with the T7 RNA polymerase promoter and ends with the T7 terminator. The used plasmid are stated for each sequence.

Fluorescent RNA aptamers were transcribed from double stranded linear DNA templates, which were hybridized from single stranded oligonucleotides. Structural sequences of the aptamer are written in capital letters, small letters show regulatory sequences like terminators, promoters and primer-binding sequences.

Table A.3.1: Templates RNA Aptamers

RNA Aptamer	DNA Sequence 5'->3'
Mango-III	tgccacctgacgtctaagaataatacgactcactataggggagcgtgacGGCACGTACGAAG GAAGGTTTGGTATGTGGTATATTCGTACGTGCgtcacgctcattaccgcctttgagtg agc
dBroccoli	gggaagcctgagacggtcgggtccatctGAGACGGTCGGGTCCAGATATTCGTATCT GTCGAGTAGAGTGTGGGCTCagatgtcgagtagagtgtgggctcaggctt

Table A.3.3: Plasmids Protein Expression

Construct	Vector	DNA Sequence 5'->3'
$E_{20}F_{20}$	pET20b(+)	taatacgactcactatagggagaccacaacggtttcccTCTAGAAATAA TTTTGTTTAACTTTAAGAAGGAGATATACAATGGGCCACG GCGTGGGTGTTCCGGGCGAAGGTGTCCCAGGTGAGGGCG TACCGGGCGAAGGTGTTCCTGGTGAGGGCGTGCCGGGCG TGGGTGTTCCGGGCGAAGGTGTCCCAGGTGAGGGCGTAC CGGGCGAAGGTGTTCCTGGTGAGGGCGTGCCGGGCGTGG GTGTTCCGGGCGAAGGTGTCCCAGGTGAGGGCGTACCGG GCGAAGGTGTTCCTGGTGAGGGCGTGCCGGGCGTGGGTG TTCCGGGCGAAGGTGTCCCAGGTGAGGGCGTACCGGGCG AAGGTGTTCCTGGTGAGGGCGTGCCGGGCGTGGGTGTTC CGGGCTTTGGTGTCCCAGGTTTCGGCGTACCGGGCTTTG GTGTTCCTGGTTTCGGCGTGCCGGGCGTGGGTGTTCCGG GCTTTGGTGTCCCAGGTTTCGGCGTACCGGGCTTTGGTG TTCCTGGTTTCGGCGTGCCGGGCGTGGGTGTTCCGGGCT TTGGTGTCCCAGGTTTCGGCGTACCGGGCTTTGGTGTTC CTGGTTTCGGCGTGCCGGGCGTGGGTGTTCCGGGCTTTG GTGTCCCAGGTTTCGGCGTACCGGGCTTTGGTGTTCCTG GTTTCGGCGTGCCGGGCTGGCCGTGATAATTCGAGCTCC GTCGACAAGCTTgcggccgcactcgagcaccaccaccaccaccact gagatccggctgctaacaaagcccgaaaggaagctgagttggctgctgcc accgctgagcaataactagcataaccccttggggcctctaaacgggtcttga ggggttttttg
$R_5Q_5R_5Q_6F_{20}$	pET28b(+)	TAATACGACTCACTATAGGATAGTAAGTCTTGAGACTAGA AAGTAAGGAGGTTTTTTATGGTACCTGGCCGGGGGGTTC CCGGACGAGGAGTACCCGGGCGGGGAGTGCCAGGACGC GGCGTTCCTGGGCGAGGTGTGCCTGGTAAAGGAGTTCCT GGACAGGGAGTACCAGGACAAGGTGTCCCTGGTCAGGGT GTTCCAGGCCAAGGAGTACCTGGACGTGGAGTTCCAGGG AGAGGAGTACCGGGCCGAGGTGTACCAGGTCGCGGAGTG CCCGGACGGGGTGTCCCTGGACAGGGGGTTCCAGGTCAA GGAGTTCCTGGACAGGGAGTACCAGGACAAGGTGTCCCT GGTCAGGGTGTTCCAGGCCAAGGAGTGGGTGTTCCGGGC TTTGGTGTCCCTGGTTTCGGTGTACCAGGATTCGGCGTG CCCGGATTTGGGGTGCCAGGGTTTGGAGTCCCTGGTTTT GGTGTGCCGGGTTTTGGAGTTCCGGGGTTTGGTGTCCCC GGTTTTGGAGTGCCTGGGTTTGGCGTTCCTGGGTTCGGG GTCCCGGGCTTTGGAGTACCTGGCTTCGGTGTACCCGGA TTTGGGGTACCGGGATTTGGCGTACCAGGCTTTGGGGTT CCAGGTTTCGGAGTTCCCGGGTTTGGAGTGCCTGGGTTT GGTGTCCCAGGGTTCGGAGTTCCGGGTTGGCCTCACCAC CACCACCACCACTGAGATCCGGCTGCTAACAAAGCCCGA AAGGAAGCTGAGTTGGCTGCTGCCACCGCTGAGCAATAA CTAGCATAACCCCTTGGGGCCTCTAAACGGGTCTTGAGG GGTTTTTT

Construct	Vector	DNA Sequence 5'->3'
pRNA	pSB4K5	GTAATACGACTCACTATAGGGttgtcatgtgtatgttgggGGATCC CGACTGGCGAGAGCCAGGTAACGAATGGATCCcccacatact ttgttgatccCGCAGGATTCGGCTCGTGTAGCTCATTAGCTCC GAGCCGAGTCCTCGAATACGAGCTGGGCACAGAAGATAT GGCTTCGTGCCCAGGAGGTGTTCGCACTTCTCTCGTGTT CGATTGTGgatcaatcatggcaaATGCGGCCGCCGACCAGAA TCATGCAAGTGCGTAAGATAGTCGCGGGTCGGTGGTCGC ATtactTAGCATAACCCCGCGGGGCCTCTTCGGGGGTCTCG CGGGGTTTTTTGCTGAAACGGCTGCTAACAAAGCCCGAAA GGAAGCTGAGTTGGCTGCTGCCACCGCTGAGCAATAACT AGCATAACCCCTTGGGGCCTCTAAACGGGTCTTGAGGGG TTTTTTGCTGAAAGGAGGAACT
6His-PCP-EX-C	pET28b(+)	TAATACGACTCACTATAGGGGAATTGTGAGCGGATAACAA TTCCCCTCTAGAAATAATTTTGTTTAACTTTAAGAAGGAG ATATACCATGGCACACCACCACCACCACCACAGCAGCGG CGAGAACTTATACTTCCAAGGAAGCAAGACTATCGTTTTG TCCGTCGGCGAGGCTACCCGTACCTTGACCGAAATTCAAT CCACCGCGGACCGTCAAATTTTTGAGGAAAAAGTCGGTC CTCTGGTGGGTCGTCTGCGTCTGACCGCGAGCCTGCGCC AGAACGGTGCCAAAACGGCATACCGTGTTAATCTGAAACT GGATCAGGCCGACGTTGTGGACAGCGGTCTGCCGAAAGT CCGCTACACCCAGGTGTGGAGCCACGATGTGACGATCGT TGCGAATAGCACCGAAGCGAGCCGCAAGAGCCTGTACGA CCTGACCAAGAGCCTGGTGGCAACGTCCCAAGTTGAAGA TCTGGTTGTTAACCTGGTGCCGCTGGGTCGTTCGGGGGG AGGTGGATCCGGCGGTGGTGGATCAGGTCTCCTTCAGCT ACCTTCTGACAAGGCTCTTTTGTCTGACCCTGTATTCCGC CCTCTCGTTGACAAATATGCAGCGGACGAAGATGCCTTCT TTGCTGATTACGCTGAGGCTCACCAAAAGCTTTCCGAGCT TGGGTTTGCTGATGCCTAATGAGATCCGGCTGCTAACAAA GCCCGAAAGGAAGCTGAGTTGGCTGCTGCCACCGCTGAG CAATAACTAGCATAACCCCTTGGGGCCTCTAAACGGGTCT TGAGGGGTTTTTT

Construct	Vector	DNA Sequence 5'->3'
6His-BIV-N-AP	pET28b(+)	TAATACGACTCACTATAGGGGAATTGTGAGCGGATAACAA TTCCCCTCTAGAAATAATTTTGTTTAACTTTAAGAAGGAG ATATACCATGGCACACCACCACCACCACCACAGCAGCGG CGAGAACTTATACTTCCAAGGATCCGGCCCGCGTCCTCGT GGTACCCGTGGCAAAGGTCGCCGTATTCGCCGTTCGGGG GGAGGTGGATCCGGCGGTGGTGGATCAGGAAAGTCTTAC CCAACTGTGAGTGCTGATTACCAGGACGCCGTTGAGAAG GCGAAGAAGCGGCTCGGAGGCTTCATCGCTGAGAAGAGA TGCGCTCCTCTAATGCTCCGTTTGGCATTCCACTCTGCTG GAACCTTTGACAAGAGAACGAAGACCGGTGGACCCTTCG GAACCATCCGCTACCCTGCCGAACTGGCTCACAGCGCTA ACAGTGGTCTTGACATCGCTGTTAGGCTTTTGGAGCCACT CAAGGCGGAGTTCCCTATTTTGAGCTACGCCGATTTCTAC CAGTTGGCTGGCGTTGTTGCCGTTGAGGTCACGGGTGGA CCTAAGGTTCCATTCCACCCTGGAAGAGAGGACAAGCCT GAGCCACCACCAGAGGGTCGCTTGCCCGATCCCACTAAG GGTTCTGACCATTTGAGAGATGTGTTTGGCAAAGCTATGG GGCTTACTGACCAAGATATCGTTGCTCTATCTGGGGGTCA CACTTTAGGAGCTGCACACAAGGAGCGTTCTGGATTTGAG GGTCCCTGGACCTCTAATCCTCTTATTTTCGACAACTCAT ACTTCACGGAGTTGTTGAGTGGTGAGAAGGAATGAGATC CGGCTGCTAACAAAGCCCGAAAGGAAGCTGAGTTGGCTG CTGCCACCGCTGAGCAATAACTAGCATAACCCCTTGGGG CCTCTAAACGGGTCTTGAGGGGTTTTTTG

Construct	Vector	DNA Sequence 5'->3'
6His-YPET-PCP	pJ431	TAATACGACTCACTATAGGGGAATTGTGAGCGGATAACAA TTCCCCTCTAGAAATAATTTTGTTTAACTTTTAAGGAGGT AAAAAATGGGTTCTTCTCACCATCATCATCATCACACTCG CGGCGGCGGCGGTAGCATGTCTAAAGGTGAAGAACTGTT TACGGGTGTCGTGCCGATTCTGGTCGAGTTGGACGGCGA CGTGAACGGTCACAAATTCAGCGTGAGCGGCGAGGGCGA GGGTGACGCGACGTACGGTAAGCTGACTCTGAAGCTGCT GTGCACCACGGGTAAATTGCCGGTTCCGTGGCCGACCCT GGTCACGACGCTGGGTTATGGTGTACAATGTTTTGCACGC TATCCGGACCACATGAAACAGCACGATTTCTTCAAGAGCG CGATGCCGGAAGGCTATGTTCAGGAACGTACCATCTTTTT CAAAGATGATGGTAATTACAAAACCCGCGCAGAAGTGAAG TTCGAGGGTGACACCCTGGTGAACCGTATTGAGCTGAAG GGTATTGACTTCAAGGAAGATGGCAATATTCTGGGTCACA AACTGGAGTACAACTATAACAGCCATAACGTCTACATCAC CGCGGATAAGCAAAAAAATGGTATCAAAGCAAATTTCAAG ATTCGCCACAACATCGAAGATGGCGGCGTGCAACTGGCC GATCATTATCAGCAGAATACCCCAATCGGTGACGGTCCG GTGCTGTTGCCGGATAACCACTACCTGAGCTATCAAAGCG CGTTGTTCAAAGACCCGAATGAAAAACGTGACCACATGGT TCTGCTGGAATTTCTGACCGCTGCGGGCATCACTGAAGG CATGAATGAACTGTACAAGACGCGTGGTGGCGGCGGTTC GATGAGCAAGACTATCGTTTTGTCCGTCGGCGAGGCTAC CCGTACCTTGACCGAAATTCAATCCACCGCGGACCGTCAA ATTTTTGAGGAAAAAGTCGGTCCTCTGGTGGGTCGTCTGC GTCTGACCGCGAGCCTGCGCCAGAACGGTGCCAAAACGG CATACCGTGTTAATCTGAAACTGGATCAGGCCGACGTTGT GGACAGCGGTCTGCCGAAAGTCCGCTACACCCAGGTGTG GAGCCACGATGTGACGATCGTTGCGAATAGCACCGAAGC GAGCCGCAAGAGCCTGTACGACCTGACCAAGAGCCTGGT GGCAACGTCCCAAGTTGAAGATCTGGTTGTTAACCTGGTG CCGCTGGGTCGTTAACCCCCTAGCATAACCCCTTGGGGC CTCTAAACGGGTCTTGAGGGGTTTTTT

Construct	Vector	DNA Sequence 5'->3'
YPET	pSB1C3	TAATACGACTCACTATAGGGTAGCGCAGCGCTCAACGGG TGTGCTTCCCGTTCTGATGAGTCCGTGAGGACGAAAGCG CCTCTACAAATAATTTTGTTTAATCATGAGaaagaggagaaa ACTAGATGTCTAAAGGTGAAGAACTGTTTACGGGTGTCGT GCCGATTCTGGTCGAGTTGGACGGCGACGTGAACGGTCA CAAATTCAGCGTGAGCGGCGAGGGCGAGGGTGACGCGAC GTACGGTAAGCTGACTCTGAAGCTGCTGTGCACCACGGG TAAATTGCCGGTTCCGTGGCCGACCCTGGTCACGACGCT GGGTTATGGTGTACAATGTTTTGCACGCTATCCGGACCAC ATGAAACAGCACGATTTCTTCAAGAGCGCGATGCCGGAA GGCTATGTTCAGGAACGTACCATCTTTTTCAAAGATGATG GTAATTACAAAACCCGCGCAGAAGTGAAGTTCGAGGGTG ACACCCTGGTGAACCGTATTGAGCTGAAGGGTATTGACTT CAAGGAAGATGGCAATATTCTGGGTCACAAACTGGAGTAC AACTATAACAGCCATAACGTCTACATCACCGCGGATAAGC AAAAAAATGGTATCAAAGCAAATTTCAAGATTCGCCACAA CATCGAAGATGGCGGCGTGCAACTGGCCGATCATTATCA GCAGAATACCCCAATCGGTGACGGTCCGGTGCTGTTGCC GGATAACCACTACCTGAGCTATCAAAGCGCGTTGTTCAAA GACCCGAATGAAAAACGTGACCACATGGTTCTGCTGGAAT TTCTGACCGCTGCGGGCATCACTGAAGGCATGAATGAAC TGTACAAGACGCGTGGTGGCGGCGGTTCGATGAGCAAGA CTATCGTTTTGTCCGTCGGCGAGGCTACCCGTACCTTGAC CGAAATTCAATCCACCGCGGACCGTCAAATTTTTGAGGAA AAAGTCGGTCCTCTGGTGGGTCGTCTGCGTCTGACCGCG AGCCTGCGCCAGAACGGTGCCAAAACGGCATACCGTGTT AATCTGAAACTGGATCAGGCCGACGTTGTGGACAGCGGT CTGCCGAAAGTCCGCTACACCCAGGTGTGGAGCCACGAT GTGACGATCGTTGCGAATAGCACCGAAGCGAGCCGCAAG AGCCTGTACGACCTGACCAAGAGCCTGGTGGCAACGTCC CAAGTTGAAGATCTGGTTGTTAACCTGGTGCCGCTGGGTC GTTAAaGCATGCcggaGGAAACACAGAAAAAAGCCCGCAC CTGACAGTGCGGGCTTTTTTTTTC

A.4. Membrane composition

Following are the membrane compositions of the vesicles used in this thesis. The main components are given in the upper parts of the tables and individual addition of other components for specific measurements like biotin-streptavidin interaction are given in the lower part of the tables.

Table A.4.1: Composition Liposomes: *Composition membrane of liposomes for measurements*

Component	C_{sample} (µM)
DOPC	135
DPPC	202.5
Cholesterol	112.5
DOPE-RhodB	0.075
DOPE-Bio	4.5

Table A.4.3: Composition ELP Vesicles: *Composition membrane of ELP vesicles for measurements*

Component	C_{sample} (µM)
ELP $EF_{20}/(R_5Q_5)_{20}F_{20}$	290
EF20-Atto488	1.5

Table A.4.5: Composition Hybrid Vesicles: *Composition membrane of hybrid vesicles composed of lipids and ELPs for measurements*

Component	C_{sample} (µM)
DOPC/DOPS	135
ELP EF_{20}	202.5
Cholesterol	112.5
EF_{20}-Atto488	1.5
EF_{20}-Cy5	5
DOPE-Bio	4.5
DOPE-RhoB	0.075

Acknowledgements

Finally, I want to thank all people who made this work possible. First of all I want to thank Prof. Friedrich Simmel for giving me the possibility at his chair to pursue the research on synthetic biology.
I want to thank Helene Budjarek, Daniela Härtwig and Susanne Kinzel, without whom work in the lab and administration would have been chaos.
A special thanks goes out to Kilian Vogele as great supervisor during my Master's thesis and great colleague during my doctoral thesis. I thank Tobias Pirzer for his feedback and detailed discussions concerning my work.
I also want to thank Julia Müller being a great support during the more difficult times during this PhD and helping me to bring some order into my chaos. Florian Katzmeier and Elisabeth Falgenhauer for being great office buddies and problem solvers.
After countless sessions in the clean room, I want to thank Lukas Aufinger and Louis Givelet for introducing me into the 'rewarding' world of microfluidics. I am grateful for the constructive, beer-supported discussions with Markus Eder and Thomas Mayer helping me figuring out new approaches for problems. Thanks also goes to Andrea Mückl for our hours spent in front of the ÄKTA and autoclaving bacteria.
I thank the whole iGEM2018 team for the experience, especially Quirin Emslander, Johann Brenner and Keno Eilers for their hard work when it counted.
I want to thank Yash Bogawat for his help concerning DNA origami and his professional input. Anna Pastucha with her help using confocal microscopy. Jonathan List and Tamara Breitinger for their professional feedback on the thesis itself.
It has been a pleasure working with all of you!

I want to thank the Hanns-Seidel-Stiftung for enabling me to pursue my doctoral thesis and providing the possibility to develop as a person.

Lastly, I want to thank my family and friends for supporting me during my whole time in academia and especially all the way to the end of this thesis.

"A mother is she who can take the place of all others but whose place no one else can take."

– Gaspard Mermillod